NANOFILM - New metallic nanocomposites for micro and nanofabrication

Fischer, Søren Vang

Publication date:
2015

Document Version
Publisher's PDF, also known as Version of record

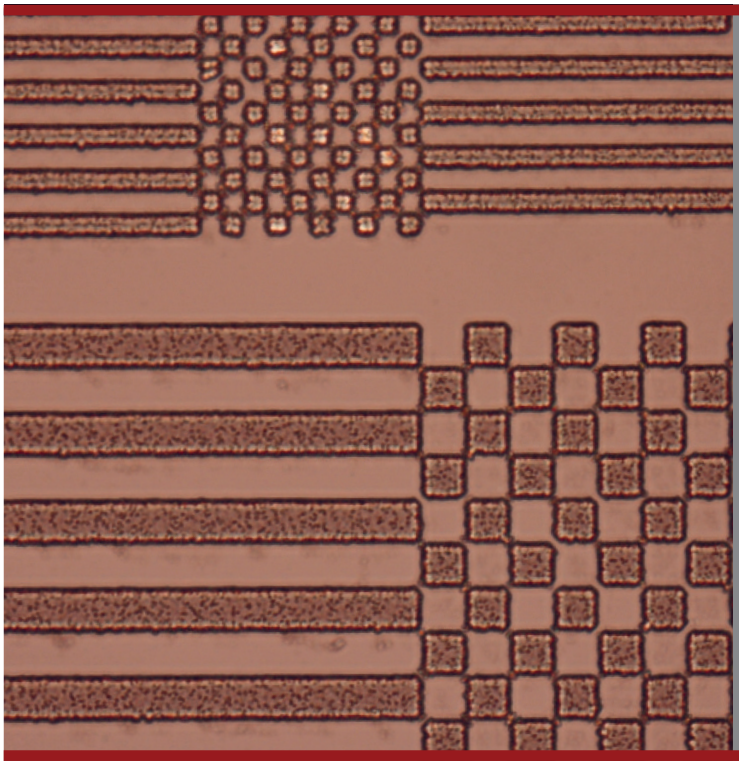

NANOFILM

New Metallic Nanocomposites for Micro- and Nanofabrication

Søren Vang Fischer
PhD Thesis April 2015

DTU Nanotech
Department of Micro- and Nanotechnology

DTU Nanotech
Department of Micro- and Nanotechnology

NANOFILM – New Metallic Nanocomposites for Micro- and Nanofabrication

Ph.D. Thesis

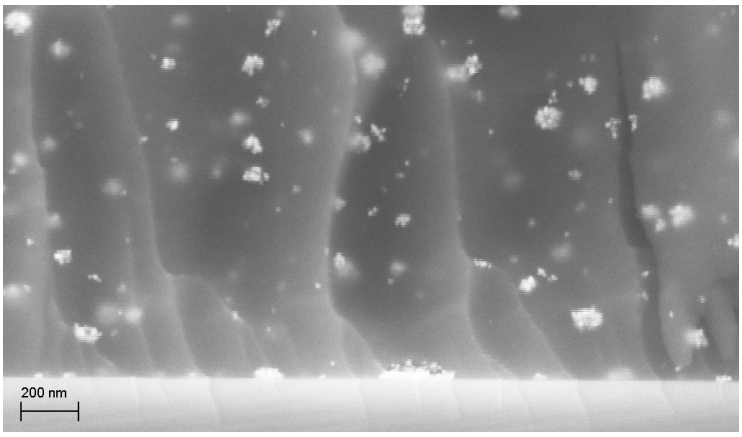

Søren Vang Fischer

14th of April 2015

DTU Nanotech - Department of Micro- and Nanotechnology
Technical University of Denmark

Supervisor: Senior Researcher Mogens Havsteen Jakobsen
CO-supervisor: Postdoc Basil Uthuppu

Partly founded by Copenhagen Cleantech Cluster

Front Page Picture

The picture on the front page shows an epoxy nanocomposite with silver nanoparticles.

Preface

This Thesis is submitted as partial fulfilment of the requirements to obtain a Ph.D. degree at the Technical University of Denmark (DTU). The work has been carried out at the Department of Micro- and Nanotechnology (DTU Nanotech) at DTU from the 15^{th} of December 2011 until the 14^{th} of Januar 2015.

The work has been supervised by senior researcher Mogens Havsteen Jakobsen, group leader of the Surface Engineering group at DTU Nanotech and CO-supervised by postdoc Basil Uthuppu also from the Surface Engineering group.

The project has been supported by Copenhagen Cleantech Cluster.

Abstract

Metal nanoparticles are of great interest because of their unique physical properties such as plasmonic absorption. By incorporating nanoparticles into polymers, nanocomposites with interesting properties can be made. These nanocomposites can be useful within optoelectronics, electrochemistry or catalysts. The possibility to effectively structure the nanocomposites are however a limiting factor.

In this project the UV sensitive photoresist SU-8 gold and silver nanocomposites have been fabricated which can be deposited and structured using standard micro and nanofabrication processes.

In the beginning, a method named as *ex situ* has been attempted to develop the nanocomposites. In this method, synthesised nanoparticles were incorporated into the photoresist matrix through effective solvent exchange from water to cyclopentanone, the solvent of the primarily used SU-8. The solvent exchange was achieved by first stabilizing the nanoparticles using the block co-polymers PVP/VA and PVA-COOH. The water was then secondly removed by co-evaporating under reduced pressure in the presence of target solvent. PVA-COOH was discarded after a jellification when in contact with cyclopentanone was discovered. A technique called pre grafting was found to be most effective for the stabilisation process. In pre grafting the nanoparticles were formed in the presence of PVP-VA. For the two metal nanocomposites attempted to be fabricated only the gold SU-8 nanocomposite was successfully and reproducibly produced with the *ex situ* method.

An *in situ* method was then tried for the development of both gold and silver SU-8 nanocomposites. In this procedure, the metal precursors were incorporated with SU-8 and the respective nanoparticles formed within the photoresist matrix. The nanoparticles should preferably be formed during the heat treatment or UV irradiation after spin coating. It was able possible to dissolve the gold precursor directly into the photoresist, but nanoparticles with large size distribution were formed within a time frame of 20 s. This made further processes such as spinning and formation of a homogeneous thin layer of nanocomposite tedious. In the case of silver, a co-solvent was needed to incorporate silver nitrate into SU-8. In the first attempt DMSO was used as the co-solvent, but as DMSO is a Lewis base, it prohibited complete cross-linking during the UV irradiation step. Acetonitrile was then chosen for as co-solvent which resulted in a successfully structured *in situ* silver SU-8 nanocomposite.

For both the *ex situ* and *in situ* nanocomposites structuring was initially found to be troublesome. Complete cross-linking of the SU-8 was only found to be possible after removing the filter from the aligner which blocks wavelengths below 350 nm. The obtained resolution was similar to what could be obtained with unmodified SU-8.

It has been found that for the silver nanocomposites a further hard bake step at 300°C in the end of the process resulted in the additional formation of numerous nanoparticles. The heating does not result in growth or agglomeration of the nanoparticles. It was also found that for high loads of silver in the nanocomposite, the additional heating results

in a conductive composite. The conductive silver nanocomposite has been compared to a commercially available product, and although SEM investigations show that the structure of the fabricated composite appears to be preferable compared to the commercially available one, the obtained conductivity needs to be improved before it is competitive.

All nanocomposites have been investigated to show that the nanoparticles maintain their plasmonic absorption and that the absorption is proportional to the nanoparticle concentration. The position of the plasmonic absorption peak was found to be red shifted with approximately 10 nm compared to that of pre synthesised nanoparticles in SU-8 or cyclopentanone. It was for the silver nanocomposites found that the additional heat treatment blue shifted the plasmonic absorption peak such that it again resembled that of the synthesised nanoparticles.

In conclusion this project has resulted in the successful fabrication of new metallic nanocomposites which can be used for micro- and nanofabrication. The process for the *in situ* formation of nanoparticles is, however, not completely understood and should be investigated in the future.

Dansk Resumé

Formålet med denne Ph.D. har været nye materialer som kan anvendes til nano- og mikrofabrikation. Mere specifikt er der blevet kigget på nanokompositter bestående af metal nanopartikler i fotoresisten SU-8. SU-8, som primært består af en epoxy resin, opløst i cyclopentanon, er valgt til dette projekt, grundet materialets transparens ved synlige bølgelængder, samt store biokompatibilitet, når først det er hærdet.

De overordnede fokuspunkter for projekter var:

- Syntese af metal nanopartikler.
- Overføre nanopartikler til SU-8.
- Nye metoder til fremstilling af nanokompositter.
- Karakterisering af nanopartikler og -kompositter.

Guld og sølv nanopartikler er blevet syntetiseret på flere forskellige måder. En metode er blevet brugt til fremstilling af guld nanopartikler mens to forskellige metoder er blevet benyttet til at fremstille sølv nanopartikler.

Guld og sølv nanopartikler er blevet udvalgt grundet deres store plasmoniske respons som gør dem velegnede til optiske sensorer.

For at forøge den kolloide stabilitet er nanopartiklerne efterfølgende blevet coatet med en polymer. To forskellige polymerer er blevet benyttet, henholdsvis poly(vinyl pyrrolidone/vinyl acetate), PVP/VA, og PVA-COOH. Polymererne er udvalgt da de er opløselige i både vand og organiske opløsningsmidler og derudover er biokompatible. Det har dog vist sig at PVA-COOH ikke er forenelig med SU-8 hvorfor denne er blevet droppet. Der blev oprindeligt benyttet en stabiliseringsmetode hvor nanopartiklerne blev coatet efter fremstilling.

Nanopartiklerne er fremstillet i vand for at minimere brugen af giftige og skrappe kemikalier hvilket nødvendiggør at vandet udskiftet med et SU-8 kompatibelt opløsningsmiddel. Tre forskellige metoder er blevet benytter til udskiftning af vandet; centrifugering, frysetørring og rotationsfordampning. For centrifugering og rotationsfordampning har det vist sig at fuldstændig udtørring af partiklerne umuliggør suspension i organiske opløsningsmidler.

Frysetørring har vist sig ikke at være mulig med sølv nanopartikler på grund af faseadskillelse og agglomeration af nanopartiklerne. Et lignende fænomen dog på mindre skala blev oprindeligt også observeret for guld nanopartikler. En gradvis udskiftning af vandet med det ønskede opløsningsmiddel ved hjælp af rotationsfordampning har dog vist sig mulig. Det er lykkedes at overføre både guld- og sølv nanopartikler til cyclopentanon med denne metode. Stabiliteten af nanopartiklerne har dog vist sig yderst svær at opretholde når SU-8 tilsættes.

For at opnå nanopartikelstabilitet når SU-8 tilsættes er en alternativ metode til at fremstilling og coatning af nanopartikler blevet udviklet. I stedet for at syntetisere partiklerne hvorefter de coates, er polymeren PVP/VA tilstede under fremstillingen. Dette resulterer en større stabilitet af partiklerne. Dette har resulteret i at guld nanopartikler der er stabile i SU-8. Rotationsfordampning er igen blevet benyttet til at udskifte vandet med SU-8. Det ser også ud til at denne alternative coating metode muliggør brugen af frysetørring for guld nanopartiklerne. Det er også lykkedes at opnå stabile sølv nanopartikler i SU-8 ved hjælp af rotationsfordamperen, men disse resultater har dog ikke været reproducerbare.

Disse metoder hvor fremstillede nanopartikler coates med en polymer hvorefter de bliver blandet med SU-8 er blevet navngivet *ex situ* kompositter. Der er også udviklet procedurer for *in situ* kompositter hvor nanopartiklerne først dannes i selve SU-8 fotoresisten.

In situ kompositterne fremstilles således at de metalsalte som skal bruges til at fremstille nanopartiklerne blandes direkte med SU-8. Dette er muligt for guldklorid som bruges til at fremstille guld nanopartikler, men ikke for sølvnitrat som bruges til fremstilling af sølv nanopartikler. Det har derfor været nødvendigt at finde et opløsningsmiddel der kan opløse sølvnitrat og samtidig være kompatibelt med SU-8. Flere forskellige opløsningsmidler er blevet afprøvet, men de tre som er blevet brugt til fremstilling af nanokompositter er DMSO, ethanol og acetonitril. Brugen af DMSO har dog vist sig at resultere i ufuldstændig krydsbinding af SU-8 hvorved det opløsningsmiddel ikke kan benyttes.

Når opløsningsmidlet med sølvnitrat blandes med SU-8 vil der over tid blive dannet nanopartikler. Denne proces er yderst hurtig for guld og sker inden for 20 s, mens det for sølv går noget langsommere. For sølv er det derfor meget nemmere at benytte de processer som er nødvendige i nano- og mikrofabrikation. Den største formation af sølv nanopartikler er blevet observeret til at ske under opvarmning. Den præcise kemiske proces ansvarlig for formationen af nanopartiklerne er dog ukendt.

For alle nanokompositter, *in situ* og *ex situ*, har det været nødvendigt at fjerne det filter der normalt blokerer for lave bølgelængder under UV eksponeringen for at opnå fuldstændig krydsbinding. Uden fuldstændig krydsbinding kan nanokompositterne ikke struktureres som ønsket. Det er derudover også fundet at brugen af ethanol og en anden SU-8 en primært benyttet muliggør strukturering af en nanokomposit uden at filteret fjernes fra maskinen. Brugen af ethanol begrænser dog mængden af opløseligt sølvnitrat betragteligt i forhold til acetonitril.

Det har vist sig at de bedste nanokompositter opnås ved at benytte *ex situ* metoden for guld nanokompositter og *in situ* metoden for sølv nanokompositter. For alle fremstillede nanokompositter har det vist sig at UV litografi kan benyttes til strukturering og at en opløsning på 5 μm kan opnås. Belysningstiden er dog væsentligt forhøjet i forhold til

standardprocesser.

Det er også blevet fundet at en yderligere opvarmning til 300°C efter fremstilling af sølv nanokompositten resulterer i en massiv dannelse af nanopartikler uden at de allerede tilstedeværende nanopartikler vokser eller agglomererer. For høje koncentrationer af sølv vil dette ligefrem føre til en ledende nanokomposit. Den samme effekt er ikke umiddelbart blevet fundet for guld nanokompositten.

Den udviklede *in situ* metode til fremstilling af SU-8 sølv nanokompositter løser flere problemer beskrevet i litteraturen omkring netop SU-8 sølv nanokompositter. Det har tidligere ikke været muligt at benytte spin coatning til deponering af resisten eller opnå fuldstændig krydsbinding ved forsidebelysning. Begge disse problemer er blevet løst hvilket øger anvendelsesmulighederne.

Ex situ nanokompositterne har dog stadig de fordele i forhold til *in situ* nanokompositterne at der er bedre kontrol med partikel form og størrelse samt at nanopartiklerne kan funktionaliseres såfremt dette ønskes.

Helt konkret har det vist sig muligt at fremstille og strukturere tre forskellige kompositter. En *ex situ* guld komposit samt to *in situ* sølv kompositter. For høje koncentrationer af sølv er det blevet observeret at en opvarmningsproces på først 150°C efterfulgt af 300°C resulterer i et ledende materiale. Materialet viser indtil videre lavere ledningsevne end et kommercielt tilgængeligt produkt, men har en overfladestruktur som ser mere favorabel ud.

Der er dog stadig masser af ting som kan undersøges og forbedres før nanokompositterne er fuldt forstået og anvendelige for et bredt publikum.

Så som en konklusion kan man sige at der har været; masser af succes og det der hører til, af adskillige fiaskoer, utallige frustrationer og ting der bare ikke har virket undervejs, men det er til slut lykkedes at skabe et materiale med en masse anvendelsesmuligheder og som forhåbentligt viser sig brugbart for mange personer.

Acknowledgements

I would like to thank all the people who in some way have contributed towards the completion of this report and Ph.D. No one should be forgotten however tiny their contribution might be, if none is mentioned, none have been forgotten. I though have to give a special thanks to Basil for all his help regarding nanoparticles as this would otherwise have been a very lonely journey. Stephan Keller is also greatly appreciated for lending me UV lithography masks with resolution marks. The fantastic four also deserves praise for cake, corrections and contemplations.

A thank to my entire research group for making the three years a good time, and of course a warm thank to my main supervisor for being there when needed, and providing insightful comments to help the project progress.

Contents

List of Figures

List of Tables

List of Abbreviations

Ex situ composite	Nanoparticles are synthesised following standard protocols and then later incorporated into SU-8, page 14.
In situ composite	The metal precursor is mixed directly with SU-8 and the nanoparticles later formed inside the polymer matrix, page 14.
Sol	Nanoparticles dispersed in a continuous medium, page 27.
Ag(acac)	Silver acetylacetonate, page 25.
$AgNO_3$	Silver nitrate, page 23.
AZ® resist	Positive tone photo resist used for micro- and nanofabrication, page 71.
$C_5H_7AgO_2$	Silver acetylacetonate, page 25.
DMSO	Dimethyl sulfoxide, page 14.
$HAuCl_4 \cdot 3H_2O$	Gold(III) chloride hydrate, page 19.
HEPA	High-Efficiency Particulate Air, page 5.
HF	Hydrofluoric acid, page 70.
HMDS	Hexamethyldisilazane, page 70.
IPA	Isopropyl alcohol (2-propanol), page 63.
ISO 14644-1	ISO standard for cleanrooms and associated controlled environments – Part 1: Classification of air cleanliness, page 5.
MEMS	Micro Electro-Mechanical Systems, page 1.
MOEMS	Micro Optical Electro-Mechanical Systems, page 1.

$Na_3C_6H_5O_7 \cdot 2H_2O$	Sodium citrate dihydrate, page 19.
$NaBH_4$	Sodium borohydride, page 23.
PEB	Post exposure bake, page 70.
PGMEA	Propylene glycol monomethyl ether acetate, page 63.
PVA	Polyvinyl acetate, page 30.
PVA-COOH	Poly(vinyl alcohol-co-vinyl acetate) containing carboxylic groups, page 14.
PVP	Polyvinylpyrrolidone, page 29.
PVP/VA	Poly(vinyl pyrrolidone/vinyl acetate), page 14.
RCF	Relative centrifugal force, page 35.
RPM	Revolutions per minute, page 35.
SEM	Scanning electron microscope, page 48.
SU-8	Negative tone photoresist used for micro- and nanofabrication, page 8.
TEM	Transmission electron microscope, page 20.
TMS	Trimethylsilyl, page 70.

Chapter 1

Introduction

In this chapter an introduction to the subject of this Ph.D. will be given. In the beginning a short description in semi-popular language is included to allow people who are not knowledgeable within this field to get an idea of the concept.

A more thorough introduction explaining follows, explaining the possibilities and limitations as well as prior art known within the areas of this Ph.D.

In the end a short description of the remaining chapters is given.

1.1 What is This Thesis About?

Within every intelligent device, be it a computer, a smart phone or an air back sensor, small components fabricated using micro- and nanotechnology is found. In every computer millions of transistors transforms inputs into outputs allowing you to play you favourite computer game, make 3D drawings or just use a spreadsheet to calculate how much money you can spend on a new car. None of this would be possible without the ability to structure, primarily, silicon on the micro- and nanoscale.

Transistors, sensors and other miscellaneous components are all Micro Electro-Mechanical Systems (MEMS) and in general the method of fabricating these devices is called MEMS technology. If optical applications are further added to the functionality the name is sometimes changed to MOEMS.

In this project the goal is to end up with new materials for use in micro- and nanofabrication. This could allow even more advanced applications than currently available, or better performance of already existing components.

At first it is important to understand that particle contamination is extremely important when fabricating MEMS devices as just a single particle can destroy an entire device. This is because of the very small structures which are easily short-circuited by a single particle. All fabrication therefore have to take place in a dedicated cleanroom which is designed to be as particle free as possible, meaning 1000 – 10 particles per cubic meter or even less. This can be compared to ambient air in an urban environment which typically

consist of 35 million particles per cubic meter of a size of 0.5 μm or more.

In cleanroom fabrication a lot of standardized processes exist in order to keep the cost down. The most used process for making small structures are UV lithography or variations hereof for more advanced systems. In UV lithography a UV sensitive polymer or polymer precursor is used to transfer the desired pattern into the substrate.

UV lithography works in the way that the polymer or polymer precursor, is dissolved in a solvent together with a material which reacts when exposed to UV light. This mixture, called a photoresist, is then deposited on a substrate, most likely silicon, using a variety of different methods including spin coating, a commonly used technique. In spin coating the substrate is rotated at a speed of maybe 2000 RPM and some photoresist is then poured onto the substrate. The rotation of the substrate results in most of the photoresist being flung or spun of the substrate leaving only a thin layer of for instance 2 μm behind covering the entire surface. Afterwards the photoresist is exposed to UV light through a mask which has the desired pattern. The UV light activates the photo reactive material in the photoresist which then again takes part in a chemical reaction with the polymer. After the exposure the substrate is dipped in a solvent to develop the structures. Photoresists can be acquired as a positive resist, where all exposed resist is removed, or as a negative resist, where all the unexposed resist is removed.

This is the basics of UV lithography although the complexity is somewhat higher. A thorough explanation of the entire UV lithography process is given in chapter 7.

As mentioned, the goal of this project is to produce new materials that can be used within MEMS and cleanroom fabrication. The development of these new materials is focused on nanocomposites made of nanoparticles and photoresists. The nanocomposites are interesting if they maintain the properties of the nanoparticles. As will be explained nanoparticles behave much different than bulk materials. The main challenge is to be able to make such a composite while still maintaining the possibility to manipulate it using standard fabrication techniques.

If you are hooked on learning more please read on, otherwise skip to chapter 9 for the conclusion to see what have been achieved, or return to the real world rejoicing in the fact that people are constantly trying to improve the world we live in.

1.2 Nanocomposites

After this general and brief introduction to the subject a deeper description is needed for the different areas covered. First we will take a look nanocomposites starting out with just a regular composite.

A composite can be described as a material which is constituted of two or more materials which are chemically or physically different. It is also described as; *a solid material that results when two or more different substances, each with its own characteristics, are combined to create a new substance whose properties is superior to those of the original components in a specific application. The term composite more specifically refers to a structural material (such as plastic) within which a fibrous material (such as silicon carbide) is*

embedded [1].

Composites have been used for thousands of years from Egyptians mixing mud and straws to make bricks, till today's vast consumption of concrete. Composites have also had a great development from wooden planks on metal frames [2] to the current uses within almost any application. Regular composites, how interesting they may ever be, are however not really relevant within this project as we need things to be small, hence a nanocomposite.

A nanocomposite basically means that at least one of the materials in the composite are in the nanometre range, which most likely mean that some "regular" composites could also get that label since they also contain elements in the nano range. Nanocomposites are of great interest as they make it possible to develop and utilize unique mechanical, electrical, optical or other properties [3].

Of the many current uses of nanocomposites the most widespread is lightweight materials within the airplane industry and composites in car manufacturing [4]. The use of different materials such as carbon nanotubes added to epoxy to increase the elastic modulus has been utilized for many years [5].

Although nanocomposites are of very high interest and can be used for things such as self-healing materials, a problem often encountered are the tendency of nanoparticles to cluster and aggregate by which the properties associated with the individual nanoparticles are negated [3].

To understand the nanocomposite better, it is important to look at the nano component, here the nanoparticles.

1.3 Nanoparticles

One of the constituents of a nanocomposite needs to be in the nanometre range. In this project the focus is on metallic nanoparticles, but engineered nanoparticles come in many forms, shapes and materials ranging from metal oxides over diamonds [6] to noble metals.

Nanoparticles have been used for centuries, but the first scientific description came from Faraday [7]. Since then, nanoparticles have been widely explored because of their unique properties such as optical, electrical or magnetic [8, 9], but nanoparticles are also extremely interesting within drug delivery [10].

Although extremely interesting, many questions have also been raised about human exposure to nanoparticles and their toxicity [11], but this should not be a problem in this project as the nanoparticles are supposed to be completely encased within the polymer matrix. Depending on the final application and the type of nanoparticles which have been used, toxicity studies should be performed if necessary.

Nanoparticles can, as mentioned, be made from almost any material, but as the title betray this project only looks into the possibilities of metallic nanoparticles. One reason to choose metallic nanoparticles is their optical properties which makes them very interesting for optical sensors. Other reasons are their electrical conductivity and their physiochemical properties, which makes them extremely useful in biological sensors [12].

Metal nanoparticles are easily synthesized using a large variety of chemical processes ranging from using plant extracts [13] to organic solvent including thiols and chloroform [14], and anything in between such as sodium borohydride [15], alcohols [16] or polymers [17].

Each synthesis method has advantages and disadvantages of its own, but the focus in this project is to synthesise them without using harsh chemicals in compliance with the requirements of green chemistry.

1.4 Green Chemistry

Green chemistry is a term introduced and explained by Anastas in 1991 and later defined into 12 principles [18]:

1. Prevent waste
2. Atom economy
3. Less hazardous chemical synthesis
4. Designing benign chemicals
5. Benign solvents and auxiliaries
6. Design for energy efficiency
7. Use of renewable feedstocks
8. Reduce derivatives
9. Catalysis over stoichiometric
10. Design for degradation
11. Real-time analysis for pollution prevention
12. Inherently benign chemistry for accident prevention

By following these principles the chemistry will result in a safer environment and a more efficient use of resources.

The idea behind the points 1-6 are that it is better to prevent waste than treat and clean up whatever waste have been created. Synthetic methods should incorporate as much of the used material into the final product as possible. During synthesis the chemicals used or created should have little toxicity towards the environment or human health. This also means that new chemical products should be designed to minimize toxicity. The use of organic solvents and auxiliaries should be avoided whenever possible, or be as harmless as

possible when used. The energy used should be minimized and if possible the synthesis should be done at room temperature.

The points 7-10 consider that a material should preferably be renewable rather than depleted. The use of blocking groups, protectors or temporary modifications should be avoided as they add more reagents and thereby more waste. Catalytic reagents are superior to stoichiometric reagents. At the end of use, all substances should degrade to harmless products which do not persist in nature. The last two points, 11 and 12, are about inventing methods for direct monitoring and minimizing the potential for accidents.

Green chemistry has since the late 90'ies been adopted by many, or at least used in the title of many research papers [19].

To comply with the principles of green chemistry this project will not use any of the many synthesis methods of nanoparticles which involve harsh organic solvents, but use water-based synthesis with a minimum of waste. Green chemistry will be a consistent consideration throughout this project even if when not mentioned.

1.5 Micro- and Nanofabrication

Before the nanocomposite becomes really useful it needs to be structured. Structuring is done using micro- and nanofabrication, or MEMS technology as it is often called. In MEMS technology special machinery, environments and processes are used to achieve the desired result.

First of all very clean and controlled environments are needed as a single particle contamination can easily destroy whatever device is being manufactured due to the very small sizes involved.

To get an idea of the scale in which these processes are taken place a good place to start is always to look how far Intel has come with their processors. Some of the newest processors from Intel have dimensions of only 22 nm [20] which will then easily be affected, or in fact be rendered useless, by a dust particle landing on the structure. A dust particle can be anywhere in the size of 0.5 μm to 10 μm [21] which is even for the small particles more than 20 times larger than the structures.

To avoid dust and many other particles such as pollen (sizes of several micrometre [22]) or bacteria (sizes from 0.5 μm to several hundred micrometres) a cleanroom is needed. A cleanroom can basically be described as a closed sealed room equipped with HEPA filters (High-Efficiency Particulate Air) to remove most particles from the air going into the room. Depending on the amount particles in a cubic meter of air the cleanroom can then be classified by the ISO 14644-1 standard ranging from the best (ISO 1) with only ten particles of a size equal to or greater than 0.1 μm to ISO 9 corresponding to room air, where the maximum amount of particles of 0.1 μm or greater is one billion.

Besides the many filters to get very clean air, a cleanroom is also equipped with a lot of specialised equipment such as high temperature furnaces, reactive ion etchers or electron beam writers to accommodate the different requirements within growth and etching of materials needed for MEMS technology.

When both the environment and the advanced processes on specialised equipment is in place, everything can come together making it possible to fabricate these very small structures which many do not know, or tend to forget, make up an integral part of our everyday life.

One of the very important steps within micro- and nanofabrication is photolithography in which photons are used to define the structures needed. A similar method which uses electrons instead of photons can also be used for extremely small structures. This is called e-beam lithography. The important parameter for these processes is the minimum feature size.

The minimum feature size is the smallest structure which can be made using photolithography and is directly proportional to the wavelength of the used light. In standard photolithography the light source will be a mercury lamp used together with a filter to get the spectral line at 365 nm, but you can also get more advanced commercial systems which uses deep UV at for instance 248 nm, while extreme UV at 13.5 nm is currently under development.

In this Ph.D. project standard photolithography at 365 nm is used, meaning that any mentioning of UV lithography refers to this 365 nm wavelength processing.

The UV lithography process is a very crucial part of this Ph.D. as new materials for micro- and nanofabrication should be developed and these will be kind of useless if it is then not possible to structure them with the available standard processes. The UV lithography process is thoroughly described in chapter 7 where each step involved is explained in details.

The detailed description of UV lithography also includes another important step called spin coating in which the photoresist is deposited on the substrate and the film thickness defined. The film thickness is also a parameter that controls the minimum feature size.

After a successful fabrication the entire device is subjected to some kind of protection and packaging to ensure that it will still be operational once being removed from the cleanroom. Before moving onto the actual work of this project some other nanocomposites will be described.

1.6 Gold Composites

One focus of this project is gold nanocomposites. Gold nanocomposites have been intensely studied and are interesting within solid-state potentiometric sensors, batteries, supercapacitors or catalysis [23].

The surface plasmon resonance peak of gold nanoparticles can be controlled from near infrared to the visible region by changing the shape and structure. This could typically be nanospheres, nanorods, nanoshells and nanocages [24]. Gold nanoparticles are also good for delivery of protein-based drugs as they can carry multiple active groups [25].

Gold nanocomposites have been used for fabricating films for plasmonic biosensing [26] holographic gratings [27] or to increase biocompatibility [28].

Gold nanocomposite preparation is normally categorised into three different methods; direct-synthesis, graft-to and graft-from [29]. All of which thiol groups play an important

factor in stabilising and functionalising the gold. Thiol chemistry will be avoided in this project, which means that other methods will have to be found.

The primary focus of this project is however silver nanocomposites which are also much more explored.

1.7 Silver Composites

A lot of work has been done through the years on silver composites as they have attracted great attention due to the antimicrobial effects of silver which have been known for ages [30].

The antimicrobial effect of silver is not fully understood, but it appears that although silver nanoparticles plays a role the dominant part is the silver ions [31]. The antimicrobial effect of silver has also meant that it has found its way into socks and textiles [32], but also many other consumer products, which raises a concern about cytotoxic and genotoxic effects should the concentration in the environment become too great [30].

There are numerous examples of different methods to make silver-polymer nanocomposites for anti-microbial purposes [33] and many applications for those as well. These applications could be within controlling biofouling in membranes for water purification [34] or for indwelling devices [35].

An effect of silver nanoparticle composites could be the one described by Lischer et al. [36]. They have an antibacterial burst of silver cations within the first day, after which cells can start to grow on the device. This could be very suitable for implant where you want to avoid bacterial infections in the beginning, but allow tissue cells to attach later on. It is however not very useful for something like water purification where you would want a constant suppression of bacterial growth.

Although not really a composite Shirwaiker et al. [37] have made an interesting design consisting of interdigitated areas of silver and an isolating polymer which could be used for water purification purposes. This design applies a constant voltage, but will only have a current running once a bacterium short-circuits a silver anode and cathode, killing the bacteria in the process. A schematic of the principle can be seen in Figure 1.1.

Besides the many antimicrobial applications of silver nanocomposites other applications can also be found.

A nanocomposite consisting of epoxy and silver nanoparticles can yield a dielectrics with high dielectric constants above 100 at low frequencies [38], some have even managed to get dielectric constants above 1000 even at high frequencies [39]. High dielectric constants are very interesting for making for instance super capacitors.

Conductive silver nanocomposites can be used for methanol sensing [40], oxygen reduction by nanocomposite silver-ion exchanger [41], plasmonic coupling [42] or as a catalyst in reduction of for instance Rhodamine 6G [43].

It should therefore be clear that silver nanoparticles and composites are intensely studied, but also very interesting. Functional silver nanocomposites are also the main goal within this Ph.D. because it can be used within such a large range of applications. These

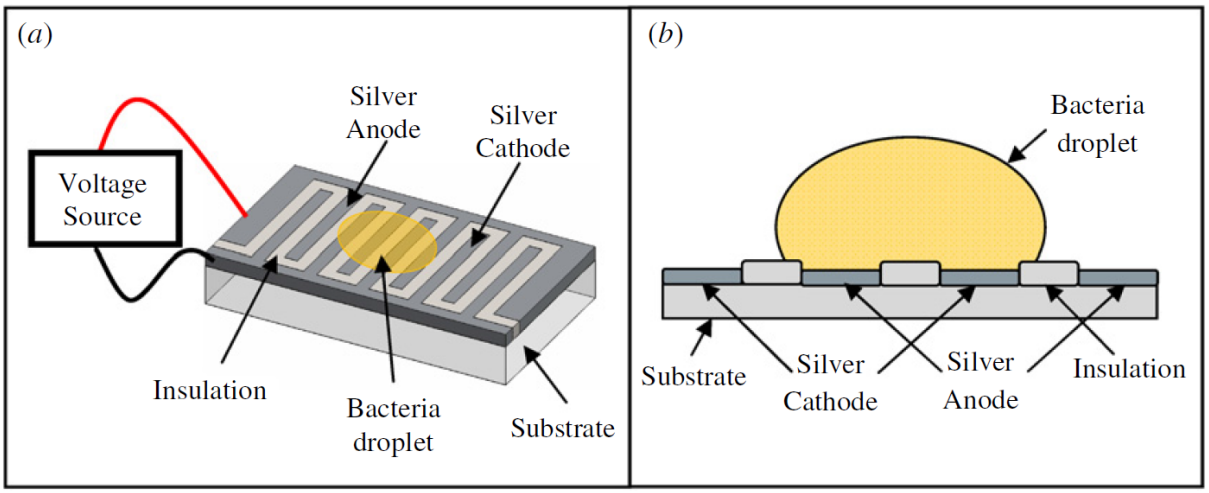

Figure 1.1 – *(a) three-dimensional view of silver electrode. (b) Cross-sectional view of electrically activated silver-polymer electrode [37].*

applications can utilise the antibiotic effect [44, 31], the optical and plasmonic properties [45, 46] or the electrical conductivity [47]. For both the gold and silver nanocomposites a requirement is that they can be easily structured, which requires the polymer matrix to be a photoresist.

1.8 SU-8

The final use of the composite is very important while choosing the polymer, as different applications requires different properties. At the same time the possibilities of manipulation during fabrication also needs to be considered as the total process is very different depending on the chosen material. As this thesis is about new materials for micro- and nanofabrication, the processing capabilities have been the main focus while choosing the polymer. As UV lithography is the main method for structuring within MEMS technology the chosen polymer has to be a photoresist.

SU-8 was chosen as the initial photoresist as it is one which has gathered a lot of knowledge through the years at DTU Nanotech and DTU Danchip where the cleanroom work has been performed. SU-8 is an epoxy based photoresist and was invented by IBM in the late 80'ies. It is an interesting polymer as it has properties making it useful for many different applications. Being a photoresist it can be structured using standard UV lithographic processes, but unlike many other photoresists it is epoxy-based and hence much more durable once hardened and can therefore be used as a free standing structure in itself [48]. It is at the same time transparent in the visible wavelength range [49] making it suitable for optical components and it is also a biocompatible material meaning that it can be used for biological applications [50].

SU-8 is based on the EPON^{TM} SU-8 epoxy resin which has the structure sketched in

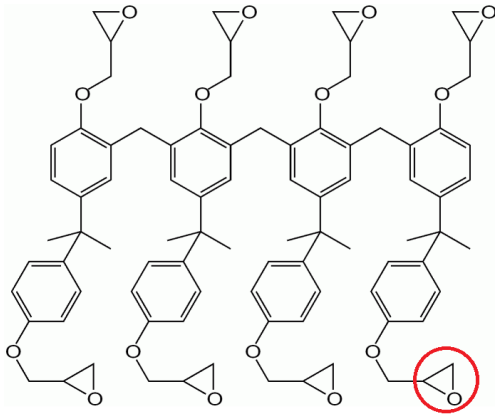

Figure 1.2 – *A schematic of the SU-8 epoxy resin. One of the eight epoxy groups has been marked.*

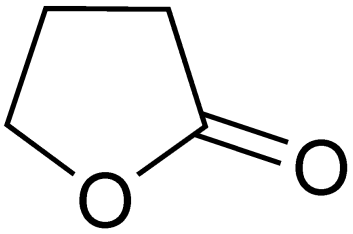

Figure 1.3 – *The chemical structure of γ-butyrolactone used as solvent in the original formulations of SU-8.*

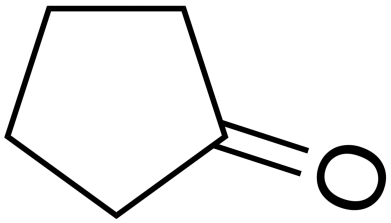

Figure 1.4 – *The chemical structure of cyclopentanone used as solvent in the SU-8 2000 series which is preferred due to higher process throughput.*

Figure 1.2.

SU-8 can be obtained containing two different solvents; γ-butyrolactone or cyclopentanone, where the one in cyclopentanone is generally recommended due to its improved capabilities regarding; drying and coating quality compared to the one in γ-butyrolactone [51]. One of the main differences between these two solvents, which are relevant for this project, is that γ-butyrolactone is miscible with ethanol while cyclopentanone is not. None of the two solvents are miscible with water although very small amounts can be dissolved in γ-butyrolactone.

The structure of γ-butyrolactone and cyclopentanone can be seen in Figure 1.3 and Figure 1.4 respectively.

The SU-8 also contains small amounts, 1-5 %, of a mixture between triarylsulfonium- and hexaflourantimonate salts. The salts act as a photo initiator creating a Lewis acid when exposed to UV-light. The Lewis acid then initiates the cross-linking of the epoxy.

As will be mentioned in section 1.9, SU-8 has previously been used in combination with silver nanoparticles to make conductive photoresists, but with several difficulties. One of

Table 1.1 – *The ingredients of SU-8 vary between formulation and within batches of the same formulations, but should lie within the boundaries given in this table.*

Chemical	SU-8	SU-8 2000
EPON^{TM} SU-8 epoxy resin	35–75 %	3–75 %
γ-butyrolactone	22–60 %	-
Cyclopentanone	-	15–96 %
Propylene carbonate	1–5 %	0.1–5 %
Triarylsulfonium salt	1.9–3.0 %[1]	0.25–2.5 %
Hexafluorantimonate salt	1.9–3.0 %[1]	0.05–2.5 %

the goals will therefore be to make a very simple process with both acceptable resolution and adhesion to the surface while being able to spin coat the resist.

SU-8 is a complex material consisting of several ingredients. The ingredients for the SU-8 2000 series are as follows.

- The precursor for the EPON^{TM} SU-8 epoxy resin: 2-(chloromethyl)oxirane; formaldehyde; 4-[1-(4-hydroxyphenyl)-1-methyl-ethyl]phenol (CAS: 28906-96-9)
- Cyclopentanone (CAS: 120-92-3)
- Propylene carbonate (CAS: 108-32-7)
- Bis[4-(diphenylsulfonio)phenyl]sulfide bis(hexafluoroantimonate) (CAS: 89452-37-9)
- Diphenyl(4-(phenylthio)phenyl)sulfonium hexafluoroantimonate (CAS: 71449-78-0)

The first complex chemical is the epoxy resin precursor, while the cyclopentanone is the solvent. The two salts are used for initiating the cross linking as they form Lewis acids when exposed to UV light. The last ingredient, propylene carbonate, is the solvent for the salts.

The original formulations of SU-8 contains the same ingredients, but instead of cyclopentanone the solvent is instead γ-butyrolactone.

The amount of each chemical changes between the different formulations of SU-8. Table 1.1 gives the boundaries between which the chemicals are varying. Small variations are also found between batches of what should be identical formulations of SU-8. The different SU-8 formulations also results in different viscosities and densities. The properties of the most commonly used SU-8's and the variation in solid content is given in Table 1.2. The table shows some of the formulations of SU-8 available. SU-8 2 and SU-8 2002 have been highlighted as these are the two formulations used in this project. The common final designation of 2 should make them comparable, but there are differences besides the main solvent. Both formulations contain a low, but not identical, epoxy amount. The low epoxy

[1] Only the combined total amount of the Triarylsulfonium and Hexafluorantimonate salts are given.

Table 1.2 – *Table of properties for the SU-8 series and SU-8 2000 series resists gathered from several sources [51, 52, 53, 54]. The two highlighted formulations are those used in this project.*

SU-8	% solids	Viscosity [cSt]	Density [g/ml]
2	**39.5**	**45**	**1.123**
5	50–55	290	1.164
10	60–65	1050	1.187
25	60–65	2500	1.200
2000.5	10–15	2.49	1.070
2002	**25–30**	**7.5**	**1.123**
2005	45–50	45	1.164
2007	50–55	140	1.175
2010	55–60	380	1.187
2015	60–65	1250	1.200

amount formulations are chosen for the possibility to achieve higher particle loadings in the final composite. The formulations have identical densities, but vary in viscosity which is an important parameter during spin coating.

The stated solid content approximately corresponds to the amount of epoxy resin in the SU-8. For the used SU-8 2002 resist the goal was, as stated by the manufacturer, 29 % epoxy resin, but ended up being 29.7 % as shown in the certificate of analysis given in appendix A.

As should be clear the SU-8 is a complex chemical and the processing of it even more complex. SU-8 has also been the subject of thorough studies, which means that more information about SU-8 and how to process it can be found [55, 56].

1.9 SU-8 Composites

SU-8 has been used by others in their attempts to make nanocomposites with varying functionalities. The use of metallic nanoparticles have been used for making conductive composites [57, 58, 59], but with some difficulties. They used pre-synthesised nanoparticles which are mixed with SU-8, but had problems with spin coating as nanoparticles in a liquid significantly change the rheological properties of the mixture [60, 61]. As spin coating was impossible, a scraper was used for deposition instead, which puts a limit on how thin the resist film can be made. At the same time adhesion problems between the polymer and the substrate also forced Jiguet et al. [62] to do backside exposure where the UV light is shined through the wafer in comparison to standard lithography where the light is shined directly on the photoresist. This backside exposure also limits the substrates which can be used as it should be transparent at the used wavelength. This means that silicon which is by far the most used substrate within MEMS technology cannot be used in this case. Fused

Figure 1.5 – *A sketch of the problems with UV exposure through the backside of a substrate. Although adhesion to the surface is ensured the absorption and shadowing effect of the nanoparticles will result in a surface with a very high surface roughness after development. The blue part symbolises a fused quartz wafer, the grey spots nanoparticles and the yellow part cross-linked polymer. The nanoparticles results in an uneven removal of the polymer.*

silica can be used as an alternative, but this significantly reduces the possible applications.

The problem with adhesion between substrate and photoresist is actually due to a lack of polymerisation during the UV exposure. A lack of polymerisation of the lower layers results in the complete removal of the photoresist during development. If the photoresist in direct contact with the supporting surface is not cross-linked it will be removed during the development, resulting in the detachment of also the cross-linked polymer. The lack of polymerisation comes from absorption and shadowing by the nanoparticles which prevents the lower layers of the polymer to be cross-linked.

The lack of lower layer polymerisation is the reason for using backside exposure as they thereby ensure that the polymer at the substrate surface is cross-linked. This does not only limit the number of usable substrates, but also results in a surface roughness of the final nanocomposite. This is due to uncross-linked areas on top of the nanocomposite which will now be removed. The problem of missing cross-linking has just been moved from the bottom to the top. The principle of the rough surface due to photoresist above the nanoparticles being removed is sketched in Figure 1.5.

For SU-8 composites containing gold or silver nanoparticles, those containing silver nanoparticles are the most studied. More SU-8 nanocomposites can, however, be found involving other materials. These includes barium titanate embedded capacitors [63], low stress SU-8 with silica particles [64], titanium oxide composites for acoustic matching in lab-on-chip systems [65], or general improvement of the tribological behaviour [66].

These are just some of the applications in which SU-8 has been used, many more including thermal conductivity can be found [67].

1.10 Work Outline

The conducted work in this project features several tracks which have been pursued. These tracks will be explained here to give a better overview of the total work involved which can otherwise seem quite comprehensive. The total work flow is schematically presented in Figure 1.6.

Figure 1.6 – *A schematic representation of the work flow followed during this project. Several experiments can have been done within each major area. The smiley at the end of each branch indicates the ultimate success of the protocol achieved during this project.*

The overall goal is to make SU-8 composites for use in micro- and nanofabrication. The focus is metal nanocomposites, where gold and silver are the preferred materials for nanoparticles. Experiments have therefore been done in parallel with one part focusing on gold and one part focusing on silver.

The first branch of both gold and silver is what is called the *ex situ* route. This means that nanoparticles are synthesised following standard protocols and later mixed with SU-8. One protocol has been used for gold nanoparticles while two protocols for silver nanoparticle synthesis have been explored.

In the *ex situ* branch the first of both gold and silver is called post grafting, which means that the after synthesis the nanoparticles are coated with a polymer to increase the colloid stability and enhance transferring between solvents. Post grafting has been tried with two different polymers poly(vinyl pyrrolidone/vinyl acetate) (PVP/VA) and poly(vinyl alcohol-co-vinyl acetate) containing carboxylic groups (PVA-COOH). PVA-COOH turns out to not be compatible with SU-8 resulting in a dead end. PVP/VA can in some extent be used for making a SU-8 gold composite, but cannot be used for a SU-8 silver composite.

Stepping back to *ex situ* a second branch called pre grafting was followed. Pre grafting means that the stabilising polymer (PVP/VA) is present during the synthesis of the nanoparticles. This branch results in a functional SU-8 gold nanocomposite, but did not give any reproducible results regarding a SU-8 silver nanocomposite.

Stepping back to gold and silver in the work flow a second branch called *in situ* has been explored. *In situ* means that the nanoparticles are not pre synthesised, but that the metal precursor is instead mixed directly with SU-8 and the nanoparticles then formed later inside the polymer matrix. The *in situ* method does work to some extent for the gold nanocomposite. For the *in situ* silver nanocomposite further branching is done.

Two different formulations of SU-8 have been tried for the *in situ* silver nanocomposite, namely SU-8 2002 and SU-8 2. The SU-8 2 protocol was found to result in a functional nanocomposite, while the SU-8 2002 protocol branches out further.

For the SU-8 2002 silver nanocomposite two different co-solvents have been tested namely DMSO and acetonitrile. The DMSO branch has not led to any good results, while the acetonitrile branch resulted in a functional SU-8 silver nanocomposite.

In total nine different routes have been explored resulting in four not preferred routes of which one is a dead end. Three routes resulted in functional nanocomposites, namely one gold nanocomposite and two working silver nanocomposites. For the remaining two routes nanocomposites have been obtained, but not of sufficiently high quality.

The work has been performed both in a DTU Nanotech lab as well as inside the DTU Danchip cleanroom.

1.11 Sum-Up

This chapter has given a very brief introduction to the subject of this Ph.D. as well as explaining nanocomposites, nanoparticles, the principles of green chemistry and micro- and nanofabrication. An overview some gold and silver composites were given followed by

composites involving SU-8. Silver nanoparticles are the most interesting and a glimpse of their countless uses has been supplied.

This thesis will describe the making of new materials useful for some of the mentioned applications. Description on nanoparticle synthesis and nanocomposite fabrication will be given as well as the encountered challenges. The problems described in section 1.9 which have limited the use of silver SU-8 nanocomposites so far will be solved during the remainder of this work.

An outline of the total work performed was also given.

1.12 Thesis Outline

The first part of this thesis will describe how to synthesise nanoparticles and the characterisation of these.

Gold nanoparticles are explained in chapter 2 and silver nanoparticles in chapter 3. Afterwards the process of stabilising the nanoparticles and transferring them into organic solvents are explained in chapter 4.

The second part of this thesis focusses on the nanocomposites. Chapter 5 describes how the synthesised nanoparticles can be used to make a *ex situ* nanocomposites before a new developed *in situ* processes for nanocomposite fabrication are described in chapter 6.

Chapter 7 describes the process optimisation done at DTU Danchip. UV lithography is thoroughly explained and the challenges encountered towards a functional protocol documented.

Chapter 8 briefly describes the work done on conductive composites and compares these to commercially available composites.

In the end everything is summarised and concluded on in chapter 9 before chapter 10 provides suggestions on things which have to be done to move forward with the nanocomposites.

appendix B explains materials and methods for all nanoparticle synthesis and polymer stabilisation, while appendix C contains the obtained process flow to be used within the DTU Danchip cleanroom.

Part I

Nanoparticles

Chapter 2

Gold Nanoparticles

Gold nanoparticles can easily be synthesised and are stable for long periods of time. These factors make gold nanoparticles an excellent choice to use as a model system before moving on to silver or other more complex nanoparticles.

The Turkevich method for synthesizing spherical gold nanoparticles was established in 1951 by Turkevich et al. [68] and has since then been used intensively for the synthesis of gold nanoparticles. Synthesis does however often follow one of the modified versions as for instance the one by Frens [69].

The basics are that a dilute aqueous solution of chloroauric acid at boiling temperature is reduced by citrate ions. The solution becomes supersaturated with sub-nanometre neutral gold atoms. The small nanoparticles will act as nucleation sites for other gold atoms and will start to grow in size. In order for the nanoparticles not to start aggregating, a stabilising agent will also have to be present. In the Turkevich method the stabilising agent is citrate ions which are electrostatic attracted to the surface of the particles.

The size of the nanoparticles can within some boundaries be controlled by the amount of reducing-/stabilising agent. Higher concentrations of sodium citrate will result in smaller particles. This is due to the stabilising process being the limiting factor, such that high concentration of citrate ions allow this process to happen faster compared to the reduction.

2.1 Synthesis

A slightly modified version of the gold nanoparticle synthesis method has been used during this project. The result is extremely stable nanoparticles with very little deviation in the average particle diameter between batches.

$HAuCl_4 \cdot 3H_2O$ $\geq$99,9 % and $Na_3C_6H_5O_7 \cdot 2H_2O$ $\geq$99 % was bought from Sigma Aldrich. Milli-Q water with a resistivity of 18.2 MΩ cm was used for all solutions.

The procedure is as follows:

1. 45 ml of 0.2 % weight to volume $HAuCl_4$ is added to a 500 ml round bottomed flask.
2. 155 ml of Milli-Q water is added to the flask to dilute the solution.

3. The flask is fitted with a reflux condenser and the solution heated to reflux with vigorous stirring.
4. 5 ml of preheated 5 % weight to volume sodium citrate is added to the boiling solution of $HAuCl_4$.
5. The colour changes from colourless through black to wine red in a couple of minutes.
6. The solution is left with stirring and heating for at least 15 min before being cooled to room temperature.

If complete reduction is assumed the theoretical concentration of gold is 0.22 mg/ml. If contaminants are avoided the particles will be stable almost indefinitely, no sign of agglomerations can be seen at least three years after synthesis.

2.2 Particle Characterisation

The synthesised particles are characterised such that the exact size is known and the assumed spherical shape confirmed. This is done with plasmonic absorption measurements using a UV-Vis spectrophotometer, and by looking at the particles in a transmission electron microscope (TEM).

2.2.1 Particle Diameter

For gold nanoparticles the diameter of the particles can be estimated from the plasmonic absorbance peak by the formula [70]:

$$D = \Sigma_{n=0}^{3} A_n (\lambda_{max} - 500)^n, \tag{2.1}$$

where λ_{max} is the wavelength of the maximum absorption, and A_n is a summation coefficient. The values of A_n are $A_0 = 12.558$, $A_1 = -2.593$, $A_2 = 0.1921$ and $A_3 = -0.00253$. A typical value for λ_{max} could be 524 nm which according to the formula means that the nanoparticles are 26 nm in diameter.

This equation for estimating the particle diameter is, however, limited to a certain range and can only be expected to give somewhat reasonable results for a λ_{max} between 518 nm and 536 nm. This corresponds to a particle diameter between 13 nm and 50 nm.

2.2.2 Absorption Measurements

The plasmonic absorption of the synthesised particles is measured using a Shimadzu UV-2600 spectrophotometer. The absorption measurements can then be used to estimate the diameter using equation 2.1 and to see variations between each synthesis.

Measurements are made and displayed from 350 nm to 650 nm as this is the interesting area. At lower wavelengths there is a very large absorption by the used cuvettes and at higher wavelengths the measurements tend towards zero.

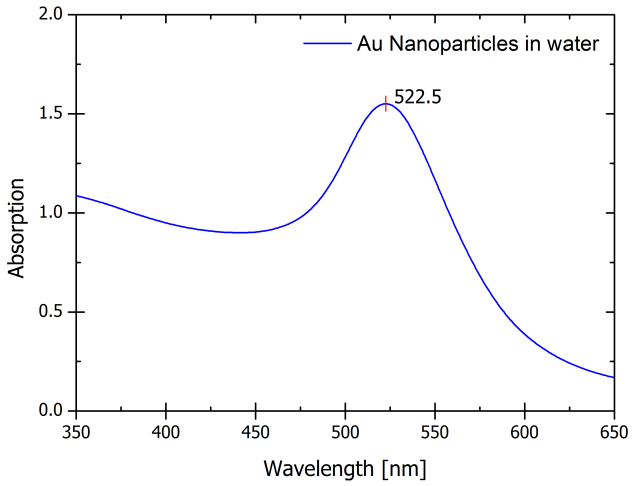

Figure 2.1 – *A typical absorption spectrum of gold nanoparticles synthesized by a modified Turkevich method. The absorption at 522.5* nm *indicates an average particle diameter around* 22-23 nm.

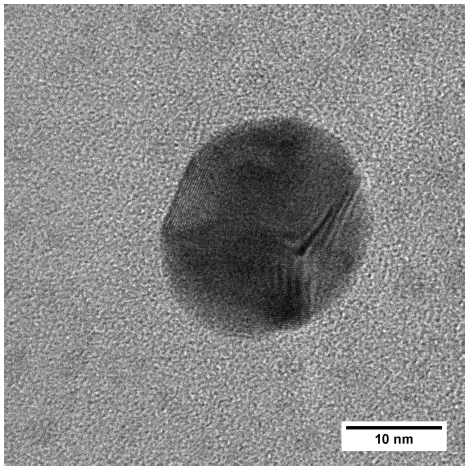

Figure 2.2 – *TEM image of a gold nanoparticle synthesized using the modified Turkevich method. The diameter of the particle is around 23* nm *and the particle is seen to be spherical.*

A typical absorption measurement for gold nanoparticles is shown in Figure 2.1.

The displayed absorption spectrum of a gold nanoparticle batch shows a very distinct absorption peak at 522.5 nm. Other batches show values ranging from 518 nm to 523 nm, but with a clear majority of absorption maxima at around 522 nm, which is equivalent to a particle diameter of 21.5 nm according to equation 2.1.

To confirm the estimated diameter as well as the shape of the particles a Technai T20 G^2 TEM was used to analyse the particles. Figure 2.2 shows the image of a single particle.

The measured diameter of 23 nm from the TEM image agrees very well with the expected diameter from the absorption measurement in Figure 2.1 confirming the validity of equation 2.1. The difference in size is well within the uncertainty as the measurement interval for the absorption measurements is 0.5 nm. At the same time the high resolution TEM image also shows that the particle is spherical as expected, and the crystal planes are even seen.

With the gold nanoparticles working as expected it is time to move on with silver nanoparticles.

Chapter 3

Silver Nanoparticles

Silver nanoparticles should also be easy to synthesise with good stability. Many different methods for synthesising silver are being used in contrary to gold where the Turkevich method is by far the most used. Two different methods have been tested in this project to find the best one regarding nanoparticle concentration, nanoparticle size and size distribution.

3.1 Synthesis – Sodium Borohydride

A well-established method for making stable silver nanoparticles has been well described by Mulfinger et al. [71], but can at least be traced back to Creighton et al. [72]. A similar method has also been used by Lee and Meisel [73].

The process involves using ice cold sodium borohydride as reductant for silver nitrate. The silver nitrate is added drop wise under vigorously stirring to ensure a complete and homogeneous reaction.

The reaction can be described as follows [71].

$$AgNO_3 + NaBH_4 \rightarrow Ag + \frac{1}{2}H_2 + \frac{1}{2}B_2H_6 + NaNO_3 \tag{3.1}$$

This process generates particles of around 12 nm in diameter. The particles are stabilised by borohydride ions as shown in Figure 3.1. This method is a good way to create stable silver nanoparticles with small standard deviations from the average diameter. The individual concentrations of the reagents must however be precisely controlled as a change in concentration ratio between sodium borohydride and silver nitrate will result in unstable particles. Using room temperature sodium borohydride or adding the silver nitrate too fast will also affect the reaction.

It is also important that the stirring is stopped after the addition of all the silver nitrate. Continuously stirring will result in further particle growth or agglomeration [49].

$AgNO_3$ $\geq$99.0 % and $NaBH_4$ $\geq$98.0 % was bought from Sigma Aldrich. All solutions was prepared using milli-Q water with a resistivity of 18.2 MΩ cm.

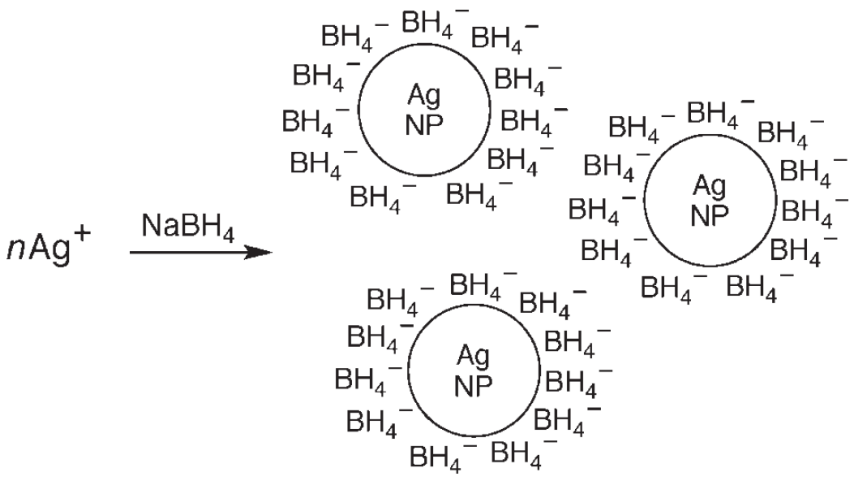

Figure 3.1 – *Image showing how silver nanoparticles are formed and stabilised by borohydride ions [71].*

The exact procedure followed in this work was:

1. 30 ml of 2.0 mM $NaBH_4$ in water is chilled in an ice bath.
2. 10 ml of 1.0 mM $AgNO_3$ in water is added drop wise at roughly one drop pr. second, under vigorously stirring.
3. The addition takes around 3 min after which the stirring is stopped.

If complete reduction is assumed the concentration of silver nanoparticles will be 27 μg/ml or roughly a factor of ten less than for gold.

An excess of sodium borohydride compared to silver nitrate is needed as it is both used as a reducing agent as well as a stabilising agent. When using a 1.0 mM $AgNO_3$ solution the initial concentration of sodium borohydride must be twice that of silver nitrate or a product breakdown will occur within half an hour [71].

3.1.1 Particle Characterisation

As with the gold nanoparticles these silver nanoparticles are examined using the spectrophotometer and the TEM. No formula has been derived which can estimate the particle diameter from the absorption maximum, but some ranges can be found from for instance Kamat et al. [74]. An absorption spectrum for a batch of these silver nanoparticles can be seen in Figure 3.2.

The absorption spectrum is similar to what could be expected by looking in the literature [72, 73] and according to Mulfinger et al. [71] the particle size should lie between 10 nm and 14 nm. To confirm this TEM images like the one shown in Figure 3.3 was taken to find the size.

The found particle diameters agree well with the expected values although particles above and below the mentioned size can be found. The size distribution between the silver

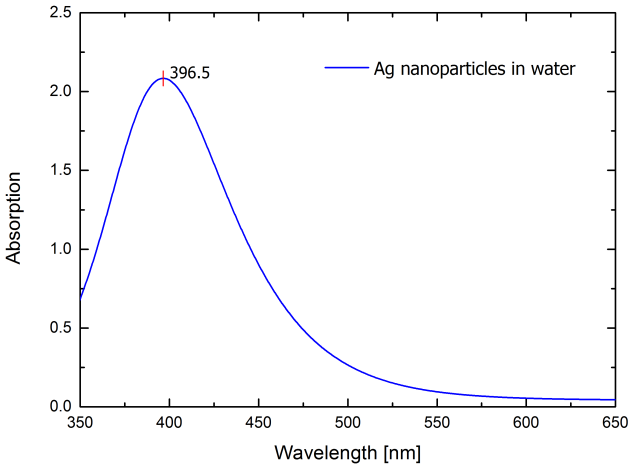

Figure 3.2 – *A typical absorption spectrum of silver nanoparticles synthesized following the approach of Mulfinger et al. [71]. The absorption max at 396.5* nm *agrees well with literature.*

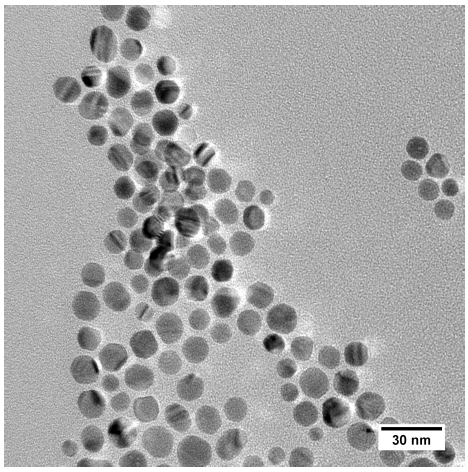

Figure 3.3 – *TEM image of silver nanoparticles synthesized following the approach of Mulfinger et al. [71]. The diameter of the particles varies between 7* nm *and 15* nm *with the majority lying between 11* nm *and 14* nm.

nanoparticles is larger than what was found for the gold nanoparticles, and the variations between syntheses are also larger. Absorption maxima for silver nanoparticles synthesised using this method have varied between 394 nm and 413 nm.

The particles are very stable as no sign of agglomeration or sedimentation can be seen after three years storage in plastic centrifuge tubes.

3.2 Synthesis – Giuffrida Method

A different method of producing stable silver nanoparticles is to use argon saturated water and silver acetylacetonate (Ag(acac)) according to Giuffrida et al. [75]. This process results in silver nanoparticles without any specific surface coating for stabilisation. The particles are dependent on a high zeta potential to keep the particles from agglomerating.

The reaction scheme is assumed to be as shown in Figure 3.4. This method is extremely suitable when considering green chemistry as no reducers or stabilisers are used and the only solvent necessary is water. The disadvantage with this synthesis method is, however, that the result will be larger particles with a very broad size distribution.

It is also expected that the lack of an initial stabiliser will result in less stable particles should they be exposed to further stimulants.

$C_5H_7AgO_2$ 98 % was bought from Sigma Aldrich.

The exact procedure is:

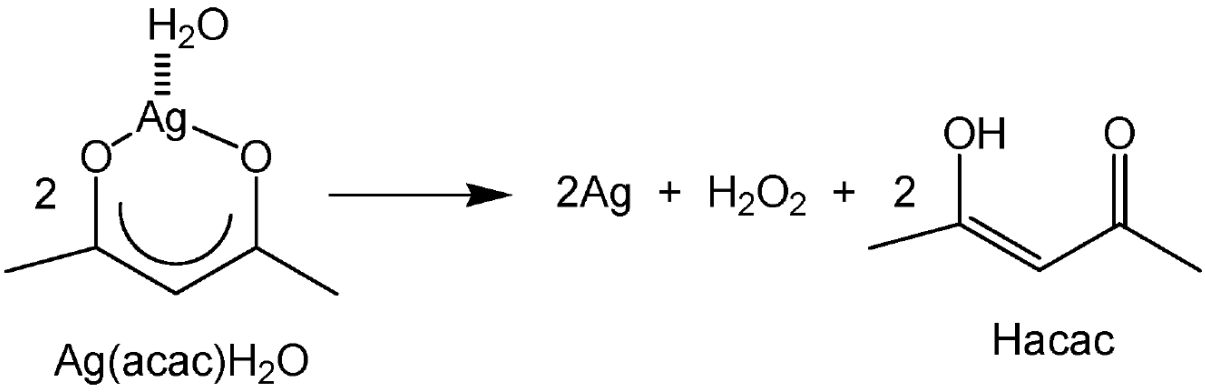

Figure 3.4 – *The probable reaction between Ag(acac) and argon saturated water. Silver, hydrogen peroxide and Hacac are the products [75].*

1. 200 ml of Milli-Q water is saturated with Argon in a gas washing bottle.
2. 10 mg of Ag(acac) is added to the water and dissolved using a magnetic stirrer.
3. Stirring is stopped and the mixture is left to react for a couple of hours at room temperature.

With this method the theoretical maximum concentration of silver is 26 μg/ml which is almost the same as for the sodium borohydride reduction.

3.2.1 Particle Characterisation

As before the particles are investigated using both UV-Vis spectroscopy and TEM. The absorption spectrum for a single batch of particles can be seen in Figure 3.5.

The larger wavelength for the absorption maximum indicates larger particles and from Kamat et al. [74] the particle size could be expected to be as large as 35-50 nm. This peak is also wider than the one from Figure 3.2 indicating a larger size distribution. The particles are investigated using TEM to find the exact size and get an idea about the size distribution. A representable image for nanoparticles synthesised using this method can be seen in Figure 3.6.

The TEM image shows that particles around 25 nm are found, which is also the average particle size reported by Giuffrida et al. [75]. At the same time many small particles down to 3 nm can easily be seen, showing that there is a wide size distribution.

Considering that the nanoparticle concentration is basically the same with the two methods, and that the size distribution is much smaller following the approach of Mulfinger et al. the Giuffrida method is not preferred, but both are tested for coating and stability. The advantages of the Giuffrida method is the scalability of the process as more can be produced without altering the process.

These particles are also very stable as no sign of agglomeration or sedimentation can be seen after three years storage in plastic centrifuge tubes.

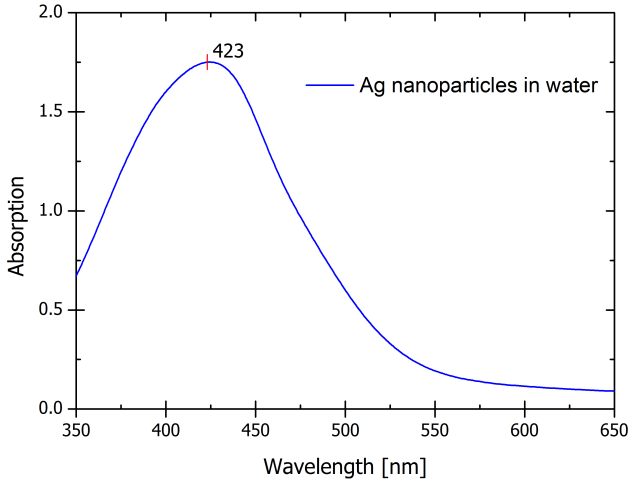

Figure 3.5 – *A typical absorption spectrum of silver nanoparticles synthesised using the Giuffrida method. The absorption maximum at 423* nm *is around the expected value*

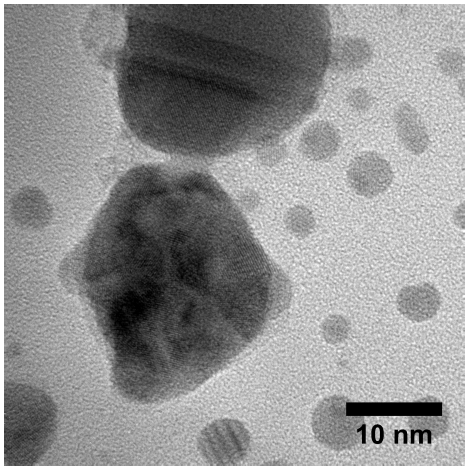

Figure 3.6 – *TEM image of silver nanoparticles synthesised using the Giuffrida method. Two large particles of around 25* nm *can be seen, but also many small ones of less than 10* nm *in diameter.*

3.3 Nanoparticle Sum-Up

As described in chapter 2 gold nanoparticles stabilised by citrate ions have been synthesised. This chapter has then explained the synthesis of silver nanoparticles stabilised by borohydride ions as well as a synthesis where the silver nanoparticles are stabilised by a high zeta potential. All methods are functional and with long time stability of at least three years.

The Giuffrida method does however result in a larger size distribution which is not an advantage as this result in a wider absorption peak.

The colloidal suspensions of both gold and silver nanoparticles will be designated with the term sol from physical chemistry. This is done for easy distinguishing between colloidal suspensions and other solution.

The synthesised nanoparticle sols are either stabilised by inorganic ligands, high zeta potentials or a combination of both. To be transferred into SU-8 and maintain a homogeneous particle distribution additional coating with organic ligands need to be applied. This creates stable core-shell particles which can form stable colloid suspensions in organic solvents compatible with SU-8. All this will be explained in the next chapter.

Chapter 4

Particle Coating, Solvent Exchange and Colloidal Stability

The nanoparticles have been synthesised and are very stable in water as found in the previous chapters. They do however need to be transferred from water into SU-8 before a nanocomposite can be made.

The primary choice has been made to transfer the particles into cyclopentanone the solvent of SU-8 2002, but other solvents compatible with SU-8 can be used as well. To accommodate the transfer the nanoparticles are first coated with a polymer as this both increases colloidal stability, but also ease the transfer due to clever selection of the polymer. Organic biocompatible polymers were chosen to ensure stable suspensions of the nanoparticles in organic solvents while keeping the toxicity low at the same time.

4.1 Coating of Nanoparticles

By exchanging the inorganic stabilizing agents with organic polymers it should be possible to transfer the nanoparticles into almost any solvent. The polymers should be compatible with both water and organic solvents, while maintaining an affinity towards the nanoparticles.

Diblock copolymers with a hydrophilic and a hydrophobic block should accommodate this demand, and diblock copolymers are often used as stabilisers for nanoparticles [76]. Many methods have utilized some form of thiol functionalized organics as these readily attach to gold surfaces [77]. As described in section 1.4 the goal is however to follow the principles of green chemistry and us chemicals with as little toxicity as possible. No thiol functionalized polymers will therefore be used.

Instead polyvinylpyrrolidone (PVP) will be used as the basic polymer, as PVP is a well-known stabiliser for gold nanoparticles. In a former project regarding gold nanoparticles [78] the block co-polymer PVP/VA was chosen as the stabilising polymer. This polymer was chosen because of the mentioned stabilising effect of PVP, while polyvinyl acetate

(PVA) ensures that the transfer into organic solvents can be accommodated. PVP/VA is biological friendly and an approved substance for cosmetic products.

A second polymer, PVA-COOH, has also been used for these experiments as the polymer in another project in the group has shown to be a good stabiliser for zero valent nano iron.

While the initial stabilising ions ensure electrostatic repulsion adsorption of polymers on the surface results in a more stable steric stability instead. Another big advantage of stabilising the nanoparticles by using polymers is the possibility of functionalization such that the nanoparticles can be used in an even larger variety of applications. The diversity of applications can be seen by looking at the thematic series from Ritter [79].

Two different methods for coating the particles have been applied in this project. The first method is called post grafting where the synthesised nanoparticles from chapter 2 and chapter 3 after synthesis are coated with the polymer. The second method is called pre grafting and involves the polymer being present during synthesis, which will change the protocols.

Post grafting will be described first.

4.1.1 Post Grafting

In post grafting the polymer is added to the nanoparticle sol after synthesis and then the entire mixture is shaken to ensure complete polymer coverage. The post grafting is used due to zero influence from the polymer during synthesis. The downside is the risk of incomplete covering due to bad ligand exchange or insufficient shaking.

Gold Nanoparticles

Gold nanoparticles synthesised as described in section 2.1 are used for the post grafting method.

Luviskol® VA 64 (PVP/VA) was kindly gifted from BASF and Poval (PVA-COOH) acquired from Kuraray.

First stock solutions are made by dissolving the polymers in water. For PVP/VA the stock solutions contains 100 mg/ml while the PVA-COOH stock solution contains 10 mg/ml.

The process for coating the nanoparticles with PVP/VA was the following.

1. 350 μl of 100 mg/ml of PVP/VA in water is added to 10 ml of gold nanoparticle sol.
2. The nanoparticle sol and polymer mixture is placed on a shaker and shaken for several hours, preferably overnight.

This amount of added polymer results in a polymer to particle weight ratio of 16:1. The long shaking should ensure complete coverage of all the nanoparticles.

For PVA-COOH the process is slightly different due to the concentration of the stock solution being lower. To have the same polymer to particle ratio the procedure was as follows.

1. 3.5 ml of 10 mg/ml of PVA-COOH in water is added to 10 ml of gold nanoparticle sol.
2. The nanoparticle sol and polymer mixture is placed on a shaker and shaken for several hours, preferably overnight.

As the concentration of the polymer in the stock solution is not identical more water is added in the latter case diluting the sol. This should not be of any concern as equal nanoparticle concentrations should be obtainable after the solvent exchange.

It was later found during the transfer of the particles into cyclopentanone that PVA-COOH forms a gel when in contact with cyclopentanone. This means that PVA-COOH is not compatible with SU-8 and leads to a dead end. For silver nanoparticles the only polymer tested was therefore PVP/VA.

Silver Nanoparticles

Two different synthesis methods of silver, those from section 3.1 and section 3.2, where used for the post grafting procedure. It is known that PVP easily reduces silver due to the lone pair electrons of PVP [80]. This should in principle be a good thing as the polymer will then ensure that the silver does not oxidise. It is, however, unknown whether this affects the stability of the nanoparticles negatively of positively. Remaining by-products from the synthesis have not been removed and these could also influence the coating.

A series of experiments is therefore conducted in which the amount of polymer is changed. For all experiments a stock solution containing 100 mg/ml of PVP/VA in water is used. The general process used is as follows.

1. An amount of 100 mg/ml of PVP/VA in water is added to 1 ml of silver nanoparticle sol.
2. The nanoparticle sol and polymer mixture is placed on a shaker and shaken for several hours, preferably overnight.

The amount of polymer solution added to the nanoparticle sol varies from 5 μl to 1000 μl. Between 50 μl added polymer solution and up to the final added amount of 1000 μl, the difference between samples is 50 μl added polymer solution. Below a total added amount of 50 μl polymer solution, the difference between samples is 5 μl added polymer solution.

After being shaken the nanoparticles are left for the next day ($\sim$20 h) and visually inspected. Due to the colour of the nanoparticles any significant change should be easily seen. The result is summarised in Table 4.1.

As seen from the table the nanoparticles synthesised following the Mulfinger procedure is stable as long as the added amount of polymer does not increase above 200 μl while the Giuffrida particles are only stable until 45 μl added polymer solution. An increase above these values first results in a colour difference from yellow to orange, which appears to be stable agglomerates, while further addition results in large agglomerates and precipitation.

Table 4.1 – *Table showing the effect on colloidal stability when adding varying amounts of* 100 mg/ml *PVP/VA solution in water to* 1 ml *of two different silver nanoparticle sols. The added polymer solution amount varies with 50 µl except below 50 µl added polymer solution as the variation between samples are only 5 µl in this case. The samples are visually inspected one day after coating.*

Added polymer [µl]	Mulfinger procedure	Giuffrida method
0-45	Stable	Stable
50-200	Stable	Colour difference observed
250-300	Colour difference observed	Unstable
300-1000	Unstable	Unstable

Storage for several weeks did not result in any change. The conclusion is that an increase in polymer amount results in an increased instability.

It must also be noted that since the concentration of the polymer solution is kept constant, adding more polymer increases the amount of water, thereby diluting the sol.

From this post grafting experiment the nanoparticles synthesised using the Mulfinger procedure appears to be the best alternative of the two synthesis methods. As commented earlier the Mulfinger procedure also results in a smaller size distribution compared to the Giuffrida method, which was also preferred. The conclusion following this experiment is therefore to not do any additional work with the particles synthesised using the Giuffrida method.

If the amount of added polymer solution is chosen to be 10 µl the polymer to particle weight ratio will be 37:1. This weight ratio is more than double as high as obtained for the gold nanoparticles, which should also be considered.

4.1.2 Pre Grafting

A different approach in which the stabilising polymer is present during the synthesis has also been explored. The idea is that this guaranties complete coverage of all particles and thereby increased stability. This process is called pre grafting.

As the PVA-COOH polymer has already been discarded the only polymer used will be PVP/VA. The synthesis process will, however, be different as the polymer effects the formation of nanoparticles.

Coated Gold Nanoparticles

The pre grafting process for gold nanoparticles is based on the Turkevich method from section 2.1 trying to change as little as possible. The final procedure used is as follows.

1. 15 ml of 0.2 % (w/v) $HAuCl_4$, 15 ml of 10 mg/ml PVP/VA in milli-Q water and 5 ml of milli-Q water is heated to reflux in a 250 ml round bottomed flask.

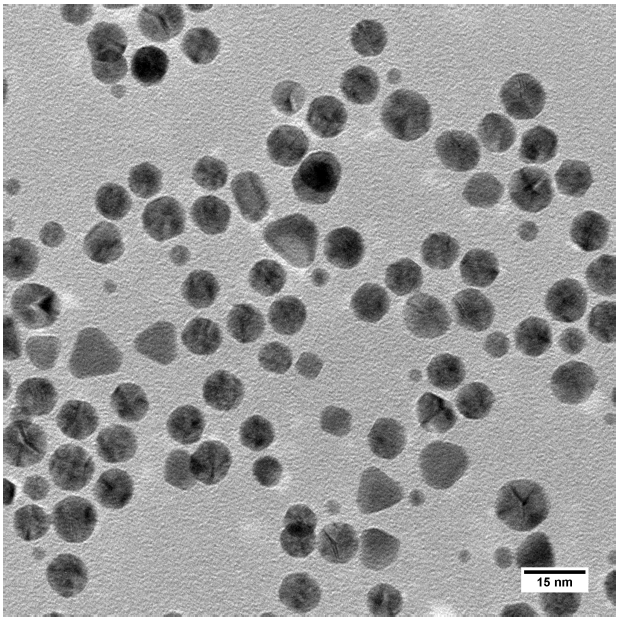

Figure 4.1 – *TEM image of pre grafted nanoparticles. It can be seen that some particles are more triangular in shape than spherical. The polymer to particle weight ratio for this sample is 1:1.*

2. 5 ml of preheated 3 % weight to volume sodium citrate is added to the solution.
3. After achieving wine red colour the solution is left with stirring and heating for at least 15 min before being cooled to room temperature.

The result is very stable gold nanoparticles in a concentration of 0.375 mg/ml if complete reduction is assumed. The polymer to gold ratio is 10:1. No agglomeration of nanoparticles has been observed after two years of storage.

Some changes, compared to the standard synthesis, have however been observed using the pre grafting technique. By introducing the polymer during synthesis the process complexity increases which can result in nanoparticles of different shapes than spherical. The amount of polymer present during synthesis has an influence although not thoroughly investigated. Figure 4.1 shows a TEM image of some pre grafted nanoparticles where the polymer to particle weight ratio is 1:1.

The image shows that although most particles are still spherical and around the same size, some particles do instead appear to be more triangular in shape.

As written a higher concentration of gold nanoparticles has been achieved with the pre grafting technique, and the polymer to particle weight ratio has been reduced compared to post grafting as well. This point towards pre grafting being preferable to post grafting. The polymer does however affect the synthesis resulting in some particles with a triangular shape instead of spherical.

Coated Silver Nanoparticles

A pre grafting method has also been developed for silver nanoparticles. The process is developed by a bachelor student in the group under co-supervision.

All the syntheses so far have been done in water to keep the toxicity low. This process is however done ethanol instead. Ethanol is not considered a toxic (unless you drink too much) so the principles of green chemistry are still followed.

The basis for this procedure has been the one described by Mulfinger where all water has been exchanged with absolute ethanol and then trying to introduce as few changes as possible. The exact developed procedure for producing pre grafted silver nanoparticles is as follows.

1. 1 g of PVP/VA and 0.1 g of $AgNO_3$ is dissolved in 50 ml of absolute ethanol.
2. 0.02 g of sodium borohydride together with 0.2 g of PVP/VA is dissolved in 10 ml of absolute ethanol.
3. The sodium borohydride solution is under vigorously stirring added drop wise at the rate of one drop per second to the $AgNO_3$ solution.
4. A colour change from clear over yellow to a more yellow-brownish colour should be observed.
5. 30 s after complete addition of the sodium borohydride solution the stirring is stopped.

By following this procedure the nanoparticle concentration will be 1.06 mg/ml if complete reduction is assumed. This concentration is around 40 times larger than the other two methods for synthesising silver. The polymer to particle weight ratio is 19:1. This ratio is almost half of what was chosen for the post grafting.

4.1.3 Grafting Sum-Up

Some interesting results were found during the experiments with post grafting and pre grafting. The main conclusions from the post grafting were:

- Post grafting works well for gold nanoparticles.
- Post grafting can affect the colloidal stability of silver nanoparticles.

For pre grafting two new methods for synthesising the nanoparticles while coating them at the same time was developed. The main finding of the pre grafting was:

- Higher concentrations of nanoparticles can initially be obtained with pre grafting than with post grafting.
- Pre grafting appears to be functional for both gold and silver nanoparticles.

In general the concentration of the nanoparticle sols is higher using the pre grafting method than the post grafting method. This should not have much influence on the choice of grafting method as the concentration is expected to be increased when removing the water. It was found that high amounts of polymer can influence the colloidal stability of the post grafted silver nanoparticles. As it is unknown if this is caused by the very high amount of polymer to particle weight ratio no direct conclusion can be drawn from this.

All in all the pre grafting appears to be preferable, but no clear conclusion can be drawn. Both types of grafted particles are therefore tested for transfer into organic solvents.

4.2 Solvent Exchange

To transfer the nanoparticles from the water or ethanol in which they are synthesised and into the SU-8, a solvent exchange has to be performed. Cyclopentanone, the main solvent of SU-8 2002 is not miscible with either water or ethanol. Most photoresists are indeed dissolved in organic solvents which mean that a solvent exchange will always have to be done for nanoparticles synthesised in water.

There are several methods which can be used for a solvent exchange; some being as simple as shaking a two phase system causing the nanoparticles to migrate due to higher affinity for one of the solvents. As this simple approach is not possible with the nanoparticles in this project, different solvent exchange methods have been investigated. The three main tracks investigated are centrifugation, freeze-drying and evaporation done either in a rotary evaporator or a desiccator. These solvent exchange methods all have the common characteristic of removing water before adding or suspending in organic solvent.

The three tested methods will be described in the following.

4.2.1 Centrifugation

Centrifugation is a well-known technique used for concentrating nanoparticles, and it has also been used in a previous project [78].

In centrifugation, rotation at very high speed results in sedimentation of the nanoparticles, leaving a water supernatant which can then be removed. Unfortunately the very low mass of nanoparticles means that extremely high speed of up to 100,000 g is needed [81].

The relative centrifugal force (RCF) expressed in units of gravity can be calculated from the revolutions per minute (RPM) using the formula [82]:

$$RCF = (1.118 \times 10^{-5}) r S^2, \tag{4.1}$$

where r is the radius of rotation in centimetres and S is the speed of the centrifuge. Sometimes a centrifuge will only have the possibility to input RPM, which should then be recalculated to RCF to ensure that identical conditions can be achieved on different equipment.

Centrifugation results in a layer with high concentration of nanoparticles in the bottom of the centrifuge tubes and a supernatant with very few or none nanoparticles. This top

layer can then be removed. The remaining water in the nanoparticle containing layer can afterwards be removed in a desiccator.

A disadvantage of centrifugation is that the small particle size can result in high process time in order to sediment all the nanoparticles. The amount of liquid which can be processed is also limited by the size of the centrifuge.

Optimisation of nanoparticle centrifugation is in principle very simple because of the distinct colour difference seen when there are nanoparticles in the liquid. To optimise the procedure these simple rules have to be followed: After an initial centrifugation with estimated values of time and speed the result is investigated. If the supernatant is still coloured, the time or speed has to be increased. If the nanoparticles are deposited on the side of the centrifugation tube, the speed has to be decreased. After the optimal speed has been found the time can be optimised by reducing the time until the supernatant starts to be coloured again.

As mentioned, previously nanoparticle synthesis in the research group has used centrifugation for solvent exchange, but as the synthesis and coating protocols are not identical the old method cannot be expected to work without further modifications.

Centrifugation was tested on gold nanoparticles using a *Thermo Scientific SL16R* centrifuge and the following procedure.

1. The synthesised nanoparticles are transferred to an even number of 45 ml centrifuge tubes.
2. Each centrifuge tube is paired with another tube and weighed such that the weight difference between the tubes in a pair is at maximum 0.1 g.
3. The centrifuge tubes are placed in an ultra-centrifuge such that the two tubes from a pair are placed opposite each other.
4. The centrifuge is set at 18,000 g for 4 h.
5. The supernatant is removed and nanoparticles dried in a desiccator.

Centrifugation was done before discovering the incompatibility of PVA-COOH and SU-8, so the procedure has been tried with both PVP/VA and PVA-COOH coated particles. It was found that the process can be used for the PVP/VA coated particles, but that the PVA-COOH coated particles could not be sedimented.

After centrifugation the nanoparticles were dried in a desiccator. The resulting pellets could be resuspended in water, but it was found that the pellets could not be suspended in organic solvents rendering centrifugation inapplicable.

4.2.2 Freeze-Drying

The second solvent exchange method tested was freeze-drying, in which the water is removed by sublimation. At first a shell freezing is used where the liquid is frozen on the inside of a rotating round bottom flask. Liquid nitrogen, dry ice sublimation or any other method for rapid freezing can be used. This results in a large surface area which reduces the necessary process time. The freezing is also important to avoid bumping when the pressure is later reduced.

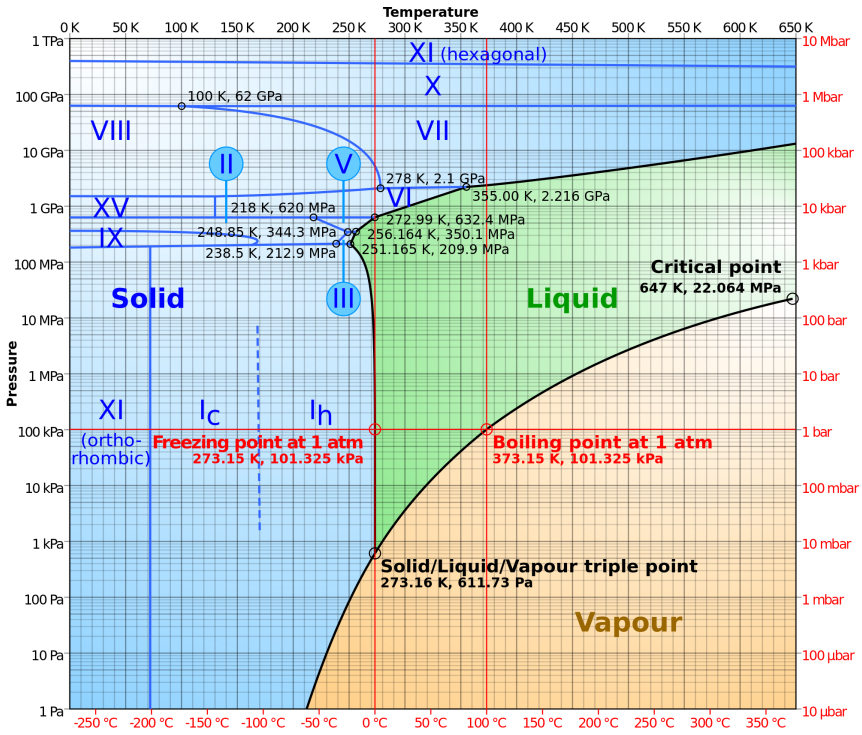

Figure 4.2 – *The phase diagram of water [83] showing which temperatures and pressures can be used for sublimation. The freeze-dryer should be set at a pressure below the triple point such that water can only exist as a vapour or solid.*

After freezing the flask with the nanoparticles is transferred to a freeze-dryer and the temperature and pressure adjusted according to the phase diagram of water, Figure 4.2.

After the water vapour leaves the flask due to the reduced pressure, it is condensed on the cold condenser plates. It can from the phase diagram be seen that a pressure of 2 mbar is suitable for frozen water at 0°C to accommodate sublimation. Condenser coils at -20°C water will then result in a desublimation as ice on the coils.

The processing time for freeze-drying can be long, several days, depending on the sample size. It is, however, and advantage that large volumes can be processed simultaneously, and that samples can be added or removed at any point without interfering with the remaining samples.

A *Christ Alpha 1-2 LDplus* freeze-dryer and the following procedure were used for freeze-drying.

1. A round bottomed flask containing the nanoparticles is connected to a rotary evaporator.
2. The flask is rotated at maximum speed while being partly dipped in a bath of liquid nitrogen or dry ice and ethanol.
3. After complete freezing of the nanoparticle sol the flask is transferred to a freeze dryer.

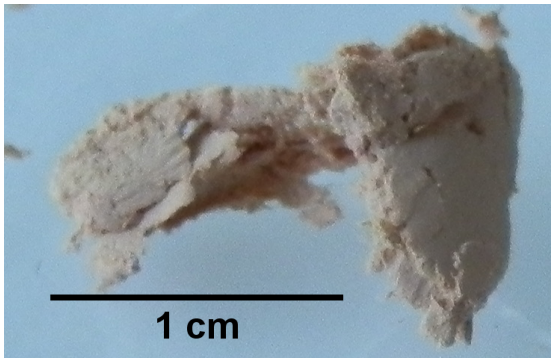

Figure 4.3 – *A lump of silver-polymer powder which has been obtained through freeze-drying. The powder is very voluminous and can be dissolved in many different solvents.*

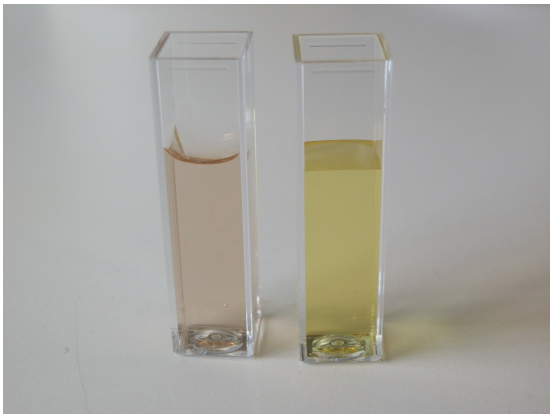

Figure 4.4 – *After dissolving the freeze-dried powder in water it can be compared with the original suspension. The cuvette on the left contains the freeze dried silver and the one on the right the original suspension. A distinct colour difference can be seen as well as a difference in surface tension.*

4. The flask is wrapped in aluminium foil and left on the freeze-dryer until the flask reaches room temperature.

The used procedure has in general been found to work for post grafted gold nanoparticles resulting in voluminous powder which can be suspended in water or a long range of organic solvents. On some occasions freeze-drying has resulted in changes of the post grafted gold nanoparticles. It was found that freeze-drying was never suitable for silver nanoparticles of this project as major changes were observed each time.

During the rapid freezing of the silver nanoparticle sol a change in colour can be observed which indicates agglomeration of the particles. After freeze-drying a powder as shown in Figure 4.3 is obtained. This powder is then dissolved in water to compare with the original silver nanoparticle sol. Figure 4.4 shows a cuvette containing freeze-dried resuspended silver nanoparticles and a cuvette containing the original sol.

It can from the colour of the liquids be seen that something has changed. At the same time it can also be observed that the surface tension is different between the two samples. The absorption of both sols is found to further quantify the difference. The result can be seen in Figure 4.5.

The absorption spectra clearly shows that although there is still a peak at the same wavelength as before freezing, a big shoulder has appeared at higher wavelengths for the freeze-dried powder. The peak broadening and colour change supports the idea that particle agglomeration has happened during the initial freezing step.

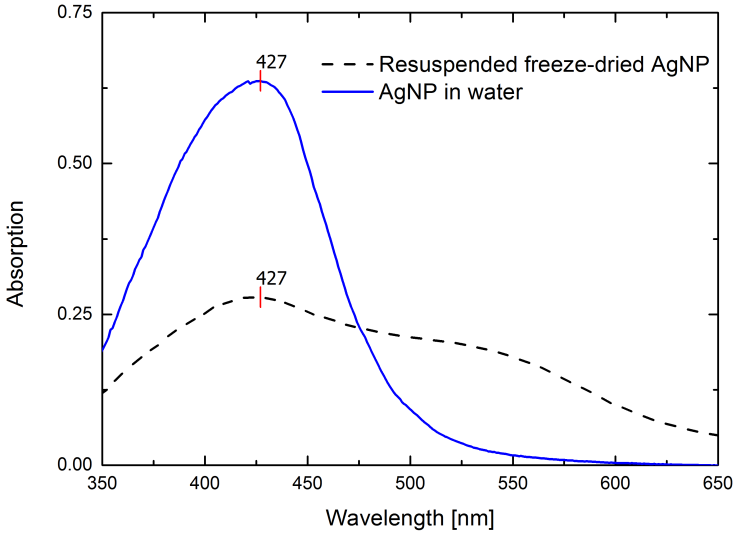

Figure 4.5 – *Absorption spectra of two silver nanoparticle sols. The original untreated sol has a well-defined peak, while the resuspended freeze-dried particles have a much wider peak. The absorption maximum for both sols are at the same wavelength, but the wide peak and shoulder of the freeze-died particles indicates some large particles or agglomerates.*

The problem is assumed to be phase separation during freezing as this is not an unknown problem within freezing [84]. A well-known method for avoiding phase separation is to use a cryoprotectant. PVP is an example of a well-known and used cryoprotectant [84]. As PVP is also one of the polymer blocks for the used polymer coating the problem could perhaps be avoided by adding more polymers. It was however shown in Table 4.1 that large amounts of polymer destabilises the silver nanoparticles.

Freeze-drying was first later revisited with the pre grafted gold nanoparticles. All samples with pre grafted freeze-dried gold nanoparticles have resulted nanoparticle powders which can be suspended in organic solvents or SU-8.

The conclusion for freeze-drying is therefore that it appears to be useful for pre grafted gold nanoparticles, but not for any silver nanoparticles.

4.2.3 Rotary Evaporation

The third method for solvent exchange tested was rotary evaporation, or evaporation under reduced pressure. In a rotary evaporator the pressure is reduced such that evaporation can happen without excessive heating. The flask containing the liquid is rotated in a bath with heated water. The rotation ensures a large surface which is good for evaporation and also counters bumping of the liquid. The vapour is after evaporation condensed on condenser coils and collected in a separate flask.

A rule of thumb for rotary evaporation is that the condenser coils should have a temperature of 0°C, the pressure should be reduced such that the liquid boils at 20°C and

the heating bath set at a temperature of 40°C. This is called a 0/20/40 setting. If the cooling water is not that cold a 20/40/60 setting can be used as well. The pressure should be reduced to approximately 20 mbar according to Figure 4.2 in order for the boiling temperature of water to be 20°C.

Rotary evaporation can also be optimised past these values. In an optimised evaporation process, condensation can be seen on 3/4 or 4/5 of the condenser coils. This can either be achieved by reducing the pressure or increasing the temperature of the water bath.

A couple of different methods can be applied when using rotary evaporation. The process can be continued until complete drying, or it can be stopped at low volumes and then remaining drying done in a desiccator. Another method is to gradually exchange the solvent during evaporation to avoid complete drying of the nanoparticle suspension.

Complete drying in the flask is not recommended as the result will be a thin film covering most of the inside of the flask. This film can be tricky to remove or dissolve in small amounts of liquid. Using a desiccator for the final drying is therefore preferred. This means that the procedure followed for rotary evaporation was as follows.

1. The round bottomed flask containing the nanoparticles are transferred to the rotary evaporator.
2. The cooling water is connected and turned on and the water bath set at 60°C.
3. The flask is rotated and the pressure lowered to 20 mbar. Be wary of bumping which could result in loss of sample.
4. The rotating flask is lowered into the water bath such that it is barely touching. Be wary once more about bumping and remove the flask from the water should it occur.
5. Leave the flask rotating in the water bath until most of the water has been removed.
6. Remove the flask from the rotary evaporator and dry the nanoparticles in a desiccator.

As mentioned either a 0/20/40 or 20/40/60 setting can be used, most likely depending on the temperature of the cooling water. The 20/40/60 setting has been used in this project, but there has clearly been room for further optimisation as the condenser coils have not been any way near 3/4 covered by condensation. Without optimisation the time to reduce 50 ml to around 2 ml is roughly 30 min.

After the final drying in a desiccator the same problem as with centrifugation was encountered. The nanoparticle pellets can be dissolved in water, but are hard to dissolve in other solvents. Different salts to control the humidity in the desiccator have been tried, but this did not solve the problem.

As complete drying appears to be a problem an approach with co-evaporation of solvents was tried instead. In this approach the target solvent is gradually added during evaporation to avoid reaching a dried state.

When applying this method the used solvents must be carefully considered. The target solvent must preferably have a higher boiling point than the original as the low boiling solvent will then most easily be removed.

Both post and pre grafted gold nanoparticles according to section 4.1.1 and section 4.1.2 have been tested, while only the pre grafted silver nanoparticles from section 4.1.2 were included. The procedure is a bit different for gold and silver nanoparticles.

The procedure for gold nanoparticles is as follows.

1. 10 ml of gold nanoparticle sol is attached to the rotary evaporator and 2 ml water evaporated.
2. 1 ml of cyclopentanone is added to the sol.
3. The process is repeated five times.

As cyclopentanone and water is not miscible two phases are observed when adding the cyclopentanone. As the water is evaporated the nanoparticles will transfer to the cyclopentanone. It can easily be seen when all water has been removed as there will then be only one phase.

The procedure for transferring silver nanoparticles are as follows.

1. 10 ml of the nanoparticle sol is attached to the rotary evaporator and 1 ml of ethanol evaporated.
2. 1 ml of cyclopentanone is added to the sol.
3. 3 ml of ethanol is evaporated and 1 ml of cyclopentanone added.
4. The remaining 6 ml of ethanol is evaporated and 1 ml cyclopentanone added.

Once the nanoparticles have been transferred to cyclopentanone there should be no problem mixed with SU-8 2002.

Solvent Exchange Sum-up

After testing these three different methods for solvent exchange some conclusions on the feasibility can be made.

For centrifugation only gold nanoparticles where tested and the following observations have been made.

- PVA-COOH coated particles cannot be used for centrifugation.
- Centrifuged and dried PVP/VA coated particles can in most cases be resuspended in water.
- Centrifuged and dried PVP/VA coated particles **cannot** be suspended in organic solvents.

Both gold and silver nanoparticles were tested for use with freeze-drying. The following observations were made,

- Freeze-drying can work for gold nanoparticles and the obtained powder can be suspended in many solvents.
- Freezing of silver nanoparticles causes phase separation and thereby agglomeration of particles.

For the final method of rotary evaporation two different approaches was tested and the observations were as follows.

- Complete drying of particles cannot be used as the resulting pellets can only sometimes be dissolved in water and never in organic solvents.
- Gradual transfer from water to cyclopentanone can be done with both post grafted and pre grafted gold nanoparticles.
- Gradual transfer from ethanol to cyclopentanone can be done for pre grafted silver nanoparticles.

The final conclusions with regard to the solvent exchange are therefore that rotary evaporation should be used. The nanoparticles should however never be dried completely as they can then only be resuspended in water. A gradual transfer into cyclopentanone has proven successful for post and pre grafted gold nanoparticles as well as pre grafted silver nanoparticles.

Freeze-drying was originally discarded as it cannot be used for silver nanoparticles because freezing causes agglomeration. Agglomeration during freezing has been observed with post grafted gold, but unagglomerated nanoparticle powders have also been obtained. Later experiments with pre grafted gold indicate that freeze-drying is well suited for these particles as no agglomeration during freezing has been observed.

4.3 Suspendability and Colloidal Stability

The range of solvents in which the obtained gold nanoparticle powder can be suspended was investigated. The experiment was done using good freeze-dried samples of post grafted gold particles with PVP/VA and PVA-COOH coatings. The procedure for the experiment was as follows.

1. Gold nanoparticles were synthesised according to section 2.1.
2. 40 ml of the gold nanoparticle sol is mixed with 1.4 ml of 100 mg/ml PVP/VA in a 45 ml centrifuge tube and placed on a nutating mixer overnight.
3. The mixture is poured into a 250 ml round bottomed flask and rotated in liquid nitrogen using a *Rotavapor® R-210* from *Buchi*.
4. After complete freezing of the liquid the flask is transferred to a *Christ Alpha 1-2 LDplus* freeze dryer and wrapped in aluminium foil.
5. The flask is left on the freeze dryer until it reaches room temperature and a powder can be observed.
6. 30 mg of the powder is weighted off and placed in a 4 ml vial.
7. 1 ml of solvent is added and the vial shaken by hand.
8. Suspendability and stability are evaluated by visual inspection.

Table 4.2 – *Suspendability and stability data for gold nanoparticles coated with PVP/VA and PVA-COOH. The nanoparticles have been freeze-dried and then suspended in various solvents.*

Solvent	PVP/VA	PVA-COOH
9:1 toluene and cyclopentanone	Stable	-
Acetone	**Unstable**	Stable
Acetonitrile	Stable	Stable
Cyclopentanone	Stable	**Not suspendable**
Dichloromethane	Stable	Stable
DMF	Stable	Stable
DMSO	Stable	Stable
Ethanol	Stable	Stable
Hexane	Stable	Stable
Isopropanol	Stable	Stable
NMP	Stable	-
THF	Stable	Stable
Toluene	**Not suspendable**	-
Water	Stable	Stable

The process for PVA-COOH coated particles is similar. Silver nanoparticles have not been included in this experiment due to phase separation and agglomeration during freezing.

The previous work on gold nanoparticles dried using centrifugation and a desiccator done in the group showed that gold nanoparticles are stable in several solvents [78]. The same solvents are tested once more and some additional ones added. The stability was checked by visual inspection immediately after mixing. If no colour change was observed, after mixing, between the suspended particles and a reference in water, the particles were deemed stable. This was then confirmed by a second inspection several days later where no further colour change should be visible. The results are summarised in Table 4.2.

As seen from the table the coated gold nanoparticles are stable in a wide range of solvents. The tests have been done with both types of polymer coatings. The results show that the particles coated with PVA-COOH are not suspendable in cyclopentanone. This is due to a jellification of the polymer. This experiment eliminates the possibility of using PVA-COOH as a coating polymer due to lack of compatibility with cyclopentanone/SU-8 2002.

Part II

Nanocomposites

Chapter 5

Ex Situ Composites

In this Ph.D. project, *ex situ* nanocomposites are composite materials made by incorporating synthesised nanoparticles into the photoresist matrix after the needed surface modifications. The previous chapter explained how super stable PVP/VA stabilised nanoparticles were successfully transferred into the SU-8 compatible solvent cyclopentanone. Successful modification of the nanoparticles has made it possible to achieve *ex situ* composites with homogeneously distributed nanoparticles without any agglomeration in the photoresists matrix.

Very little work has been reported in the case of nanocomposites using SU-8 and gold nanoparticles. Toor et al. [85] reports a SU-8 gold nanocomposite in which they have used dodecanethiol coated nanoparticles which are dispersed in chloroform. This method clearly lacks the principles of green chemistry. The reported nanocomposite has also not been structured which is a key element in this work. The goal of their composite was to increase the dielectric constant of the material using small nanoparticles. They used nanoparticles with a diameter of 5.68 nm and achieved a generally good homogeneity, but with some clusters of 25 nm.

Chiamori et al. [86] reports a SU-8 gold nanocomposite in which the gold nanoparticles were suspended in benzene before mixing them with SU-8. This method does not follow the principle of green chemistry as well. Their goal was to achieve reduced residual stress as well as electrical conductivity, where the latter was not achieved. They used 5 nm large nanoparticles, but does not report anything about homogeneity.

Jiang et al. [87] reports of a microwave device made with gold nanoparticle doped SU-8. The used nanoparticles have an average diameter of 2 nm which means that they are too small to display any surface plasmonic response. They do not report anything about homogeneity or structuring of the nanocomposite.

Some *ex situ* nanocomposites with silver have also been reported, but these have already been explained in section 1.9.

In the following sections, *ex situ* gold and silver nanocomposites are described. The effect of the two coating mechanisms described in chapter 4 is compared in terms of colloidal stability and distribution of particles within the polymer matrix.

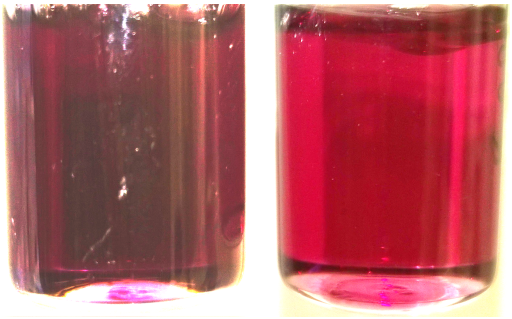

Figure 5.1 – *Picture of* 1 ml *of nanoparticles suspended in cyclopentanone mixed with* 2 ml *of SU-8 2002. The left shows post grafted nanoparticles while the right shows pre grafted particles. It is seen that the post grafted nanoparticles are purple indicating particle agglomeration while the pre grafted nanoparticles maintain the characteristic red colour.*

5.1 Gold Composite

1 ml of the PVP/VA coated nanoparticles suspended in cyclopentanone obtained according to subsection 4.2.3 is mixed with 2 ml of SU-2002 and given a gentle shake to ensure complete mixing. A difference in colour can be seen between the post grafted and the pre grafted particles as shown in Figure 5.1.

The nanoparticle stability in SU-8 is evaluated by looking at the colour of the sols. The picture shows that the post grafted and the pre grafted nanoparticles does not have the same colour after being mixed with SU-8. The purple colour of the post grafted particles indicates partially agglomeration of the nanoparticles. As no further agglomeration is observed over time, both sols are considered stable. The two sols are further investigated by looking at the plasmonic absorption spectrum as seen in Figure 5.2.

It is clear from the absorption measurements that the pre grafted gold nanoparticles are more stable in SU-8 than the post grafted particles. The shoulder on the spectrum for the post grafted particles show that partial agglomeration has happened.

Differences between batches of post grafted particles can be observed as some mixtures have resulted in blue sols including large particles visible by naked eye. Some of these batches are also not long term stable in SU-8. For the pre grafted nanoparticles the SU-8 sol was found to be stable for at least one year. In some batches particles showed a tendency of sedimentation. Shaking of the sedimented mixtures resulted in complete redispersion of the nanoparticles without any visible colour change, indicating good stability due to the PVP/VA coating.

The mixtures with both post grafted and pre grafted nanoparticles are spun on 50 mm silicon wafers. After heating the wafer with the post grafted nanoparticles are broken in two such that the cross section can be investigated. The cross section was investigated with a scanning electron microscope (SEM), and the result can be seen in Figure 5.3.

The marked regions can be investigated further by looking closer at each of them as done in Figure 5.4.

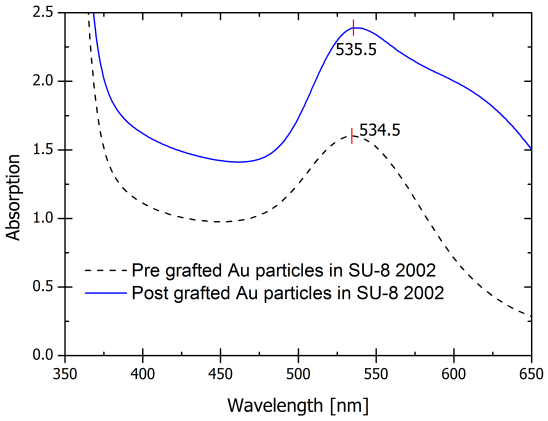

Figure 5.2 – *Absorption spectra of pre and post grafted gold nanoparticles suspended in SU-8 2002. The sols have almost identical wavelengths for the absorption maximum, but the post grafted particles also have a larger shoulder due to partial agglomeration.*

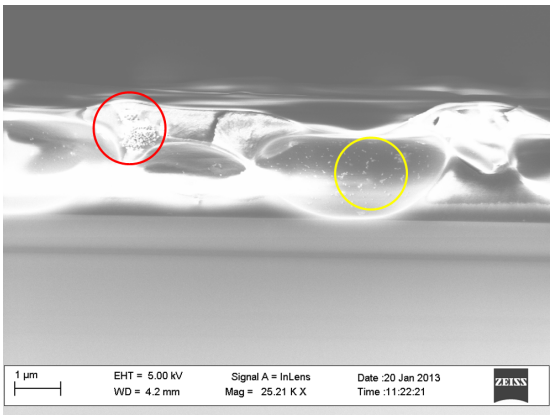

Figure 5.3 – *SEM image of the cross section of an ex situ gold nanocomposite with post grafted nanoparticles. The image is representative for the nanocomposite and two different regions have been marked to show how the composite is divided into different domains.*

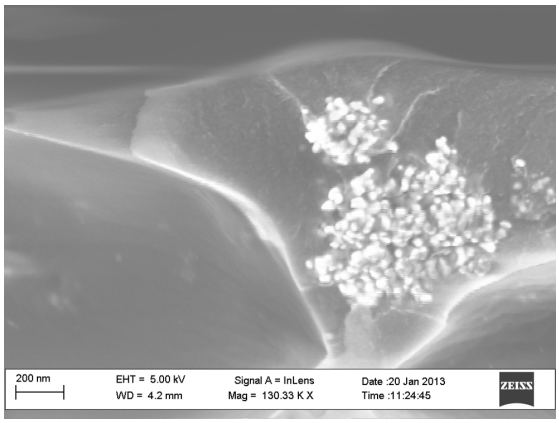

(a) *SEM image of the area marked with a red circle in Figure 5.3. One large agglomerate of gold nanoparticles makes up most of this domain.*

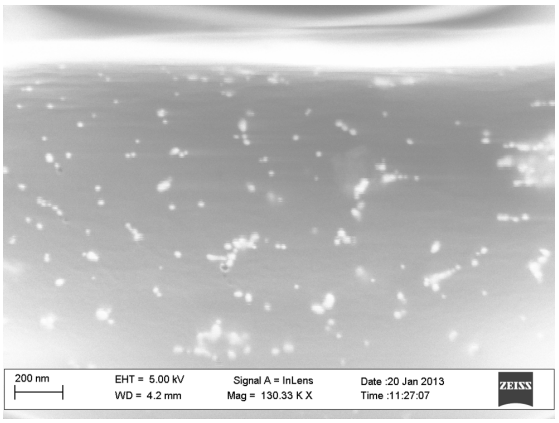

(b) *SEM image of the area marked with a yellow circle in Figure 5.3. Individual nanoparticles are randomly distributed across the domain.*

Figure 5.4 – *SEM image of the two domains marked in Figure 5.3. One domain consists of large gold nanoparticle agglomerates while the other contains individual nanoparticles. In both cases the nanoparticles have a size of around 25* nm.

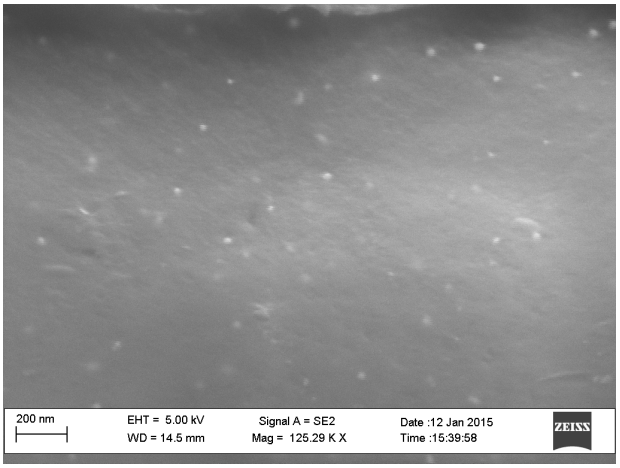

Figure 5.5 – *SEM image of an ex situ gold composite cross section made with pre grafted nanoparticles in SU-8. The nanoparticles can be hard to see, but appears to be homogeneously distributed.*

The investigation of the nanocomposite clearly shows that two distinct regions is found within the composite; one where large agglomerates are dominant, and one with individual nanoparticles. This tells us that although we have agglomerates, which is also the reason for the purple colour of the sol and the shoulder observed in the absorption spectrum, individual nanoparticles can still be found within the composite.

The wafer with the pre grafted particles is also investigated with SEM and this is shown in Figure 5.5.

The pre grafted nanoparticles have not formed agglomerates in the SU-8, but are homogeneously dispersed within the polymer.

The pre grafted nanoparticles are much better than the post grafted with regards to homogeneous distribution of the particles within the polymer. No further work has therefore been done on post grafted gold nanoparticles and the following results will only be of pre grafted particles.

5.1.1 Plasmonic Absorption and Structuring

If the nanocomposites are to be used in optical sensors the plasmonic absorption has to be distinct in the nanocomposite. As the nanoparticles have been engineered to have an absorption peak at a specific wavelength, the wavelength of the absorption peak in the composite should be in the near vicinity. If the peak has a similar shape and an absorption value close to that of the nanoparticles, then no growth or agglomeration of particles have happened.

Measurements are made on nanocomposites spun onto fused silica wafers. These measurements are then compared with measurement of the nanoparticles in SU-8. A Shimadzu UV-2600 UV-Vis spectrophotometer has been used to measure the plasmonic absorption with air as the reference.

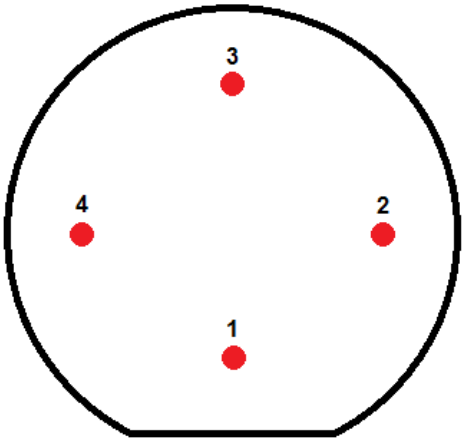

Figure 5.6 – *Sketch of the approximate position of the four measurement points on wafer using the Shimadzu spectrophotometer. Each measurement point is the same distance from the edge, meaning that the measurement point around the flat is closer to the center of the wafer. The wafer is rotated 90 degrees between each point.*

Each wafer is measured in four different points to see if there are any variations across the wafer. The angle between each measurement point is approximately 90 degrees, and all except one are at the same distance from the center of the wafer. An approximate position of the measurement points on the wafer can be seen in Figure 5.6.

These measurement points are consistent throughout all measurements made on nanocomposites on fused silica wafers for the entire project. Unless otherwise mentioned no difference has been found between the measurement points.

Two composites with pre grafted *ex situ* nanoparticles are compared to nanoparticles from the same batch suspended in SU-8 2002, to see if there is change in the plasmonic absorption. The result is shown in Figure 5.7.

The absorption spectra show that there is effectively no shift in absorption maximum between the composites and the nanoparticles suspended in SU-8 2002. It is seen that absorption is higher for higher amounts of gold as expected. The y-value of the nanoparticles cannot be directly compared with the nanocomposites as the values have been normalised to fit with the values of the nanocomposites.

Ex situ composites are structured in the cleanroom using an *EVG620* double side mask aligner following the procedure described in chapter 7. The result can be seen in Figure 5.8.

The microscope image shows that a resolution of around 5 μm can be achieved with the *ex situ* composite and the used fabrication methods.

In conclusion, the *ex situ* gold composite achieved by using pre grafted gold nanoparticles gave the best results with regards to homogeneous distribution of particles within the polymer without agglomeration and hence retention of the plasmonic properties. It has been shown that it is possible to structure the composite, and the achieved resolution of 5 μm is acceptable for micro- and nanofabrication. *Ex situ* gold composites are hence a viable option for a new material to be used in micro- and nanofabrication.

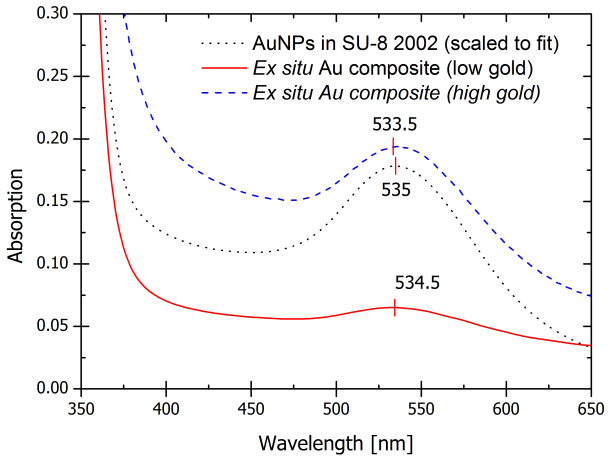

Figure 5.7 – *Plasmonic absorption spectra of two ex situ composites with different gold amounts on a fused silica wafer and of gold nanoparticles suspended in SU-8 2002. The exact gold concentration is unknown, but the one designated low is half of the one designated high. There is effectively no shift in the absorption maximum wavelength, but a reduced absorption for low gold.*

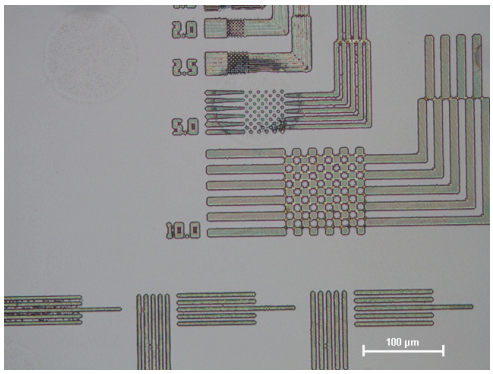

Figure 5.8 – *Microscope image at 20 times magnification of a gold nanocomposite made with ex situ synthesised nanoparticles. Ignoring the strange circle in the picture the resolution is seen to be around 5 µm. It is also possible to spot some nanoparticle agglomerates within the polymer.*

5.2 Silver Composite

As explained in subsection 4.1.1 post grafted silver nanoparticles could not easily be obtained, and successful transfer into cyclopentanone was not performed. Only the pre grafted silver nanoparticles described in section 4.1.2 are therefore used in this attempt.

The nanoparticles are transferred into cyclopentanone using the procedure described in the end of subsection 4.2.3. 1 ml of the silver nanoparticles in cyclopentanone is then mixed with 2 ml of SU-8 2002. The mixtures have in general been found to be unstable, although the student working with the procedure has been able to spin it on a 50 mm fused silica wafer as shown in Figure 5.9.

The wafer appears yellow because of the silver nanoparticles within the SU-8.

As with the *ex situ* gold composite the plasmonic absorption of the nanocomposite is measured and compared with suspended particles. The absorption spectra for the composite and silver nanoparticles in cyclopentanone can be seen in Figure 5.10.

The absorption spectrum for the silver nanocomposite shows a shoulder to the right of the absorption peak, a clear indication of agglomerates in the composite. Besides that the absorption peak of the composite is a bit blue shifted compared to that of the nanoparticles in cyclopentanone.

Because the transfer of silver nanoparticles into SU-8 for obtaining a stable nanocom-

Figure 5.9 – *Picture of a fused silica wafer on which a mixture of SU-8 and silver nanoparticles have been spun. The yellow colour shows that silver nanoparticles are present.*

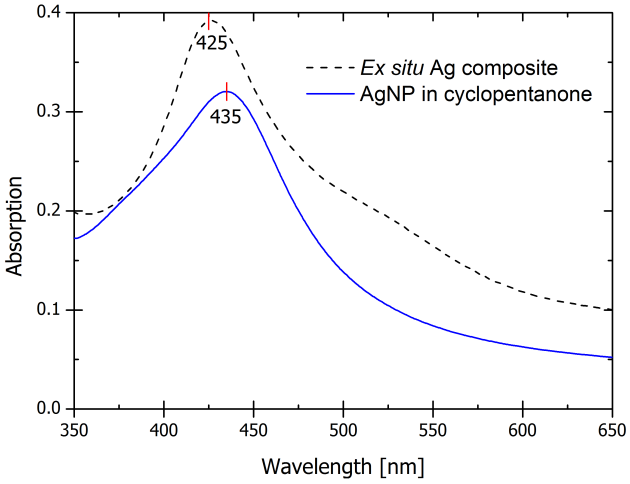

Figure 5.10 – *Plasmonic absorption spectra of an ex situ silver composite and silver nanoparticles suspended in cyclopentanone. The absorption maximum of the composite lies at a lower wavelength than the nanoparticles, but the composite also has a shoulder to the right of the peak not visible in the spectrum for the nanoparticles.*

posite material ended up with poor reproducibility, no structuring of *ex situ* silver nanocomposites were performed.

5.3 Sum-Up

It has been shown that it is possible to make an *ex situ* gold composite using gold nanoparticles stabilised with PVP/VA. The best result is obtained using pre grafted particles as this result in a homogeneous distribution of the nanoparticles whereas the post grafted particles results in a composite divided into distinct different domains.

The pre grafted nanoparticles suspended in SU-8 2002 have shown to be stable for more than a year, giving this pre composite a long shelf lifetime. The gold composite has also been successfully structured with an obtained resolution around 5 μm.

It has also been possible to fabricate an *ex situ* silver nanocomposite using pre grafted silver nanoparticles, however, not in a reproducible fashion. From this it is therefore concluded that *ex situ* composites are a viable route for gold composites, but a more robust method will have to be developed for silver composites.

Although the precise amount of gold in the final composite is not known, it is low with the used process flow. Higher nanoparticle loadings are for instance needed if conductivity is wanted. Higher loadings requires that the nanoparticle sols to have a higher

concentration of nanoparticles than what was done.

When using pre synthesised nanoparticles the final composite also includes a lot of the stabilising polymer. This additional polymer will have an effect on the final composite although which is unknown.

The situation with poor reproducibility of the *ex situ* silver composites have led to the investigation of new possible methods for silver nanocomposite fabrication. An alternative method for nanocomposite fabrication, which has also been widely exploited, is an *in situ* approach which will be described in chapter 6.

Chapter 6

In Situ Composites

The *ex situ* composites were found to be possible for the pre grafted gold particles, but was not really suitable for silver. Instead, silver composites will be made using an *in situ* approach where the particles are formed directly within the SU-8 matrix.

Many different methods for *in situ* formation of especially silver nanoparticles have been reported; purely chemical reduction [88, 89, 90], UV initiated [91, 92, 93] or thermal initiated [94, 95, 96]. Therefore, an *in situ* approach is considered as a more preferable route to achieve a silver-SU-8 nanocomposite. Although *ex situ* nanocomposites with SU-8 and both gold and silver nanoparticles have been reported as mentioned in section 1.9 nothing has been reported using an *in situ* approach.

In the *in situ* approach, nanoparticles are formed inside the photoresist matrix to obtain the desired nanocomposite material. This eliminates the requirement of prior synthesized and conditioned nanoparticles, needed with the *ex situ* method. The *in situ* method is thus easier, since no solvent exchange step is involved. The *in situ* composite also has the benefit of not having any conditioning/stabilizing polymer around the nanoparticles which influences the final composite.

The disadvantage of the *in situ* approach is the loss of control with regard to particle size and shape, as well nanoparticle functionalization.

In this chapter processes for fabricating *in situ* nanocomposites with both gold and silver are described and evaluated.

6.1 Gold Composite

To form an *in situ* composite the metal precursor needs to be mixed with the photoresist. There are two ways to do this; either the precursor can be dissolved directly in the photoresist or a co-solvent compatible with both precursor and photoresist is needed.

For the gold nanocomposite the precursor, auric chloride, can be dissolved directly in SU-8 2002, but with the disadvantage that a nanoparticle forming reaction starts immediately.

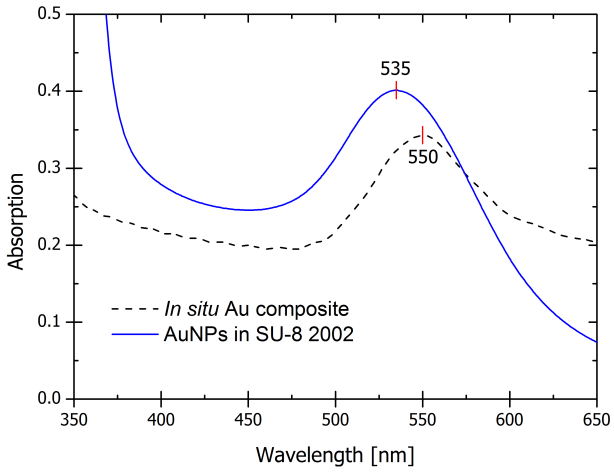

Figure 6.1 – *The absorption spectra of an in situ gold nanocomposite and gold nanoparticles in SU-8. The absorption maximum is shifted towards higher wavelength for the in situ composite compared to pre synthesised nanoparticles.*

Even though the precursor is directly soluble in SU-8, the precursor was dissolved in cyclopentanone. Auric chloride is easily dissolved in cyclopentanone resulting in a yellow/orange solution. As cyclopentanone is also the solvent of SU-8 2002 there are no problems with compatibility. It was found that when adding the cyclopentanone containing the gold precursor to SU-8 2002, an exothermic reaction occurs within 20 s or even more rapidly if shaken. The result is a viscous black solution consisting of nanoparticles.

The result is therefore not as expected as the nanoparticles are preferably formed after the photoresist mixture has been spun on a wafer. Nanoparticles change the rheology of the photoresist which could render spin coating impossible. It has, however, been shown that it is possible to spin coat SU-8 with 14 vol% gold nanoparticles in it [86]. As spin coating should therefore be possible the SU-8 and gold nanoparticle sol will be tested.

The procedure follow was:

1. 62.5 mg auric chloride is dissolved in 0.5 ml cyclopentanone.
2. 4 ml of SU-8 2002 is added and the entire mixture quickly spun on a 100 mm fused silica wafer.
3. The wafer is placed on a hotplate set at 95°C for 10 min before being given a UV flood exposure.
4. After UV exposure the wafer is given another 10 min on the hotplate at 95°C .

The plasmonic absorption of the obtained nanocomposite thinfilm is measured and compared to that of the pre grafted synthesised gold particles in liquid SU-8. The result is shown in Figure 6.1.

The absorption spectra shows that the absorption maximum of the *in situ* composite is red shifted with 15 nm compared to that of pre synthesised nanoparticles in SU-8 2002. This indicates that the *in situ* synthesis results in larger particles, or that agglomerates

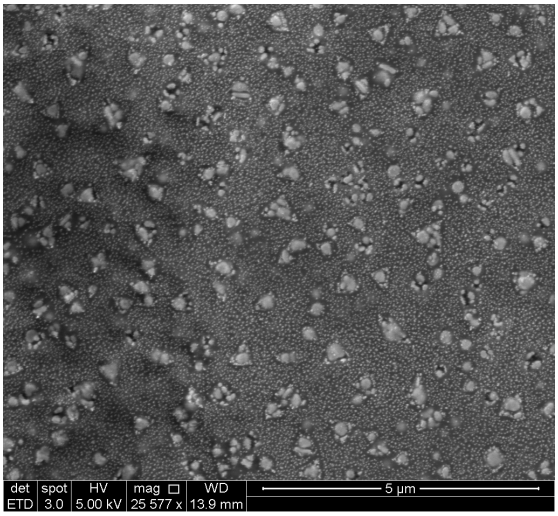

Figure 6.2 – *SEM image of an in situ gold composite made in this project. Large particles of 200-300* nm *can be seen with smaller particles of around 20-30* nm *in between.*

are present in the composite. The shoulder on the *in situ* spectrum also indicates that the composite has agglomerates.

To investigate the *in situ* gold composite further, a silicon wafer is prepared using the same procedure and investigated using a SEM. One of the SEM images is shown in Figure 6.2.

The SEM image shows that the gold composite consist of many small particles around 20-30 nm, and a number of larger particles and agglomerates of 200-300 nm as well. The large particles and agglomerates explain the red shift of the absorption maximum compared to synthesised nanoparticles.

From the plasmonic absorption and the SEM image it is clear that the *in situ* approach does not result in nanoparticles of identical size. A narrow size distribution is preferred to because of better homogeneity and sharper signal. The conclusion is therefore that for a gold nanocomposites the *ex situ* approach is the best.

6.2 Silver Composite

An *in situ* silver composite cannot be made as easily as the gold nanocomposite. Two different precursors were tested; silver nitrate and silver acetate, but none of them are soluble in SU-8.

A different approach where a co-solvent is used is therefore needed. Only experiments with silver nitrate is explained as preliminary experiments with silver acetate did not produce any results which favoured the continuation of this precursor.

The chosen co-solvent can influence the remainder of the process and must therefore be carefully selected.

Table 6.1 – *This table lists the solubility of silver nitrate in various solvents. It must be noted that the solubility data is given at different temperatures and can therefore not be directly compared. All chosen solvents are compatible with either SU-8 2002 or SU-8 2 except water which is only added as a reference.*

Solvent	Temperature [°C]	Solubility [mg/ml]
Acetone	18	3 [98]
Acetonitrile	25	879 [99]
Benzonitrile	18	1006 [99]
Cyclohexane	~ 22	None
Ethanol 95 %	15	31 [99]
Ethanol absolute	20	24 [98]
Diacetone alcohol	~ 22	Low
Dichloromethane	~ 22	Very low
DMF	~ 22	High
DMSO	25	1300 [100]
Pyridine	20	330 [99]
Water	20	2200 [98]

6.2.1 Co-Solvent Selection

It is important to choose the right co-solvent for silver nitrate to ensure that an *in situ* composite is possible. Two main criteria can be given for the solvent.

1. Silver nitrate solubility
2. Compatibility with SU-8

According to the handbook of chemistry and physics [97], ethanol should be a good solvent, but solubility data for silver nitrate are in general not that easy to find. Some solubility values have, however, been retrieved from the internet. The solubility data has mainly been extracted from two sources and converted into mg/ml. Some solvents which are all compatible with either SU-8 2002 or SU-8 2 are given in Table 6.1. The table includes water as a reference, as well as some solvents tested in the lab where the exact values are unknown.

It can be seen from the table that there is a large variation in the solubility between the solvents. A high solubility is preferred when attempting to get a high silver loading in the final composite. It was from the table chosen not to proceed with cyclohexane and dichloromethane due to the very poor solubility. Benzonitrile was also not tested due to lab availability.

The remaining solvent is then tested for stability, which means whether or not the solvents initiate nanoparticle formation during storage. This is done by dissolving silver nitrate in the solvents and observe what happens over time.

The experiment was performed as follows.

Table 6.2 – *Stability of silver nitrate in various solvents. If no formation of nanoparticles has occurred after a day or more the solvent is designated as stable.*

Solvent	Stable
Acetone	Yes
Acetonitrile	No
Ethanol 95 %	Yes
Ethanol absolute	Yes
Diacetone alcohol	No
DMF	No
DMSO	Yes
Pyridine	No

1. Three vials with 1.5 g of silver nitrate dissolved in 3 ml of a solvent is made.
2. One vial is stored as made at room temperature.
3. One vial is wrapped in aluminium foil and stored at room temperature.
4. One vial is stored in a refrigerator.
5. Colour changes are observed by visual inspection.

If the solubility of silver nitrate in the solvent is less than 500 mg/ml, then the maximum soluble amount of silver nitrate has been used instead. The stability was evaluated by observing any colour change or agglomerates in the liquid after one day or later. If colour or agglomerates could be observed the mixture was marked as unstable. In all samples no difference could be observed between the different storage methods. The results are summarised in Table 6.2.

From the stability table it can be seen that half of the solvents initiate the formation of nanoparticles while being stored. For process purposes a stable solution is preferred as a stock solution can then be made instead of preparing fresh solutions each time. Ethanol is a preferred solvent although it has a low solubility of silver nitrate. This is because it does not initiate nanoparticle formation, has no toxicity and is easily removed in later processing.

Ethanol is however only compatible with SU-8 2 and not SU-8 2002. This is due to ethanol being miscible with γ-butyrolactone, the solvent of SU-8 2, and not cyclopentanone, the solvent of SU-8 2002. It is however possible to achieve compatibility between ethanol and cyclopentanone, and thereby SU-8 2002 by adding acetone. It was found that complete miscibility is achieved when the volume ratio between ethanol, acetone and cyclopentanone are 2:1:1.

DMSO is also chosen as a preferred solvent as it does also not initiate nanoparticle formation and has a high solubility of silver nitrate. Acetone could be chosen as a third choice, but was discarded because of the lower solubility than ethanol.

Of the remaining solvents pyridine is discarded as it has the lowest solubility. Acetonitrile is preferred over DMF because of lower toxicity. Should DMSO ultimately turn out to

be a bad co-solvent acetonitrile will therefore be a backup. One of the differences between DMSO and acetonitrile is also that DMSO is a slightly oxidising solvent while acetonitrile is a slightly reducing solvent.

An effect has been observed upon mixing silver nitrate containing DMSO with SU-8 2002. The compatibility disappears when the silver nitrate concentration increases above a certain value. The exact value is not known as it appears to be changing with temperature, but in general it lies between 0.5 g/ml and 0.6 g/ml.

6.2.2 SU-8 Reactivity

When auric chloride was mixed with SU-8 nanoparticles were quickly formed. Formation of nanoparticles has also been observed when silver nitrate and the co-solvent are mixed with SU-8, although at a much slower rate. In one experiment 10 mg of silver nitrate was dissolved in 2 ml of ethanol before 1 ml of acetone and 1 ml of SU-8 2002 was added. This results in the formation of a grey precipitate over time.

To understand which chemical is responsible for initiating the formation of nanoparticles a small experiment was performed. Three vials were prepared with using the following procedure.

1. 33 mg of silver nitrate is dissolved in 6 ml of 96 % ethanol.
2. 3 vials are filled with 2 ml of the silver nitrate containing ethanol in each.
3. 1 ml of acetone is added to two of the vials.
4. 1 ml of cyclopentanone is added to one of the vials containing acetone.

The vials were then observed over time to see if any colour change appeared. It was found that as long as the vials were not stored in direct sunlight, no change could be observed.

To see the influence of UV irradiation the vials were placed in a UV box for 30 s after which the colour of the liquids were again evaluated. The resulting colours can be seen in Figure 6.3.

As seen from the figure only the vial containing cyclopentanone has experienced a colour change. It can therefore be concluded that ethanol and acetone cannot initiate the formation of nanoparticles, but that cyclopentanone together with UV light can.

An experiment was also performed with silver nitrate dissolved in DMSO and SU-8. 0.5 g of silver nitrate was dissolved in 1 ml of DMSO and mixed with 2 ml of SU-8 2002. In a timespan of roughly 10 min the colour changes to yellow similar to that of the synthesised silver nanoparticles described in chapter 3. As time passes the colour darkens before it eventually becomes clear liquid with visible grey precipitate of silver particles.

As nanoparticle formation happens when SU-8 is added, even without any UV irradiation a conclusion can be drawn. Cyclopentanone, although able to form nanoparticles are not the main initiator. One or more of the remaining SU-8 ingredients must therefore be

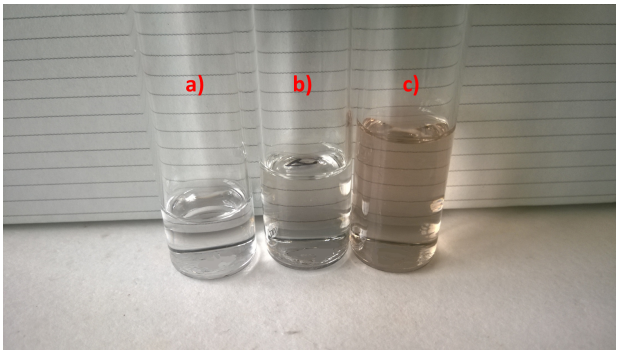

Figure 6.3 – *A picture showing the three vials containing a) silver nitrate and ethanol, b) silver nitrate, ethanol and acetone and c) silver nitrate, ethanol, acetone and cyclopentanone. The vials have been given a 30* s *UV exposure and it is clear that only the one with cyclopentanone has changed its colour indicating the formation of nanoparticles. If b) appears to be darker than a), then this is just a shadowing effect from c).*

responsible for initiating the nanoparticle formation. It has, however, not been possible to test the remaining ingredients separately.

It finally concluded that no matter which solvent is chosen as the co-solvent a SU-8 stock solution with the metal precursor cannot be made. The silver nitrate containing co-solvent must therefore be mixed with SU-8 just before use to minimise nanoparticle formation before spinning.

6.2.3 Initial Composite Test

It was found that with the use of DMSO as co-solvent, silver nitrate can be mixed directly with SU-8 2002. Nanoparticles will form over time, but a reaction time of at least 10 min makes it possible to deposit the photoresist on the wafer before nanoparticles renders spin coating impossible. Some initial tests are done in the lab to see if a structurable silver nanocomposite can be made.

A *Delta 10 TT* spinner from SÜSS MicroTec, shown in Figure 6.4, and a custom build UV chamber, shown in Figure 6.5, are used for deposition and structuring. The TT in the spinner name stands for Table Top. The initial tests are performed on 50 mm wafers.

As was previously explained, section 1.5, micro- and nanofabrication is done in a cleanroom to avoid particles. Particles on the wafer will be problem during spinning when the process is performed in a standard lab. The amount of particles will therefore have to be reduced. The method which has been adopted in this project for removing unwanted particles is the Piranha clean which is normally not used for pre-treatment of wafers before resist spinning.

A piranha clean consists of concentrated sulphuric acid (98 %) and hydrogen peroxide (30 %) in the ratio 4:1. The ratio does not have to be exact as others use ratios of 5:1 or 3:1. A correct mixing procedure is however important due to safety reasons. Hydrogen peroxide

Figure 6.4 – *Picture of the used Delta 10 TT spinner from SÜSS MicroTec. The wafer is placed on the pedestal to the left, while the control panel on the right is used for setting the parameters.*

Figure 6.5 – *Picture of the used UV chamber. The wafer is placed in the drawer with a mask on top of it when exposed to UV. The total effect of the UV chamber is unknown.*

has to be added to the sulphuric acid and not the other way around as the solution almost instantly heats up to the working temperature of $\approx 70°C$ and is potentially explosive. This is an important thing to remember as it is opposite the rule for mixing acids and water.

The piranha clean is a very aggressive process which removes all organics and alkali ions and is therefore often used for removing contaminants on wafers or cleaning glassware. The process will also hydroxylate most surfaces, meaning that there will be OH-groups at the surface making it hydrophilic. A hydrophilic surface is, however, bad when spin coating. Photoresists, and especially SU-8, have huge adhesion problems on hydrophilic surfaces. This is also why the humidity in a cleanroom is closely controlled. In an attempt to overcome the hydrophilicity caused by the Piranha clean, the wafer is placed on a hotplate with a lid, set at 250°C for at least four hours. The lid should hopefully prevent too many particles settling on the wafer again. The high temperature drives out most of the water from the wafer which makes it possible to spin coat SU-8.

After heating, the wafer is quickly transferred to the spinner and a mixture of 2 ml SU-8 and 0.5 ml of $AgNO_3$ in DMSO is immediately spun on in order to keep the particle contamination as low as possible.

A spinning speed of 300 RPM is used for 10 s while the resist is being poured onto the wafer, then the speed is increased to 1000 RPM for 30 s. It was not possible to use a higher spinning speed as this resulted in all the resist being spun off leaving an empty wafer with no resist thinfilm.

The inability to use high spinning speeds could be a result of the Piranha treatment. It has been attempted to spin coat wafers without the Piranha treatment, but this has resulted in very poor covering of the wafer due to particles. A solution could be to increase duration of the heat treatment or the temperature to improve dehydration of the wafer.

After spinning the wafers are placed on a hotplate set at 95°C for 10 min before being placed in the custom build UV chamber using non collimated light for 1 min. A patterned

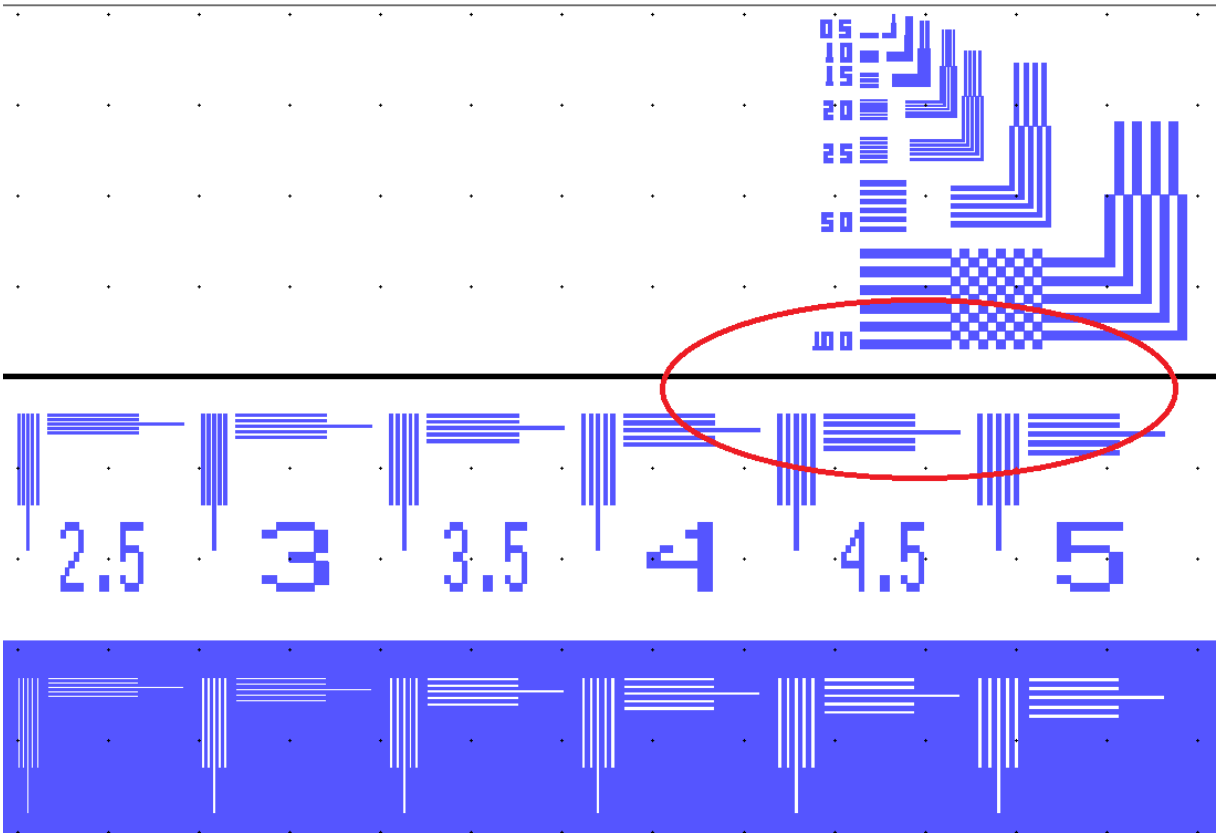

Figure 6.6 – *This illustration shows how the resolution marks on each mask is constructed. The marks can be used to see what resolution has been obtained, and if the resist is over or under exposed. The black line and the red oval are not part of the mask.*

mask is placed on top of the wafer to give some structures. The used mask includes resolution marks consisting of lines and squares. These structures, which are shown in Figure 6.6, can be used to evaluate the quality of the exposure and development.

SU-8 is cross-linked when achieving a sufficiently large energy dose at 365 nm. The dose varies depending on the film thickness, but lies below 100 mJ/cm^2. If too high a dose is applied cross-linking will happen in unwanted areas resulting in a distorted image. The used UV chamber emits light in a very broad spectrum and with a high intensity. Integrating the intensity spectrum has given a total effect of 82 mW/cm^2, but as the tubes deteriorate over time the exact value is unknown. The broad spectrum and high intensity makes it impossible to achieve good resolution, but it is possible to see if structuring is possible.

After UV exposure the wafer is again placed on a hotplate set at 95°C for 10 min before being developed for 2 min in propylene glycol monomethyl ether acetate (PGMEA). The wafer is then rinsed with isopropyl alcohol (IPA) and dried using a nitrogen gun. The total procedure can be summarised to the following.

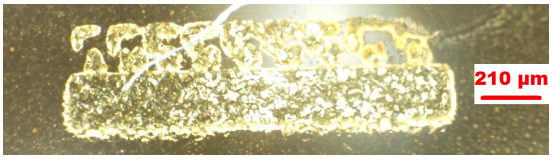

Figure 6.7 – *Microscope picture of SU-8 2002 silver nanocomposite. The structures seen are the part of the resolution marks below the black line shown in the schematics of Figure 6.6. It does not resemble that well, but the lines angled at 90 degrees can be seen as well as the large square below. The small teeth on the big squares were originally the numbers.*

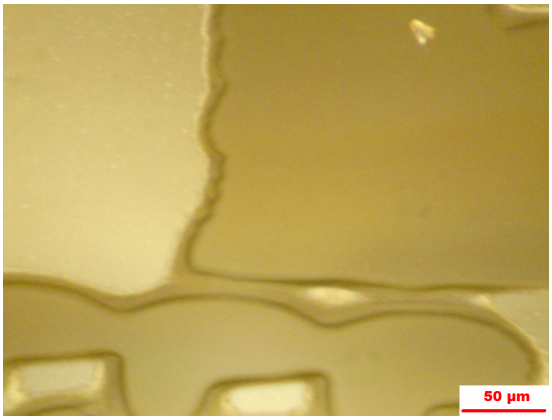

Figure 6.8 – *A microscope picture of cross-linked SU-8 2002 resolution marks. The structures should resemble the one shown in the red circle in Figure 6.6, which is does not.*

1. Silver nitrate is dissolved in DMSO to obtain a solution concentration of 0.5 g/ml.
2. A 50 mm silicon wafer is given a Piranha clean (4:1 sulphuric acid and hydrogen peroxide) for 10 min.
3. The wafer is cleaned with Milli-Q water for 10 min.
4. The wafer is placed on a hotplate with lid set at 250°C for at least 4 h.
5. 0.5 ml of DMSO with silver nitrate is mixed with 2 ml of SU-8. The silver nitrate concentration can be adjusted as preferred.
6. The wafer is placed on the spinner and the SU-8 mixture is spun on. The spinning parameters are: Dispense step; 300 RPM for 10 s, acceleration of 100 RPM/s, thickness definition; 1000 RPM for 30 s, acceleration of 300 RPM/s.
7. The wafer is transferred to a hotplate set at 95°C and baked for 10 min.
8. The wafer is transferred to a UV chamber and a mask placed on top of it before it is given a 1 min UV exposure.
9. The wafer is transferred to a hotplate set at 95°C and baked for 10 min.
10. The wafer is agitated for 2 min in PGMEA to develop the structures.
11. The wafer is rinsed with IPA and dried using a nitrogen gun.

After this process the wafer is examined using a microscope, the result is shown in Figure 6.7. The same procedure, but without any silver nitrate, has also been followed, giving the result shown in Figure 6.8.

If there had been no cross-linking of the polymer only a bare silicon wafer would have been seen. Since some resist is found cross-linking and thereby structuring has happened. Both microscope pictures show structures which, at best, can be described as terrible. It can be hard to see what the pictures resemble, but as it is known that it is the resolution marks similarities can be found.

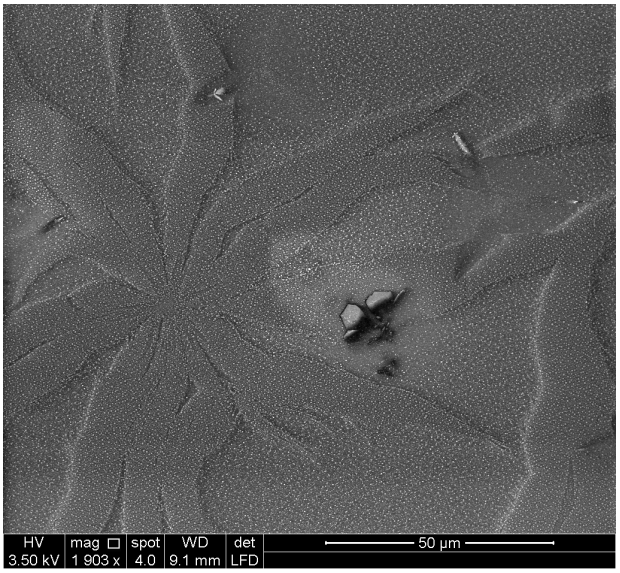

Figure 6.9 – *SEM image of an in situ silver nanocomposite. The image shows that a lot of particles have been formed.*

No attempts have been made to improve the result as this test was merely used as a proof of concept to indicate that structuring was possible.

A wafer has also been made using a process without a mask and with no development. This wafer was then examined using a SEM to confirm the formation of nanoparticles. The result is shown in Figure 6.9.

The SEM image confirms that silver nanoparticles or clusters of nanoparticles have been formed. The magnification is not high enough to determine the size, but they appear to have a size of at least 100 nm. As mentioned one of the disadvantages of the *in situ* formation of nanoparticles is the lack of control over particle size and shape. Nothing can therefore be done if the particles are too large for the desired application.

Plasmonic Absorption

The plasmonic absorption of the *in situ* silver nanocomposite is also measured and compared to that of silver nanoparticles in cyclopentanone.

A two fold dilution series have been made to also see how the plasmonic absorption changes with precursor concentration. The dilution series are made from a stock solution of 0.5 g/ml of $AgNO_3$ in DMSO. Ten samples with 2 ml of SU-8 2002 and 1 ml of the $AgNO_3$ solution are made, in a manner such that the maximum $AgNO_3$ amount is 500 mg and the lowest is roughly 1 mg. They are all spun on fused quartz wafers, exposed to UV and given a 95°C heat treatment. Some representative results are shown in Figure 6.10. The image shows that the absorption maximum only varies within 2 nm for most of nanocomposites, and that an increased precursor amount as expected results in a higher absorption. The result for the ∼3.9 mg $AgNO_3$ is the lowest which can be achieved as no peaks are seen for

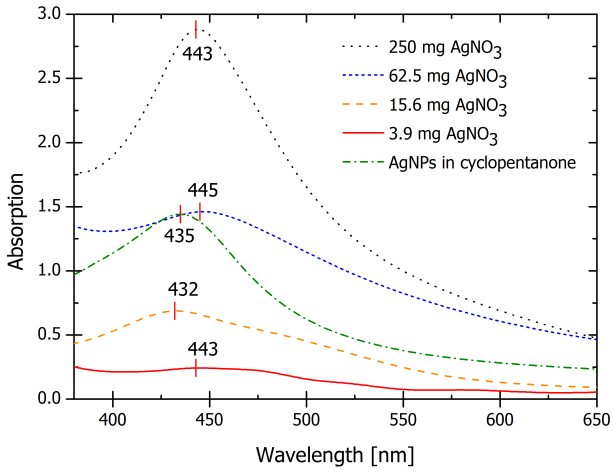

Figure 6.10 – *Absorption spectra for some selected silver nanocomposites. The position of the absorption peak only varies with 2* nm *between three of the nanocomposites, but is red shifted with roughly 10* nm *compared to the nanoparticles in cyclopentanone and the last nanocomposite.*

the 2 mg and 1 mg composites. The absorption maximum for all samples varies between 450 nm (500 mg sample) and 443 nm, except the single outlier at 432 nm shown in the figure.

The general red shift compared to pre synthesised nanoparticles in cyclopentanone is consistent with the SEM image showing 100 nm large particles. The single outlier does indicate that it is possible to achieve an absorption peak at the same wavelength as the previously synthesised particles.

6.3 Sum-Up

It was found that it is possible to fabricate an *in situ* gold nanocomposite, but with large variation of particle size. Auric chloride can be dissolved directly in SU-8, but nanoparticles are formed within 20 s.

It has all in all been shown that it is possible to fabricate an *in situ* silver nanocomposite which can be structured using UV light. Silver nitrate cannot be directly dissolved in SU-8 and a co-solvent must be used. The preferred solvent is DMSO, but ethanol can also be used together with SU-8 2.

It has been found that the plasmonic absorption increases with added precursor amount, and that the absorption maximum is in general red shifted with 10 nm. If the silver nitrate precursor amount was decreased below 3.9 mg no absorption peak could be distinguished.

From all the experiments performed so far the overall conclusions are as follows.

- *Ex situ* gold nanocomposites with pre grafted particles are preferred over *in situ* gold nanocomposite.

- *In situ* silver nanocomposites are preferred to *ex situ* silver composites.
- All nanocomposites can be structured.

The next step is to optimise the entire process such that a homogeneous spinning and a good resolution are achieved.

Chapter 7

Process Optimisation

It has been shown that both gold and silver nanocomposites can successfully be made. So far the work has mostly been on a proof of concept level, which means that in order for the nanocomposites to become really useful a process optimisation must be done.

Processing of SU-8 resulting in interesting MEMS structures have been extensively explored. Adding co-solvents, nanoparticles or nanoparticle precursors to the photoresist will dramatically influence the processing parameters relative to the original photoresist. The nanocomposites in this project are made from highly modified SU-8 and standard recipes can therefore not be expected to work without further modifications.

The first process optimisation has been carried out inside the DTU Danchip cleanroom to eliminate the effects of the poor micro- and nanofabrication environment in the lab. The cleanroom also contains more specialised equipment designed for the purpose. Each step of the UV lithography process will be thoroughly explained and the possible parameters to be adjusted will be described depending on the used machine.

In the end the final process recipe used will be stated.

7.1 UV Lithography

UV lithography is a relative simple process which only involves these steps.

1. Deposition of resist on substrate.
2. Exposure of resist with UV light through a mask.
3. Development of resist to achieve desired pattern.

After this you can transfer the pattern to the underlying substrate using various methods and then remove the resist again.

This is sort of true, but the process does involve several steps more. At the same time UV lithography is only simple once the process has been optimised as many parameters can be adjusted along the way.

The complete process involved in this project includes the following steps.

1. Pre-treatment of substrate.
2. Spinning of resist.
3. Soft bake.
4. UV exposure.
5. Post Exposure Bake (PEB).
6. Development.
7. Soft- or hard bake.

These seven steps will individually be explained followed by the actual optimisation performed.

Some steps of the process may vary with the choice of wafer material. All descriptions are based on silicon wafers, but will, unless otherwise mentioned, also work for fused silica wafers.

7.1.1 Pre-treatment of Substrate

A pre-treatment of the substrate is done to ensure that the resist will adhere to the surface and that there will be a nice and homogeneous coverage. In subsection 6.2.3 a Piranha clean was used as a pre-treatment, but this will not be considered again as particles should not be a problem within the cleanroom.

Several treatments or adhesion promoters can be used to achieve good homogeneous coverage, but the consideration here will only be on the most used one at DTU Danchip.

HF Dip

A dip in hydrofluoric acid (HF) just before spinning resist is a standard way to treat a silicon wafer. Adhesion to silicon are for the most resists better than to oxides, and by dipping a silicon wafer in HF the native oxide which has been formed on the surface will be removed leaving just the silicon.

This process is mostly used for new wafers where the surface has not been exposed to any kind of treatments. This pre-treatment sounds like a good choice for this project as well, but experience has shown that it does not work for SU-8. This is mainly because the wafers are cleaned for several minutes in water after being dipped in HF.

This step is not applicable for a fused silica wafer as it would start etching the entire wafer.

HMDS Treatment

Another popular pre-treatment of wafers are a chemical treatment with hexamethyldisilazane (HMDS). Priming the wafer with HMDS leaves a mono-layer of trimethylsilyl (TMS) on the surface of the substrate. The process will somewhat dehydrate the surface due to an elevated temperature during the process, and the mono-layer will result in a lower surface energy.

The process is the most used method for increasing adhesion by creating a hydrophobic surface. This also sounds like a promising pre-treatment for the wafer, but it is mainly used for the AZ® resists which are the most used resists in the cleanroom. It is also used for wafers with oxide layers as these cannot be dipped in HF.

250°C Oven

The preferred way to maximise dehydration of the substrate is to place them in a 250°C oven for at least four hours, preferably longer. This long baking at high temperature drives out all the absorbed water from the substrate and is especially used before spinning tricky resists like SU-8.

The process is simply to take any new wafers and place them in the 250°C oven several hours before use. In general several hours have in this project always meant at least putting the wafers in the oven the day before use. After spending the night in the 250°C oven all water should effectively have been driven out of the wafer.

Sum-Up

Of the standard pre-treatments the HF dip is the worst candidate and discarded due to the wafer being washed in water. HMDS looks like a good alternative, but previous experience with SU-8 has shown that a 250°C treatment has a higher chance of success.

The preferred pre-treatment will therefore be the 250°C which will not be tested separately, but evaluated together with the resist spinning. The entire pre-treatment should be reconsidered if the final result is not at desired.

The spinning which will be explained in subsection 7.1.2 did not result in any adhesion problems between the wafer and the resist which can be correlated to the pre-treatment. A 250°C heat treatment has therefore been used consistently throughout the remaining cleanroom work.

7.1.2 Spinning of Resist

The spinning process will be explained with regards to the possibilities of an *OPTIcoat SB20+* from *ATMsse GmbH* as this machine has initially been used.

The spinning of resist can be divided into two different steps, each with three parameters to adjust. The first step is called a spreading cycle where the wafer spins at a slow speed while the resist is being poured onto it. The spinning ensures continuously movement of the resist which helps to avoid areas with higher spin resistance due to fast evaporation. The spinning should also ensure that resist which flows off the wafer is spun away instead of attaching to the backside of the wafer due to surface tension.

The second step is called thickness definition and is where the final thickness of the resist is defined by increasing the rotational velocity.

In both steps the parameters to be varied is RPM, time and acceleration.

The RPM defines the final rotational velocity, the time defines how long time the spinning will be performed at the maximal velocity and the acceleration defines how fast the wafer will go up in speed (and down again).

In a standard recipe the spinning time would be kept constant at 30-60 seconds and the RPM varied. Using a constant spin time and varying the RPM a spin curve can be constructed showing the final resist thickness as function of spin speed.

The acceleration is mostly relevant for ensuring no abrupt velocity changes which could result in inhomogeneities or other unwanted effects.

Test of Spinning Speed

Since the adhesion properties of SU-8 is likely to change due to the addition of an extra solvent the optimal spinning speed with regards to homogeneity and defects such as edge beads have to be found. Edge beads are a common result of resist spinning, either because of low spinning speed or high viscosity of the resist. The edge beads will, if not removed, result in lower resolution during the UV exposure step due to an increased distance between mask and resist.

The maximum resolution or critical dimension can theoretically be calculated with this formula:

$$CD = \frac{3}{2}\sqrt{\lambda\left(d_p + \frac{t_r}{2}\right)}, \tag{7.1}$$

where λ is the wavelength emitted from the aligner, d_p is the proximity distance between the mask and the resist film and t_r is the thickness of the resist film.

The edge beads, which can have a thickness of several times the deposited film, increases d_p above the ideal value of zero. This could mean that for a resist thickness of 1 μm a d_p value of 4 μm compared to 0 μm would result in an increase of the critical dimension by a factor of three.

The optimal spinning speed is found by spinning 4 ml SU-8 2002 mixed with 1 ml DMSO on wafers at different spinning speeds for 30 s. A summary of the spin results can be seen in Table 7.1.

These results are not promising as no defect-free and homogeneously covered wafers have been obtained. 1100 RPM is preferred as the best compromise as it is not preferred to also include an edge bead removal step in the process. This spinning speed does also somewhat resemble what was used in subsection 6.2.3.

Besides the test of optimal spinning speed, testing was also done with regards to stationary or dynamic dispense of the polymer. In stationary dispense the spreading step is omitted and resist poured directly onto a stationary wafer, while the resist is being poured onto the wafer during the spreading step in dynamic dispense. The result of these test was that resist would get to the backside of the wafer if stationary dispense was used. Some testing was also done to find the best parameters for the spreading cycle, but ultimately it was decided to use 300 RPM for 10 s such that both the spreading and the thickness definition step resembled that of the lab experiments.

Table 7.1 – *A table showing the tested spinning speeds and the corresponding result obtained at the Opticoat.*

Spin speed	Result
2500 RPM	Most resist is spun off the wafer.
2000 RPM	Lines without resist seen on the wafer.
1500 RPM	Some spots with no resist seen.
1200 RPM	Single spot without resist observed.
1100 RPM	Good somewhat homogeneous coverage with few edge beads.
1000 RPM	Good homogeneous coverage, but large edge beads and edge defects.

Figure 7.1 – *Picture of a new Opticoat spinner. Everything within the white ring is part of the chuck and rotates. The grey part in the middle is an insert which can be exchanged depending on the use of the machine.*

An Additional feature of the *Opticoat* is that it, within some limits, can spin with or without an automatic lid. It was also tested to see which option gave the best results during the thickness definition step, but no difference could be observed. It was chosen not to use the lid during spinning as it is then possible to see if something goes wrong.

The reason for the generally bad coverage when spinning resist films on this spinner originates from a bad horizontal alignment and/or wobbling of the chuck. The spinner itself is nicely aligned as it is built into the table on which it stands. The chuck is however very large and cannot be perfectly aligned. On top of this the chuck has different insets depending on the size of wafer needed to be spun. These insets are by no means perfect. This all results in a none-horizontal wafer which experiences wobbling during spinning which then again lead to poor spinning results. A picture of a **new** Opticoat spinner is shown in Figure 7.1.

This should complete the spinning part and the process continued with UV exposure, but alas, had it only been so easy. Shortly after having done the spin speed optimisation tests on the *Opticoat*, it was taken out of use since the motor was removed to repair another machine. The spinner was therefore not available for the majority of this project.

This meant that something had to be done, and after some time permission was granted

Figure 7.2 – *Picture of a WS-650 spin coater. The spinner is placed directly on the table and the wafer on the center pedestal.*

to proceed with the process on a different spinner. This spinner was a *WS-650 spinner* from *Laurell Technologies Corporation*, and as it was a completely different machine spinning tests had to be done all over again. A picture of a *WS-650* spinner can be seen in Figure 7.2.

Better results was obtained using the *WS-650* spinner at velocities between 1000 RPM and 2000 RPM in terms of homogeneity across the wafer and edge defects. The *WS-650* is a small moveable spinner without a large chuck like the *Opticoat*. The *WS-650* has a small center pedestal resulting in no chuck wobbling. The spinner cannot be horizontally adjusted in itself, but as long as it is placed on a horizontal surface everything should be okay.

The *WS-650* is a simpler instrument than the *Opticoat*. The recipes on the *Opticoat* can contain several steps, all with different acceleration, spinning speed and spinning time, whereas the *WS-650* uses predefined recipes where you can choose the spinning speed, but the spinning time is fixed at 1 min and the acceleration at 500 RPM/s. The *WS-650* has been used for making spin curves using the following procedure.

1. The wafer is placed on the pedestal using the positioning tool, the vacuum is turned on and the lid closed.
2. 0.5 ml of co-solvent is mixed with 4 ml of SU-8.
3. The SU-8 mixture is manually dispensed to the center of the wafer through the hole in the lid using a transfer pipette.
4. The spinner procedure is then quickly started.
5. After spinning the wafer is placed on a hotplate set at 95°C.
6. The wafer is broken in half and the thickness found using SEM.

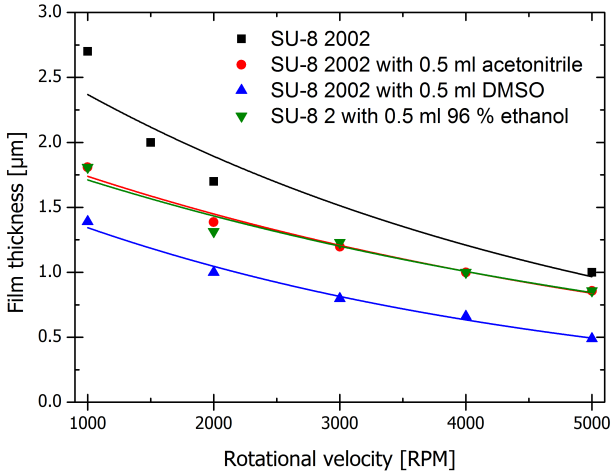

Figure 7.3 – *The result of spin test performed with 0.5* ml *of DMSO, acetonitrile and 96 % ethanol mixed with 4* ml *of SU-8. The spin curve without added solvent is taken from the DTU Danchip labadvisor while the other thicknesses are evaluated by breaking the wafer in two and examining the cross section in a SEM. All data has been fitted with a logarithmic function. The fits are seen to be in good agreement with the measurements, but with larger deviations for the pure SU-8 due to less precise measurements.*

This procedure was first used for the co-solvent DMSO and later acetonitrile together with SU-8 2002 as well as for 96 % ethanol and SU-8 2. The spinning was done at five different speeds between 1000 RPM and 5000 RPM. If the film thickness of the deposited photoresist is then measured a curve displaying the resist thickness as a function of rotational velocity can be made as shown in Figure 7.3.

It is expected that the thickness of the resist decreases when adding a co-solvent as the resist is diluted and the viscosity reduced. The results are in agreement with this. The addition of DMSO is seen to lower the thickness of the deposited resist more than with acetonitrile. The SU-8 2002 with acetonitrile and the SU-8 2 with 96 % ethanol gives almost identical results.

The most used resist thickness used at DTU Danchip is 1.5 μm. 1500 RPM is therefore chosen as this results in a similar resist thickness. The resist thickness lies between 1 μm and 1.75 μm for all co-solvents when this speed is used. Spinning time and acceleration are fixed and those predefined values are therefore used. As it also only possible to do a one step process the stationary dispense is also adopted.

The observant reader will have noted that the amount of solvent changed from 1 ml at the *Opticoat* to 0.5 ml at the *WS-650*. This change shall be seen in the light of an effect discovered when spinning resist using a stock solution of 0.5 g/ml $AgNO_3$ in DMSO.

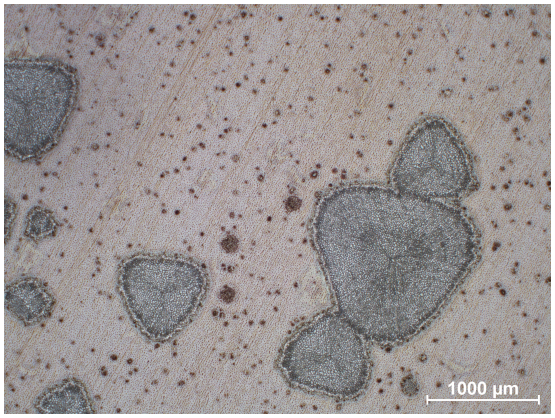

Figure 7.4 – *Optical microscopy picture at 2.5 times magnification of a wafer on which SU-8 2002 with 0.5* ml *of 500* mg/ml $AgNO_3$ *in DMSO has been spun on. The result is large islands consisting of agglomerated silver nanoparticles. The islands are very different in size and randomly distributed across the wafer.*

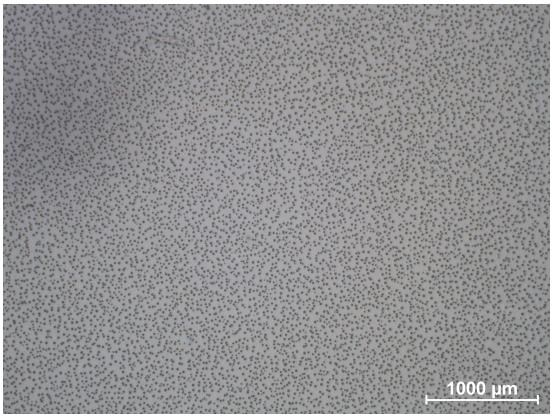

Figure 7.5 – *Optical microscopy picture at 2.5 times magnification of a wafer on which SU-8 2002 with 0.5* ml *of 250* mg/ml $AgNO_3$ *in DMSO has been spun on. The result is silver nanoparticle agglomerates of similar size homogeneously distributed within the polymer.*

Effect of Metal Precursor Concentration

It was discovered that at high silver nitrate amounts the spinning was suddenly not homogeneous at all. What can only be described as an inability for the SU-8 to contain high silver nitrate amounts while being rotated at high speeds resulted in large islands of silver visible after spinning. This effect can clearly be seen in Figure 7.4.

Reducing the silver nitrate amount when spinning, results in nice homogeneous films as seen in Figure 7.5. Silver nanoparticle agglomerates can still be seen, but as they are homogeneously dispersed it does not really matter. It must also be mentioned that the picture is taken after the polymer has been hardened as it can otherwise not be handled. Many of the particles may have been formed during this baking step, but for the high amount of silver nitrate the silver islands was definitely there after spinning.

As it was shown that high silver nitrate loadings in the co-solvent resulted in inhomogeneities it was decided to use 0.5 ml of co-solvent and not 1 ml as was initially used. It is an advantage to minimise the amount of used co-solvent to ensure as little difference between the nanocomposite mixture and the photoresist.

7.1.3 Soft Bake

After spinning, a soft bake is performed to remove most of the solvent from the resist before exposing it to UV. This step is important for the handling of the resist as it might otherwise flow of a non-horizontal wafer, or it will stick to the UV mask in the following step if in contact. The baking step can be further divided into two or more steps depending on the complexity of the baking process selected.

For a two-step process the first one will be a ramping step where the temperature is gradually increased to the desired temperature and the second step a baking step where the temperature is kept constant for a period of time.

For this two-step process three parameters can be adjusted; temperature, ramping time and baking time.

The temperature defines what final temperature the wafer should be baked at and the baking time defines for how long time. The ramping time defines how fast the final temperature is reached. The ramping could be programmed for a 1°C/min increase if desired. To achieve this the ramping time would have to be set at 30 min if the room temperature was 20°C and the final temperature wanted was 50°C.

For this two-step process the hotplate will turn off once the baking time has expired and the wafer will therefore cool down to room temperature at the same rate as the hotplate. A ramping down step can be added to ensure a slower decrease in temperature if needed, but this will only be effective at high temperature differences where the hotplate will still need to be turned on in order to prevent a too rapid decrease in temperature. At low temperature differences the desired ramping will not be possible unless a hotplate with build-in cooling is used.

The temperature ramping is used to prevent thermal stresses within the polymer due to large temperature differences during heating.

If desired this process could be expanded to include several baking and ramping steps for more advanced baking purposes, but it is hard to see the necessity for this during this process.

The supplier recommends a soft bake of 1 min at 95°C for a resist thickness of 0.5-2 μm [51]. The standard processing at DTU Danchip is however 10 min at 95°C with a ramp of roughly 1°C/min. It was decided to use the DTU Danchip standard of 10 min at 95°C, but with a much faster ramping because of the hotplate.

Due to problems in the following steps the cleverness of this decision was never really evaluated, but will have to be considered for future work.

7.1.4 UV Exposure – Part 1

The UV exposure defines the pattern in the resist when it is exposed through a mask. The pattern is defined either by cross-linking of the resist in the exposed areas (negative resist), or by bond breaking in the exposed area (positive resist). The machine used for standard UV exposures is called a mask aligner.

This step is perhaps the most important one in the micro- and nanofabrication process

Figure 7.6 – *Picture of an EVG620 mask aligner. The left part is an automated system for aligning while the left part contains the lamp, filters, hard and software etc.*

and also involves several parameters to be adjusted. There are also many different settings which can be changed in this step. For this project a *Double Side Mask Aligner EVG620* has been used and all parameters and possible settings will refer to this machine. A picture of a *EVG620* is seen in Figure 7.6.

It is important to ensure that this step is optimised as the results can otherwise be horrendous. One of the main issues to be considered is over- or under exposure. This means that the resist either receives too much or too little UV exposure. For a negative photoresist like SU-8 an over exposure will result in larger structures than desired because the photo acid generated by the UV exposure will diffuse beyond the boundaries defined by the mask. Small structures close to each other will merge into one indistinguishable blob, which is what happened back in Figure 6.7 and Figure 6.8. For under exposed SU-8 the structures will be smaller than desired and connecting structures may not be connected at all.

For all optimisation done during this step a silicon wafer is used on which SU-8 2002 with DMSO and silver nitrate has been spun on at 1500 RPM.

First of all the right filter should be chosen for the aligner. Several types can be used depending on the need. A typical mask aligner, and the *EVG620*, has a mercury lamp as the light source. This kind of lamp is usually chosen because of the spectral lines at 436 nm (g-line), 405 nm (h-line) and 365 nm (I-line). The filter then ensures that only the desired wavelength at the desired intensity will reach the resist. As an example of filters these could be an I-line filter insuring maximum intensity of the I-line or a SU-8 filter which effectively eliminates low wavelengths, but also reduces the intensity of the I-line to 50 %. It is important to remove small wavelengths when working with SU-8 as it has a high absorption at low wavelength making correct dosage hard to achieve. Other filters around the g- or h-line could also be available, but are not that interesting for this

application.

Secondly a decision can be made whether or not to do purge with nitrogen during exposure. Purging with nitrogen or other inert gasses, can be used to remove contaminants from the air. These contaminants could be oxygen or products generated when the resist is exposed to UV light. For some resists contaminants are not a problem, while others will not cross link at all without purging. Purging should not be necessary with SU-8.

Possibilities to add purges both before and after exposure also exist with some of the same arguments as before.

A third setting is also available; either constant- or interval exposure can be used. For short exposure times constant exposure should be used, while for long exposure times interval exposure should be used. Long and constant exposure with UV light will cause the resist to heat up and maybe form a protective skin on the top which prevents the underlying layers from polymerising. This phenomenon is also known as T-topping.

An interval exposure allows the resist to cool down between each exposure. A further setting can be made within both constant- and interval exposure as either constant time or constant dose can be chosen. Constant dose should in principle be the best, but the UV integrator used for constant dose is not precise enough on the *EVG620* to be a reasonable choice.

In constant exposure there is only one parameter to adjust, either the exposure time or the exposure dose depending on which type of constant exposure has been chosen. In interval exposure more parameters can be adjusted. Again there is the choice of exposure time or -dose, but this time the number of cycles should also be chosen as well as the wait time between each cycle.

A choice about positioning of the mask must also be made. Several possibilities exist regarding this as; proximity, soft contact, hard contact or vacuum contact can all be chosen. There is no contact between the mask and the wafer in proximity mode. The choice of mask positioning mainly affects the achievable resolution as proximity will result in diffraction between the mask and the resist increasing the size of the structures. If there are height differences in the photoresist thickness across the wafer the contact modes can eliminate some of these as the mask is pressed into the resist. The downside of the contact modes are that the mask will be contaminated with resist residues which again means that the mask will have to be cleaned frequently if identical results are to be achieved. Another downside especially apparent with vacuum- and hard contact is the possibility of the resist and wafer to stick to the mask which is not at all desirable. If proximity is used the separation gap between mask and substrate can also be adjusted.

There is also the possibility to use flags during mask alignment which should be considered when choosing which contact mode to be used. Flags are small metal pins used to ensure that the mask do not touch the resist during the process of aligning and adjusting the mask to the wafer. The mask is moved into contact with the wafer for wedge adjusting to ensure perfect alignment between the mask and the wafer. The flags are important when using the proximity setting as the idea of the mask not touching the resist will otherwise be lost. For hard- and vacuum contact the effect of flags are properly minuscule.

Although even more obscure settings can properly be found, these are the only to be

Table 7.2 – *There are many settings and parameters on the* EVG620 *which can be changed and adjusted. Some of the major settings which have been varied are shown in this table.*

Parameter	Possible Configurations	Comments
Exposure	Four possible configurations. Time or dose dependent, and for both of them either constant time/dose or interval.	Only the constant time or time interval options have been considered.
Filters	Four possible configurations; default, I line, SU-8 or C-TYP	All settings have been tried, but appears that it is only a software setting without any effect on the exposure.
Mask contact	Four possible configurations; proximity, soft, hard or vacuum.	Only proximity and soft contact have been used. The setting does not affect the exposure, only which critical dimensions can be achieved.
Purge during exposure	Two possible configurations; yes or no.	Flushes with nitrogen during exposure, both settings have been tried.
Alignment	First print and print, both comes in a top or bottom side and automatic or manual mode.	Only top first print manual has been used as we do not need alignment.
Purge before or after exposure	A purge can be added both before and after an exposure if wanted.	None of the possibilities for adding extra purges either before or after the exposure have been used.
Flags	Two possible configurations, in or out	Flags in has always been used.

considered during this project. Several settings have been tested, and Table 7.2 summarises the parameters of the *EVG620* together with some comments on what have been tested.

It should be clear that there are many parameters which can be adjusted during this step, which means that process optimisation can be extremely time consuming.

As standard the *EVG620* has an SU-8 filter which only leaves the I-line (365 nm), but at a reduced intensity. The intensity of the I-line has been adjusted to approximately 7 mW/cm^2, which is significantly different than the UV chamber used in the laboratory.

The SU-8 supplier recommends an exposure dose of 60-80 mJ/cm^2 for film thickness's between 0.5-2 μm [51]. With an effect of 7 mW/cm^2 this corresponds to 10 s of exposure. This exposure dose is optimised for silicon wafers and should for glass wafers be increased

by 50 % [51].

It is expected that the nanoparticles will influence cross linking and an increased exposure time of 1 min or 6 times the recommended dose is therefore initially tried. During the following step, development, all photoresist was however removed from the wafer indicating insufficient cross linking. Numerous experiments have therefore been performed where the exposure time is gradually increased up to a total exposure time of 30 min. None of these experiments did however improve the final result after development as all photoresist was removed. The exposure time has not been increased above 30 min as this is already an absurdly long exposure time.

Failure is however not an option as the initial lab experiments showed that it is possible to have deposited photoresist after development. changes will therefore have to be made to the process.

The long exposure dose entails switching to interval exposure to prevent possible T-topping. As a rule of thumb intervals should be used when the dose exceeds 250-300 mJ/cm^2, which is reached after 36-43 s with the used intensity. Interval exposures of 30 s UV followed by a 30 s waiting time was therefore chosen. The interval exposure should allow the resist to cool down between exposures. These interval exposures have again been done up to a total exposure time of 30 min. These experiments did not result in any improvement.

The next attempt was to include a nitrogen purge during exposure to see if this could help. Unfortunately no improvement was found with this approach.

Then all the possible filter combination was tried, meaning that instead of selecting the standard SU-8 filter in the software, both I-line, C-TYP and default was tried. It has however later been found that this is a software setting which is only relevant for constant dose exposures. As a result no improvement was of course found.

Despite the many attempts to structure the nanocomposite only failures were achieved. Additional consideration must therefore be given to reasons behind the inability to structure.

When SU-8 is correctly exposed a faint image of the mask should appear in the resist when placed on the PEB hotplate [51]. After the very long exposure tried in this project the mask pattern could be seen in the resist directly after the exposure. As an image can be seen something is definitely happening, but the process does not follow the guidelines of when the image should be observable and it should therefore be changed.

The best results which have been seen during development were obtained at random. At a few instances the resist fell of the wafer in the pattern of the mask which could indicate bad adhesion to the surface. The main reason for this to happen must be that the top layers of the resist have been exposed, but the bottom layer in contact with the wafer has not. If the bottom layer is not exposed, then the resist will not be cross-linked and will therefore dissolve in the developer releasing everything on top of it.

The problem with lack of adhesion was also described by Jiguet et al. [58], which they solved by exposing through the backside of a quartz wafer. This method does however impose several problems. At first you lose resolution as the distance between mask and resist becomes very large. They solve this problem by depositing amorphous silicon the

quartz wafer and then structuring this layer so it can be used as a mask. This does however significantly add to the complexity of the process, and this backside illumination method is not preferable as the possible usable materials are limited to those transparent in the near UV range. An additional problem for this method which is not addressed is the resulting surface roughness which will arise as parts of the top layer will not be exposed and thereby removed during development. The resist will in the end be irregular with very high surface roughness further limiting the possible uses.

To find the root of the problem it was decided to do an additional investigation of the added co-solvent to ensure that it did not affect the behaviour of the photoresist. The only co-solvent used until this point was DMSO and this solvent was therefore investigated.

DMSO Investigation

It was considered that DMSO could have a quenching effect on the UV light or somehow limit the photo activity of SU-8. The absorption of DMSO was measured, but showed that there should be no absorption at the used wavelengths.

Instead a test was performed to see how DMSO affects the photo activity of SU-8. Two small vials where filled with 3 ml SU-8 in both and an additional 1 ml DMSO in one of them. Then both vials were given 10 s of UV exposure in the UV chamber in the lab, after which the colour change was evaluated. To further evaluate the effect the vials were given an additional two times 10 s exposure, then 30 s followed by 1 min, 3 min, 5 min and 10 min UV exposure. The total UV exposure time after all exposures are 20 min. The colour development for both vials has been documented and is shown in Figure 7.7.

From this simple experiment it is clear that the addition of DMSO has a drastic effect on the cross-linking of SU-8 during UV exposure.

As said, DMSO does not really absorb in the wavelengths used for cross-linking SU-8 and the problem will therefore have to be explained by another effect. Instead the problem is most likely due to the fact that DMSO is a Lewis base [101] and can thereby stop the cross-linking reaction as this is initiated by a Lewis acid as explained in section 1.8. When the choice of co-solvent was made, this should have been considered, but nobody thought about that.

As DMSO cannot be used the backup co-solvent, acetonitrile, was therefore used instead for all further experiments. Acetonitrile is not a Lewis base and does not show any sign of prohibiting the cross-linking of SU-8.

7.1.5 UV Exposure – Part 2

Back in the cleanroom, but with acetonitrile as a co-solvent, the experiments with finding the correct procedure for UV exposure was continued.

Although the hopes were high with regards to the acetonitrile experiments, it was unfortunately found that there was absolutely no improvement in the final results.

Several quotes could be given here about falling and then getting back up, but I will just say that; sometimes life seems hard, and then it hits you in the face with a brick.

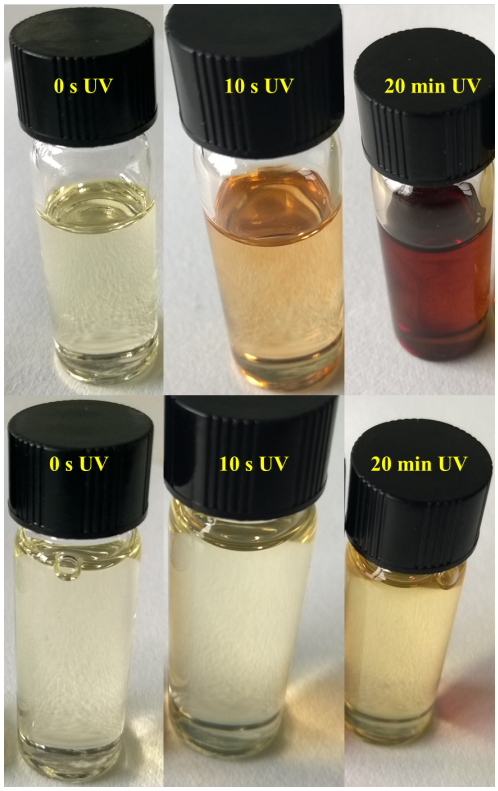

Figure 7.7 – *Picture of two vials before and after UV exposure. The top row shows a vial containing* 3 ml *SU-8, the bottom row shows a vial containing* 3 ml *SU-8 and* 1 ml *DMSO. Both vials are given the same UV exposure and some selected images; before exposure, after* 10 s *UV exposure and after* 20 min *UV exposure is shown. It is clear that the vial containing DMSO barely changes colour, which is significantly different from the pure SU-8 which darkens a lot.*

As it had been possible to structure the nanocomposite in the lab as explained in subsection 6.2.3 additional explanations to the cleanroom failure were considered. SU-8 is optimised for exposures in the range of 350 nm to 400 nm. Above 400 nm SU-8 is virtually transparent while at wavelengths below 350 nm it has a high actinic absorption. This explains why an exposure wavelength of 365 nm is used together with a filter that eliminates low wavelengths. All experiments in the lab were, however, made using a custom build UV chamber emitting in a very broad spectrum. To better resemble the lab conditions, the filter was therefore removed completely from the aligner. Intensity measurements at the I-line showed an increase from 7 mW/cm^2 to roughly 12.4 mW/cm^2 which agrees okay with the expectation of the filter normally reducing the I-line with 50 %.

The first experiment without a filter in the aligner involved an unknown, but very low concentration silver nitrate. The wafer received 5 min UV exposure and after development the result was as shown in Figure 7.8.

This first result without the filter is extremely promising. The microscope picture shows

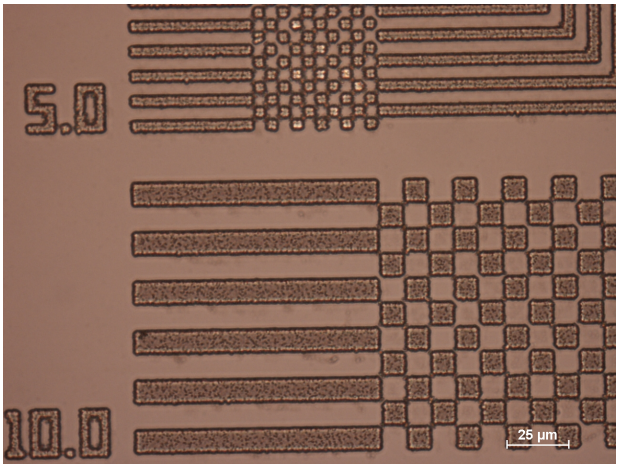

Figure 7.8 – *Microscope image at 50 times magnification showing part of the resolution marks which are on the wafer. The lines and squares are* 10 μm *and* 5 μm *respectively. The squares are supposed to touch in the corners, which mean that they are almost perfect. Clusters of nanoparticles can also be seen within the polymer.*

well defined structures with only a slight under exposure which should be possible to fix by increasing the exposure time a bit. At the same time nanoparticle clusters are also seen within the resist confirming the formation of nanoparticles.

Further testing with different concentrations of silver nitrate in the mixture revealed that the exposure dose was independent on the concentration. The optimal exposure time was found to be around 7.5 min, but this is not an exact number. The intensity of the I-line has varied between 11.80 W and 12.74 W. The intensity difference is equivalent to a missing exposure of 33 s for the low intensity if the total dose should be the same.

Although the dose appears to be independent of silver nitrate concentration a dependence can properly be found for very small concentrations indicated by the initial result of only needing 5 min UV exposure. Some additional tests were therefore performed with low concentrations of silver nitrate to find at which silver nitrate concentration an exposure of 5 min is enough. The lowest concentration of silver nitrate in acetonitrile used for these tests were 16 mg/ml, but 5 min UV exposure was found not to be enough for this. The initial result could be a random result, but it is assumed that for very low concentrations of silver nitrate the exposure dose changes.

Purging with nitrogen during exposure was used when achieving a structured nanocomposite. Although purging should not be necessary for SU-8 it was never tested whether this could be avoided or not.

SU-8 2 Composite

As it was mentioned subsection 6.2.1 ethanol was also chosen as one of the preferred solvents. It has, however, not been used that much since it requires using SU-8 2 instead of SU-8 2002. The amount of silver nitrate is also much lower than used in other experiments.

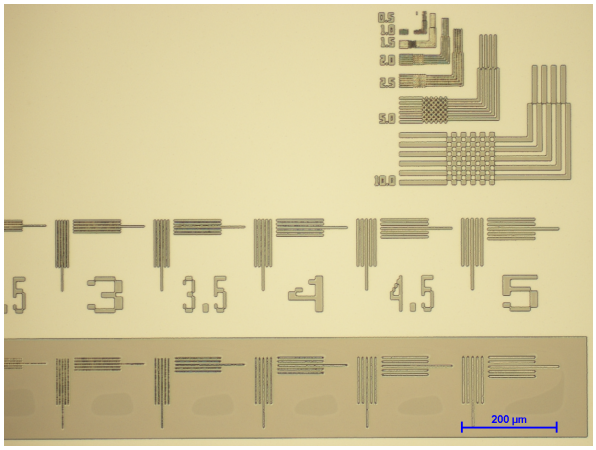

Figure 7.9 – *Microscope image of 10 times magnification of an in situ silver composite made with ethanol and SU-8 2. The resolution is seen to be good, but the nanoparticle agglomerates are hard to spot due to the low concentration.*

After successfully achieving a structured silver SU-8 2002 nanocomposite with acetonitrile a few experiments with ethanol and SU-8 2 were also performed.

The used procedure is identical to the one described for SU-8 2002 and acetonitrile, but the exposure time only 5 min. The amount of dissolved silver nitrate in ethanol was 10 mg/ml. For this combination the result after development, without removing the filter from the aligner is as shown in Figure 7.9.

The image clearly shows that this nanocomposite can be structured without removing the filter. There is still a prolonged exposure of 5 min, but this still provides a secondary silver nanocomposite.

As 5 min of exposure is enough to get good results it could indicate that the exposure time changes once the silver nitrate amount decreases to 10 mg/ml or less.

Resolution

The achievable resolution is important, and it has been shown that 5 μm seems to be the limit for the nanocomposites. The displayed images of resolution marks show that the 10 μm squares are always good while the 5 μm is bit short of perfection. It is, however, hard to evaluate if this resolution is good or bad without comparing it to what can be achieved using unmodified SU-8.

The same equipment and procedure is therefore used for a wafer with unmodified SU-8 2002. The exposure is done without removing the filter and for only 10 s. The resulting resolution marks are shown in Figure 7.10. The image shows that the resolution obtained with the pure SU-8 is almost identical to what have been obtained with the different nanocomposites. The 10 μm squares looks good, but the 5 μm could be slightly improved. The structures shown could be a bit more sharply defined, but are otherwise fine. The conclusion is that the resolution obtained for the nanocomposites are equally good as what

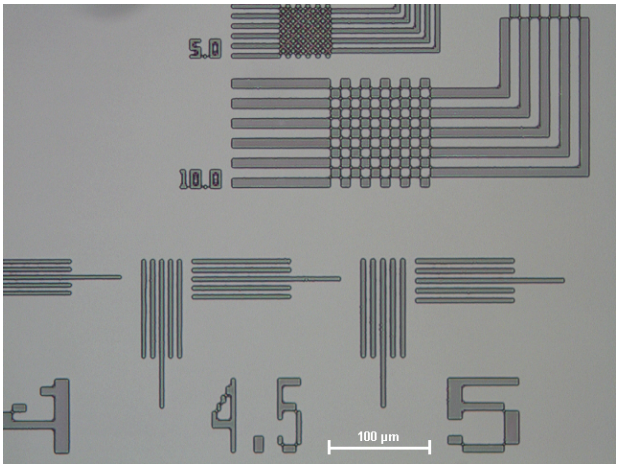

Figure 7.10 – *Microscope image at 20 times magnification of structured pure SU-8 2002. The 10 µm squares are perfectly developed, but the 5 µm squares could be better.*

can be obtained using unmodified SU-8.

This is very important since no special consideration needs to be taken with regards to resolution when using the nanocomposites of this project. It is also expected that if procedures and equipment are used which improves the resolution of unmodified SU-8, then this will equally improve the resolution of the nanocomposites.

7.1.6 PEB

Even though the nice results have already been shown, a few steps have still not been explained.

After exposure the PEB is performed. This step is very similar to the soft bake step made before the UV exposure. The PEB removes solvent from the resist and prevents diffusion of the active chemicals which could expand exposed areas. The baking also reduces any standing wave phenomenon which could have occurred. Standing waves, where reflections from the surface results in areas with high and low intensity through the resist, can result in ridges in the side walls once the resist has been developed.

The same parameters as in the soft bake, subsection 7.1.3, are available to change, and the process parameters have been chosen to be identical.

7.1.7 Development

The development step is properly the easiest of the steps as this involves agitating the wafer with exposed resist within a developer suitable for the chosen resist.

The developer dissolves any polymer which has not been cross-linked, or if it was a positive resist it would dissolve all polymers with broken bonds.

The developer for SU-8 is PGMEA and the only parameter to vary is the development time.

The developing procedure used involves two dedicated beakers with PGMEA in which the wafer is dipped in each for two minutes. The first one is to remove most of the composite, while the second is to ensure complete development of all the structures. Finally the wafer is rinsed with IPA and dried using a nitrogen gun.

The development time in each beaker is set to two minutes, but can be adjusted if necessary. The development is the least critical step in the entire process as the resist can easily be developed once more if two minutes is not enough to remove all unexposed resist. If the development time is too long, nothing really happens except whatever boredom one might experience.

Insufficient development is easy to spot as the rinsing with IPA will causes unexposed resist to become white.

7.1.8 Soft or Hard Bake

An additional baking step can be applied after development if desired. This baking step hardens the resist making it more durable such that it can better withstand further processing. The hardening of the resist is also important if it is to be used as a structure itself.

An additional heating step could also release any stresses which have appeared because of development as well as removing small cracks which could have appeared during processing.

The developed nanocomposites should be usable for fabricating free standing structures. A hard bake of 150°C or 300°C have therefore been applied to harden the resist. It was found that this drastically changes the final nanocomposite.

Dilution Series

A dilution series with DMSO was shown in section 6.2.3, if a similar dilution series is made for an acetonitrile composite the plasmonic absorption is as shown in Figure 7.11.

The spectra shows that for the highest amount of silver nitrate the maximum absorption lies at 345 nm as with DMSO, while the others are red shifted almost 15 nm. The peaks are very broad, so the actual difference might be smaller.

Figure 7.12 then shows the plasmonic absorption for the nanocomposite with the highest concentration of silver nitrate after the 95°C heat treatment and after a 300°C heat treatment for 30 min.

It can clearly be seen that the high temperature heating has a huge impact on the nanocomposite. The absorption maximum shifts towards lower wavelengths and is enhanced. The spectrum after heating also better resembles that of silver nanoparticles in cyclopentanone although there is a shoulder at higher wavelengths.

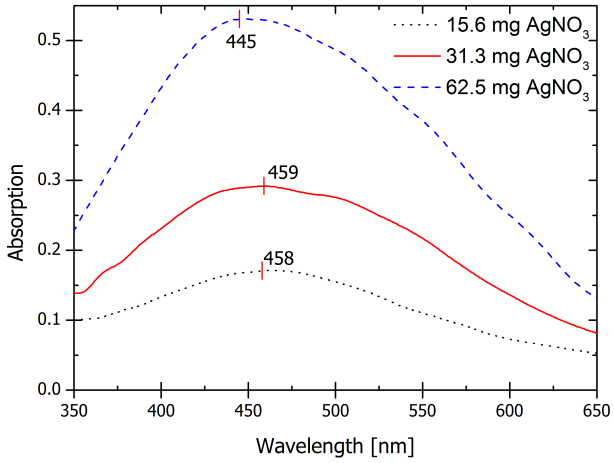

Figure 7.11 – *Absorption spectra for silver nanocomposites made with acetonitrile. The absorption maximum lie close for two of the nanocomposites while the last one is shifted more than 10* nm.

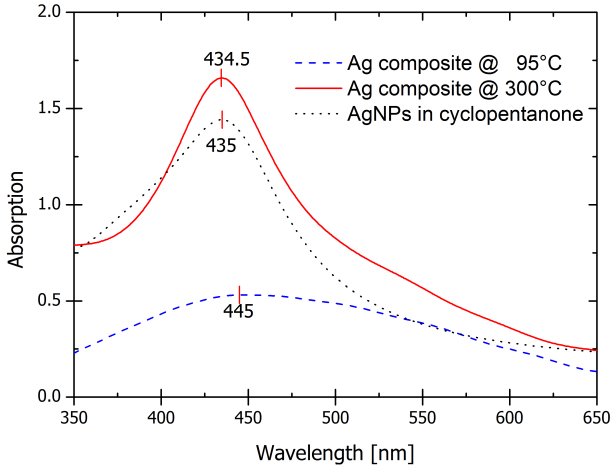

Figure 7.12 – *Absorption spectra of a silver nanocomposite after 95°C PEB and after an additional 300°C heating for 30* min. *An absorption spectrum for silver nanoparticles in cyclopentanone has been added for comparison, and it can be seen that the absorption maximum for the composites shifts towards lower wavelengths after heating and more resembles that of bare nanoparticles.*

Nanoparticle Formation

To confirm that the heating has resulted in the formation of nanoparticles a silicon wafer is prepared with the nanocomposite and broken in two pieces. One of the pieces is then investigated using SEM before it is heated to 300°C and investigated once more. The nanocomposite before the 300°C heat treatment can be seen in Figure 7.13 and after heating in Figure 7.14. The SEM images clearly show that the increased heat treatment

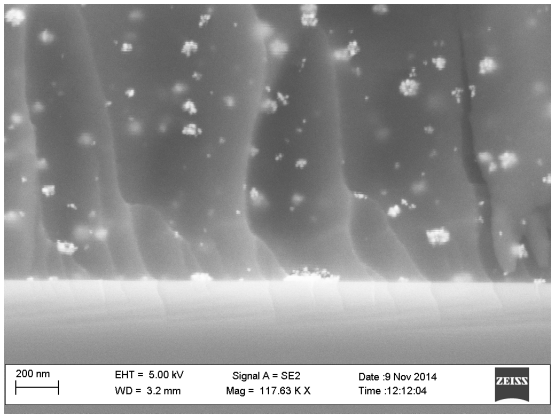

Figure 7.13 – *SEM image of a cross sectional view of a silver nanocomposite after heating to 95° C. Some larger agglomerates of around 100* nm *can be seen as well as individual nanoparticles of around 25* nm.

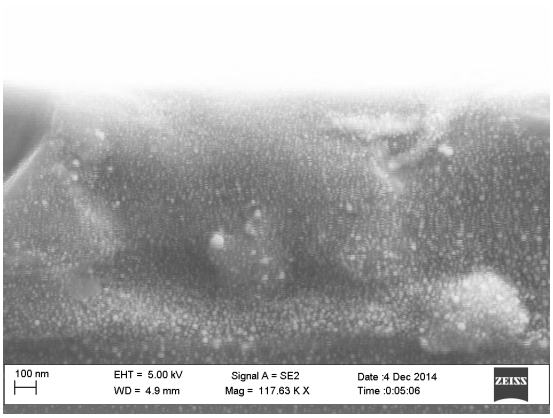

Figure 7.14 – *SEM image of a cross sectional view of a silver nanocomposite after heating to 300° C. Some larger agglomerates or particles can still be seen, but the vast majority is individual nanoparticles of 25* nm.

results in the formation of numerous new nanoparticles, and that no further growth of nanoparticles or already formed agglomerates can be seen. This explains the blue shift in wavelength for the absorption maximum as the 25 nm nanoparticles are dominant after heating, while the agglomerates are more important right after the 95°C PEB.

A silicon wafer has also been made with an *in situ* gold composite to see if the same effect could be seen here. The cross sectional images of a gold nanocomposite with 62.5 mg auric chloride before and after heating are shown in Figure 7.15 and in Figure 7.16.

From the SEM images it can be seen that the gold nanocomposite does not behave similar to the silver nanocomposite. More particles are formed, but not such that nanoparticles are all which can be seen. At the same time some larger formations of gold is also visible in between the smaller particles.

The less nanoparticle formation could be because the vast majority of auric chloride is reduced before the spinning has been completed. No matter the case, the gold composite is not as versatile as the silver composite regarding this temperature tuning.

7.2 Process Recipe

The process optimisation has been a tedious development involving a lot of variations. If all the variations should be thoroughly explained the thesis would turn in to a trilogy. Instead a sum-up is given as well as the final processes for making the nanocomposites.

The variations in UV lithography directly relevant for the possibility to structure the nanocomposite tested are:

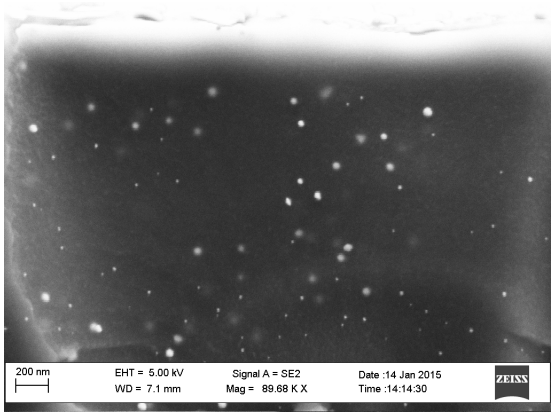

Figure 7.15 – *SEM image of the cross section of a gold nanocomposite. Nanoparticles of different sizes can be seen, the largest around 60* nm*. The particles appear to be randomly distributed, perhaps with a higher concentration towards the bottom.*

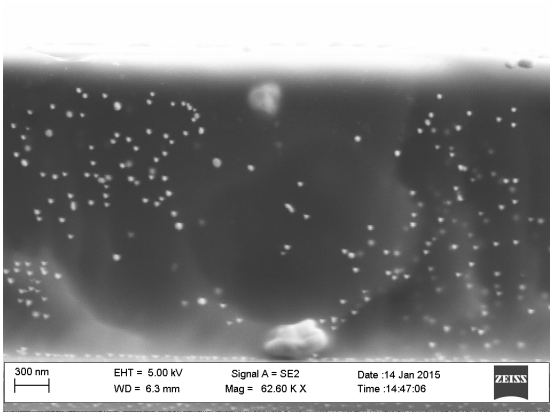

Figure 7.16 – *SEM image of the cross section of a gold nanocomposite after heating to 300° C. More particles can be seen, but also lumps of more than 200* nm*. The particles are not homogeneously dispersed in the composite.*

- Varying the exposure time between 1 min and 30 min.
- Doing constant or interval exposure, with and without nitrogen purge.
- Removing the filter from the aligner.
- Using different co-solvents.

The remaining, numerous, tests can all more less be considered to only effect the resolution, no matter how long time has been invested into that particular process step.

The majority of all tests were unsuccessful as the breakthrough was first achieved after removing the filter from the aligner. An idea conceived because of some structuring success achieved outside the cleanroom in a UV chamber.

Therefore it is great to be able to describe a working recipe obtained under great distress.

1. Place wafers, silicon of fused silica, in a 250°C oven for at least four hours.
2. Dissolve a desired amount of $AgNO_3$ in acetonitrile.
3. Add 0.5 ml of the $AgNO_3$ in acetonitrile solution to 4 ml of SU-8 2002 and give it a gentle shake to ensure complete mixing.
4. Quickly spin the SU-8 mixture on the wafer before particles start to form. The parameters for spinning is 1500 RPM for 1 min with an acceleration of 500 RPM/s.
5. Soft bake the wafers on a hotplate at 95°C for 10 min.

6. Do a UV exposure using interval exposure with 30 s exposure and 30 s wait time. The number of cycles should be around 15 and are independent on $AgNO_3$ concentration. Set the aligner to do purge during exposure and remove any filter before exposing.
7. Do a PEB of the wafers at a 95°C hotplate for 10 min.
8. Develop the wafers in PGMEA bath for 2 min followed by 2 min in a second PGMEA bath.
9. Rinse the wafers with IPA and dry.
10. Do a hard bake at 300°C if wanted.

This procedure has been used to fabricate is the best *in situ* silver nanocomposite achieved during this project. This was done with the SU-8 2002 photoresist, but a different procedure was found to work for SU-8 2 with ethanol as the co-solvent. The amount of silver nitrate which can be used is limited, but there is a clear advantage of not needing to remove any filter from the aligner.

The process which has also been found to work, involves dissolving $AgNO_3$ in 96 % ethanol which can be kept as a stock solution. This solution is compatible with SU-8 2 resulting in this alternative process flow:

1. Make a stock solution of $AgNO_3$ in 96 % ethanol, the maximum concentration possible is 31 mg/ml.
2. Place wafers in a 250°C oven for at least four hours.
3. Add 0.5 ml of the $AgNO_3$ in ethanol stock solution to 4 ml of SU-8 2.
4. Spin the SU-8 mixture on the wafer using the parameters 1500 RPM for 1 min with an acceleration of 500 RPM/s.
5. Soft bake the wafers on a hotplate at 95°C for 10 min.
6. Do an interval UV exposure with 30 s exposure and 30 s wait time. Use 10 cycles and do purge during exposure.
7. Do a PEB of the wafers at a 95°C hotplate for 10 min.
8. Develop the wafers in PGMEA bath for 2 min followed by 2 min in a second PGMEA bath.
9. Rinse the wafers with IPA and dry.
10. Do a hard bake at 300°C if wanted.

It must be mentioned that the exposure time is not optimised, but assumed to be around 5 min because of the previously mentioned experiments.

It has also been possible to produce an *in situ* gold composite with auric chloride dissolved in cyclopentanone. The process follows that of the *in situ* silver composite with SU-8 2002, but the particle formation initiates much faster, within 20 s, than for silver. Due to the rapid formation of gold nanoparticles the entire process does however need to be optimised as the obtained results are not good. It can also be argued that for gold the process is not really *in situ* as the particles are formed before spinning.

For gold it has also been possible to make an *ex situ* composite using the particles described in subsection 4.1.2 which have then been transferred to SU-8. The process has

again been identical to that of *in situ* silver, and with good results. The difference is that instead of mixing the precursor with co-solvent and SU-8 the SU-8 nanoparticle sol is used directly instead. The *ex situ* procedure is preferred for the gold nanocomposite.

Achieving metal nanocomposites which be structured at the micro scale is a great result. Although the process is not completely optimised it has been shown both gold and silver nanocomposites can be used. One of the goals of the project was also to make a conductive composite which will be described in the next chapter.

Chapter 8

Conductive Composites

It was mentioned in section 1.9, that SU-8 has been used in connection with silver nanoparticles to make a conductive composite. A conductive composite was also one of the original main goals of this research project and a lot of time has therefore gone into this work.

Nanoparticles have in general been used in many composites to enhance conductivity. Metal nanoparticles are used because of their good electric conductivity, and electric conductivity for the entire composite material is achieved when the amount of nanoparticles increase above a certain value known as the percolation threshold. Nanocomposite conductivity has been found to agree very well with theoretical percolation values where the nanoparticles form a connecting structure [102]. This means that besides the optical effects which are present even at low nanoparticle loading, high loading results in conductive materials further adding functionality. For silver nanoparticles the percolation threshold has been shown to be at 3.9 wt.% [59] while the general theory for perfectly dispersed spherical particles the percolation threshold is to be expected at 12 wt.% [103].

Even if a conductive nanocomposite cannot be achieved it might still be useful as nanoparticle loadings just below the percolation threshold can be utilized for making materials with very high dielectric constants. Although the breakdown strength of the composite might decrease when nanoparticles are introduced, an increase in dielectric constant is definitely found and nanoparticles are much better than microparticles [104]. Materials with high dielectric constants are interesting for use in for instance super capacitors.

The focus is however on conductive silver nanocomposites.

8.1 Fabrication of Conductive Composites

The attempt towards a conductive nanocomposite has only been performed outside the cleanroom because of the problems with spinning resists with high loadings of silver nitrate as shown in section 7.1.2. This problem was not encountered in the lab, or at least not noticed.

The process initially used for attempting to make a conductive composite was.

1. 1 ml of 0.5 mg/ml $AgNO_3$ in DMSO is added to 2 ml of SU-8 2002.
2. The mixture is spun on a 50 mm silicon Piranha cleaned wafer at 1000 RPM for 30 s.
3. The wafer is placed on a 95°C hotplate for 10 min.
4. The wafer is given a 1 min UV exposure.
5. The wafer is placed on a 95°C hotplate for 10 min.
6. The temperature on the hotplate is increased to 150°C .
7. The wafer is removed from the hotplate after 30 min.

This resulted in a wafer where the deposited film had a grey colour resembling that of pure silver. To see if conductivity had been achieved a quick test was done where two probes connected to a multimeter was placed on the surface. This procedure did however not result in any conductivity.

As the wafer looked very metallic it was investigated whether an additional heating would have any effect. The wafer was therefore placed on the hotplate once more, but this this time the temperature was set at 300∘C. 300°C was chosen as the SU-8 should be able to handle this temperature, and also because it is above the melting temperature for silver oxides [97]. The wafer was heated for 30 min.

After this second heat treatment no visible difference could be seen on the wafer, but measurements with the multimeter showed that the composite had become conducting. 4-point probe measurements which could give values for contact resistance, sheet resistance and if it was a surface current or structural current was unfortunately not done. The measurements with the multimeter however indicated that resistances as low as 7 Ω across the wafer could be achieved.

To test reproducibility and confirm that the high temperature treatment at 300°C was responsible for the conductivity, additional composites were made following the same procedure except they did not receive a 150°C bake, but was placed directly at 300°C after the bake at 95°C.

After 30 min of heating at 300°C the composites were tested for conductivity, but none could be found! The wafers were therefore given another 30 min at 300°C , but still showed no conductivity.

It was therefore decided to return to the exact same procedure as originally. The wafers where given a 150°C treatment followed by a 300°C treatment. When this procedure was followed the composites were again conductive. The correct heating is therefore a very critical step.

Further testing has also shown that placing the wafers on a programmable hotplate which increases the temperature with 1°C/min also resulted in conductive composites.

A possible explanation of the process has also been considered. Most likely the particles are formed at the lower temperature and then fused together when the temperature is increased. If the high temperature is used immediately the SU-8 hardens before enough particles have been formed and are thereby creating a separating layer between the particles.

A SEM investigation helps to understand the structure of the conductive nanocomposite. Although very inhomogeneous, a zoom on the conductive areas look like as shown in

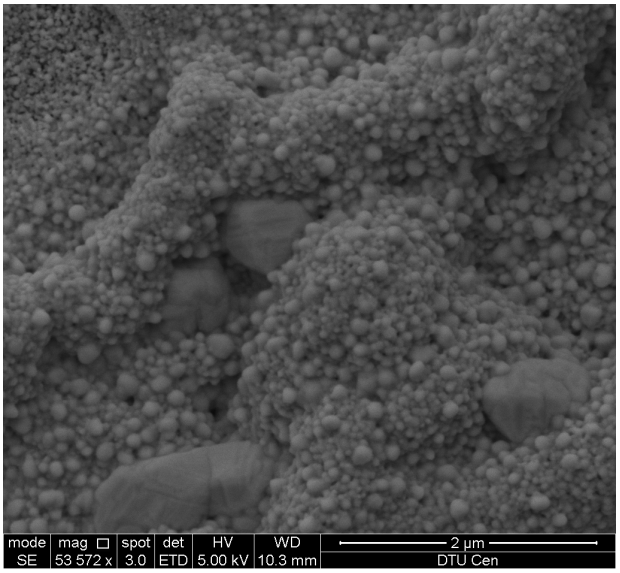

Figure 8.1 – *SEM image of fabricated silver nanocomposite. High surface roughness can be seen, but it is also clear that numerous small silver nanoparticles form a connecting structure resulting in the conductivity. Some larger particles can also be seen.*

Figure 8.1. In a small conclusion on the conductivity you could say that one small step in the process results in a giant leap for the nanocomposite functionality.

8.2 Conductive Silver Nanocomposite Comparison

The achieved conductive silver composite should be compared to what is commercially available.

The work of Jiguet et al. [62] has resulted in the possibility to buy a commercial conductive SU-8 composite with silver nanoparticles. The composite still suffers from the inability to use spin coating and problems with front side exposure, but a sample was acquired for comparison.

The commercial composite was deposited on a wafer and the conductivity measured. The exact values were again not measured, but the conductivity was definitely much higher than for the one produced in this project. The datasheet for the commercial composite reports a conductivity of 10-1000 S/cm^2 [105], which is then the target value that should also be achieved with further development.

The commercial silver nanocomposite was deposited on the wafer using the following procedure.

1. 3 ml of commercially available conductive SU-8 is spun on a 50 mm silicon Piranha cleaned wafer at 1000 RPM for 30 s.
2. The wafer is placed on a 95°C hotplate for 10 min.
3. The wafer is given a 1 min UV exposure.

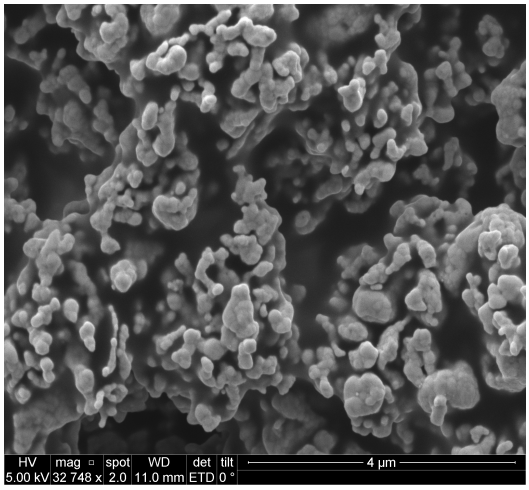

Figure 8.2 – *SEM image of commercially available SU-8 silver nanocomposite. The composite is seen to consist of a sort of weathered silver structure made from the nanoparticles in the resist.*

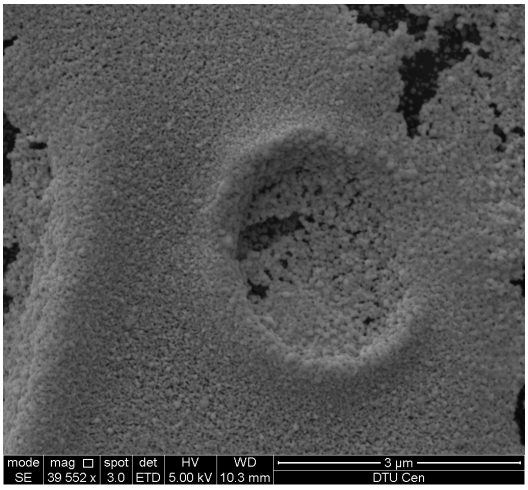

Figure 8.3 – *SEM image of conductive silver composite made in this project. The composite consist of a somewhat layered structure of connected nanoparticles.*

4. The wafer is placed on a 95°C hotplate for 10 min.
5. The temperature on the hotplate is increased to 150°C .
6. The wafer is removed from the hotplate after 30 min.

The commercial silver composite and the conductive silver composite from this project were also investigated with SEM to see the difference in structure. Images at roughly the same magnification are shown in Figure 8.2 and Figure 8.3.

While comparing, it can be seen that the commercial one has a more branched surface where the nanoparticles are fused together in a series of structures making it hard to distinguish the original nanoparticles. On the other hand, the nanocomposite from this project has a much more layered structure in which the original nanoparticles are much easier to distinguish. It was also found that the commercial composite was deposited very homogeneous across the wafer while the nanocomposite from this project had a very inhomogeneous coverage. The inhomogeneity of the deposited layer is also something which has to be improved if it should be used as a conductive nanocomposite.

From the images it is easy to conclude that the composite from this project has a more optimal structure, but as long as it is not homogeneous across the wafer, this would be a stretch. As the conductivity of the nanocomposite from this project is also much lower, the commercial composite is unfortunately at the moment the better choice.

Only a few attempts have been made on fabricating a conductive gold nanocomposite, but none of these where successful. The dielectric constant of the unsuccessful nanocomposites should however be measured in future work as the material might be useful for super capacitors.

Chapter 9

Conclusion

This Ph.D. has involved a lot of experiments, testing and process optimisation. The majority of which has been explained in the previous chapters. In this chapter the major findings are collected once more and some final remarks and conclusions are given.

It was in the introduction, with some examples, explained how nanocomposites are extremely interesting because of the unique properties of the used nanoparticles which properties are maintained in the final composite. The focus of the Ph.D. was metallic nanocomposites, in particular gold and silver nanocomposites. The nanocomposites should be useful for micro-and nanofabrication and it was chosen to go for the epoxy based photoresist SU-8. Not many SU-8 gold nanocomposites have been reported, but some SU-8 silver nanocomposites are described in literature, although with some significant process incapabilities. These process difficulties were described and one of the goals to overcome these.

The introduction also briefly touched upon green chemistry and how all processes in this project should follow these guidelines.

The remainder of this chapter follows the general structure of the thesis and the conclusions will explain how both SU-8 gold and silver nanoparticles have been successfully fabricated and how the processing problem previously experienced with SU-8 silver nanocomposites have been overcome.

9.1 Nanoparticle Synthesis and Stabilisation

The first part of the project revolved around nanoparticle synthesis, coating with organic polymers to increase colloidal stability and transfer into organic solvents.

Gold Nanoparticle Synthesis

Gold nanoparticles were synthesised using the very well-known Turkevich method and characterised using TEM and UV-Vis spectroscopy.

The nanoparticle diameter was estimated from absorption maximum and equation 2.1 and confirmed by TEM investigation. Synthesised gold nanoparticles have been stable for the entire three year duration of this project.

Synthesis of gold nanoparticles should be easy the main conclusion is in agreement with this.

- Long-time stable 22 nm large spherical gold nanoparticles have easily been synthesised.

Silver Nanoparticle Synthesis

Silver nanoparticle synthesis was not as straight forward as the gold nanoparticle synthesis as many different methods are being using by different research groups. The many synthesis methods for silver nanoparticles are also not as forgiving as the gold nanoparticle syntheses with regard to irregularities in the process parameters. It was decided to try two different, but simple methods of silver nanoparticle synthesis in water.

Both methods result in almost identical nanoparticle concentrations. The nanoparticle diameter could not be estimated from the absorption maximum, but UV-Vis and TEM investigations were done none the less. All synthesised silver particles have also been stable for the entire three year duration of this project.

The main conclusion found regarding the silver nanoparticles was then.

- Long-time stable spherical silver nanoparticles have been synthesised by two methods.
- The Mulfinger procedure is superior to the Giuffrida method regarding size distribution of the nanoparticles.

Polymer Coating of Nanoparticles

After synthesis the colloidal stability of the particles were enhanced by coating with organic polymers. Two different biocompatible amphiphilic block co-polymers were chosen, PVP/VA and PVA-COOH.

The nanoparticles were coated using a post grafting technique in which the polymer dissolved in water was added to the synthesised particles and shaken for a long time.

The colloidal stability of the coated gold nanoparticles was later tested to show that PVA-COOH is incompatible with SU-8 which led to the silver nanoparticles only being coated with PVP/VA.

The conclusions for this post grafting coating method were:

- Gold nanoparticles can be coated with both PVP/VA and PVA-COOH and shows good stability.
- PVA-COOH coated particles appear to have higher colloidal stability than PVP/VA coated particles.
- PVA-COOH is not compatible with SU-8.

- Silver nanoparticles can be coated with small amounts of PVP/VA.
- Large amounts of PVP/VA polymers results in colloidal instability of the silver nanoparticles.
- Silver nanoparticles synthesised using the Mulfinger procedure is more stable than following the Giuffrida method.
- Post grafted gold nanoparticles can be suspended and are stable in most organic solvents, but not SU-8.

To further increase the colloidal stability two pre grafting methods in which the polymer is present during nanoparticle synthesis were developed, one method for gold nanoparticles and one for silver nanoparticles. There was a general increase in stability and higher nanoparticle concentrations could be directly synthesised. The conclusions were:

- Long time stable PVP/VA pre grafted gold and silver nanoparticles have been synthesised.
- Pregrafting results in more non-spherical gold nanoparticles.
- Higher initial nanoparticle concentration can be achieved with the pre grafting method.
- The colloidal stability of the pre grafted nanoparticles is enhanced compared to comparable post grafted nanoparticles.
- Pre grafted nanoparticles can be suspended and are stable in SU-8.

Solvent Exchange

Solvent exchange proved to be one of the most difficult parts of this project. Three different methods with their own advantages and disadvantages were tried.

Centrifugation was tested as it often used for nanoparticles and had successfully been applied in another project. It was tested with both PVP/VA and PVA-COOH coated gold particles, but the PVA-COOH coated particles have a colloidal stability so high that they could not be centrifuged down. After centrifugation the PVP/VA coated particles were dried in a desiccator, but could then not be suspended in organic solvents.

Freeze-drying was found to result in nanoparticle agglomeration due to phase separation. This was always the case for post grafted silver nanoparticles and sometimes for post grafted gold nanoparticles. Later tests have indicated that phase separation is not a problem for pre grafted gold nanoparticles.

The third method tried was evaporation under reduced pressure. It was found that complete drying resulted in an inability to suspend in organic solvents similar to what was experienced when using centrifugation. Co-evaporation of solvents was adopted instead where the particles never reach a dry step. This was found to be very effective.

In total the main conclusions of the solvent exchange were:

- Completely dried particles cannot be suspended in organic solvents.
- Freeze-drying of post grafted nanoparticles result in phase separation and agglomeration.
- Co-evaporation of solvent can be used to transfer pre grafted nanoparticles into SU-8.
- Freeze-drying appears to be a viable method for pre grafted gold nanoparticles.

9.2 Nanocomposites

The second part of this thesis revolved around actual nanocomposites of SU-8 and either gold or silver. The first nanocomposites were made using the previously synthesised and described nanoparticles in a process called *ex situ*.

Ex Situ Nanocomposites

For the *ex situ* composites attempts were made to use both post and pre grafted nanoparticles. It was not possible to use the post grafted silver nanoparticles while the post grafted gold nanoparticles resulted in a nanocomposite consisting of different domains. These domains were either large gold nanoparticle agglomerates or individually suspended gold nanoparticles.

Better success was obtained using pre grafted nanoparticles which resulted in a gold nanocomposite with individually dispersed nanoparticles. It has also been possible to produce a silver nanocomposite using this method, but it has not been reproducible.

The plasmonic absorption for both the gold and silver nanocomposite was found to resemble that of the nanoparticles before cross-linking the SU-8. The gold nanocomposite was also structured with a resolution of approximately 5 μm.

The main conclusions for the *ex situ* nanocomposites were:

- Post grafted nanoparticles cannot be used for making nanocomposites.
- Pre grafted gold nanoparticles can be used to make a nanocomposite.
- The procedure for making a nanocomposite using pre grafted silver nanoparticles is not reproducible.
- The gold nanocomposite can be structured using UV lithography.

In Situ Nanocomposites

Alternative methods for nanocomposite fabrication were also developed. The *in situ* approach utilises the fact that SU-8 reduces the used metal precursors and forms nanoparticles.

The method was found to not be that suitable for gold nanocomposites as nanoparticle formation happens within 20 s. The main challenge with the silver nanocomposite was to select a suitable co-solvent as the metal precursor cannot be dissolved directly in SU-8 or cyclopentanone. DMSO was chosen as the preferred candidate while ethanol could be used in connection with the unpreferred SU-8 2 formulation.

It was found that cross-linking of the SU-8 was possible and that numerous silver nanoparticles are formed within the polymer matrix. The plasmonic absorption was also measured for nanocomposites with varying amounts of silver nitrate to find a correlation between maximum absorption and initial silver nitrate amount. The plasmonic absorption also showed that the nanocomposites behaved similarly, but that the absorption maximum was red shifted compared to pre synthesised nanoparticles.

The main conclusions for the *in situ* nanocomposites were:

- The *in situ* approach is not that well suited for a gold nanocomposite.
- The *in situ* approach is very effective in fabricating a silver nanocomposite.
- The silver nanocomposites show a red shifted position of the absorption maximum compared to pre synthesised silver nanoparticles.
- It is possible to cross-link the SU-8 making it possible to structure the nanocomposite.

Process Optimisation

The process optimisation has almost entirely been done on *in situ* silver composites. The process has for much of the time been almost good, but unsuccessful in the end due to incomplete cross-linking of the SU-8. It was discovered that DMSO is a contributing factor in preventing cross-linking of SU-8 and the co-solvent was switched to acetonitrile.

After switching to acetonitrile cross-linking was still not possible until removing the filter from the used aligner. After removing the filter an exposure time of 7.5 min was found to result in a resolution of 5 μm in the structured nanocomposite. It was also found that for the used amounts of silver nitrate the exposure time is independent on silver nitrate concentration. It was, however, discovered that the spinning became inhomogeneous for high amounts of silver nitrate.

Test with ethanol and SU-8 2 also resulted in a structurable nanocomposite with a resolution of 5 μm. This was achieved without removing the filter and with an exposure time of only 5 min. The differences in exposure can perhaps be becomes of the lower amount of silver nitrate when using ethanol. This also indicates that the exposure time could be dependent on the silver nitrate amount for low values.

It was also found that a high temperature treatment resulted in the formation of numerous new nanoparticles without growth or agglomeration of already present nanoparticles. This formation of new nanoparticles also led to a blue shift of the plasmonic absorption such that absorption maximum again resembles that of pre synthesised nanoparticles.

The main conclusions for the process optimisation were:

- DMSO inhibits cross-linking of SU-8.
- *In situ* silver nanocomposites can be structured with a resolution of 5 μm when acetonitrile is used as co-solvent and the filter removed from the aligner.
- A silver nanocomposite which can be structured without removing the filter can be achieved by using ethanol as the co-solvent and SU-8 2.
- The exposure time might vary for small amounts of silver nitrate but are independent of silver nitrate amount for large concentrations.
- High temperature treatments results in the formation of numerous new nanoparticles.

Conductive Composites

Some work did also go into achieving a conductive composite. It was never achieved for any gold nanocomposite, but high temperature treatment of silver nanocomposites containing large amounts of silver nitrate resulted in a conductive composite.

The conductive silver nanocomposite was compared to a commercially available product, and although the structure of the fabricated nanocomposite appears to be favourable the conductivity is not yet high enough to effectively compete with the commercial product.

The main conclusions for the conductive composites were:

- It has not been possible to fabricate a conductive gold nanocomposite.
- A conductive silver nanocomposite can be fabricated if the correct heating procedure is used.
- The produced conductive nanocomposite appears to have a favourable structure compared to a commercially available product.
- The achieved conductivity needs to be approved before the nanocomposite is competitive.

9.3 Final Conclusion

In some final words it can be concluded that the goal of this project was to develop new metallic nanocomposites for micro- and nanofabrication. This goal has been achieved, although with some difficulties.

A total of three working procedures have been developed resulting in one gold nanocomposite and two silver nanocomposites. One of the additional goals of making a conductive nanocomposite has also been achieved.

So with all this in mind the ultimate conclusion is that the project was a success, but possibilities do of course exist for improvements.

Chapter 10

Outlook

In this chapter some of the many ideas for moving forward are presented.

As expected everything has not gone exactly as planned, some will even claim that it has been a long series of failures before achieving the desired result, but as Niels Bohr once said; *an expert is a man who has made all the mistakes which can be made, in a narrow field.*

10.1 Fabrication and New Materials

It has been proven in this project that it is possible to fabricate nanocomposites and structure them on the micrometre scale. Some possibilities for future optimisation does however exist within the fabrication of the nanocomposites as well as some other materials could be tested.

Solvent Exchange

The solvent exchange was one of the main difficulties on the route towards *ex situ* composites. Co-evaporation of solvents was adopted, but freeze-drying seems to be a viable option for pre grafted gold nanoparticles. It should be confirmed that freeze-drying is indeed a viable option as this method is preferred.

If freeze-drying could also be found to work for silver nanoparticles this would of course also be an advantage.

Solvents

For the *in situ* silver nanocomposites the co-solvent was found to be very important. The majority of the work was focused on DMSO which did not work during this project and then acetonitrile. Other solvents should be investigated to see if they have advantageous properties. Benzonitrile which was not tested due to availability seems like an interesting alternative to acetonitrile. It has a higher solubility and is less toxic.

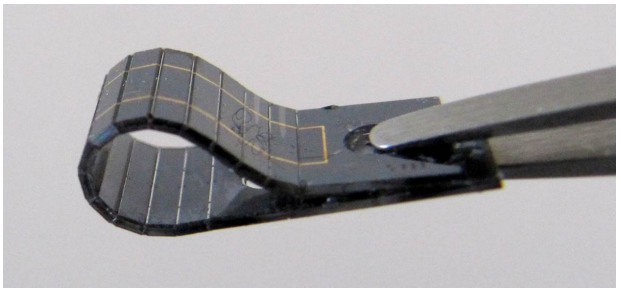

Figure 10.1 – *A flexible sensor developed at DTU Nanotech for measuring the oxygen level in the brain on premature born babies.*

Photoresists/Polymers

This work has focused entirely on SU-8 nanocomposites it could however be an advantage to have nanocomposites consisting of other polymeric materials than SU-8.

As an example more elastic polymers could be considered for fabrication of very flexible conductors which can be defined on a micro scale. Although flexible screens and electronic papers exist this new functionality could be interesting within sensor fabrication, as for instance the flexible sensor for neonatales shown in Figure 10.1.

These new polymers should preferably also be some sort of a photoresist, but this demand can be discarded as long as structuring is possible.

Other formulations of SU-8 than the primarily used SU-8 2002 should also be tested. It is unknown whether a higher amount of epoxy resin in the SU-8 formulation will solve for instance the problem of silver island formation at high silver nitrate loadings.

The entire process of nanoparticle formation for the *in situ* nanocomposites are unknown and should in general be investigated. One thing which could be considered is to add extra amounts of the photo initiated salts to the SU-8 mixture. A hunch is that the salts are the primary initiator for the nanoparticle formation. If some of the salt is depleted during nanoparticle formation this could also explain some of the problems with later cross-linking of the resist.

Nanoparticles

Gold and silver were the choice of material for this Ph.D. project. Depending on the final application of fabricated devices different metals might be advantageous. Standard metals such as aluminium and copper could therefore be interesting for the nanoparticles, but also more exotic materials such as platinum or palladium.

Conductivity

A working process for the conductive composite was never achieved inside the cleanroom. This has to be achieved before any hopes of having a competitive nanocomposite can be achieved. There are three main speculations to why it was not achieved.

One is that very poor thinfilm homogeneity was also experienced outside the cleanroom, but never considered due to less thorough evaluation of the spinning results.

The second possibility is an unknown effect of the Piranha clean. The Piranha clean is the most significant difference between the lab experiments and the cleanroom work. This can easily be tested by Piranha cleaning a wafer in the cleanroom before proceeding with the dehydration and spinning procedure.

Thirdly the spinning speed could be important. 1000 RPM has been used for several tests outside the cleanroom, but never inside the cleanroom. A slower rotational speed could give some improved results with high silver nitrate loadings.

UV Exposure and Silver Nitrate Concentration

It was found that the exposure time was independent on the amount of silver nitrate added to the SU-8. The very first structured nanocomposite did however receive less exposure indicating that an effect could be there at low concentrations.

No effect was found down to 16 mg/ml of added silver nitrate, but as the SU-8 2 and ethanol composite with only 10 mg/ml silver nitrate also needed less exposure further investigations are needed.

Experiments starting at 10 mg/ml silver nitrate and decreasing the amount from this value to see if the exposure time also decreases should be done.

Heat Treatment

The last main thing regarding fabrication which should be investigated is all the heat treatments. The supplier recommends a 1 min soft bake after spinning and before exposure. This is in contrast to the 10 min used in this project and as standard in DTU Danchip. As it is known that nanoparticles are formed during heat treatments a shorter soft bake time might be advantageous. If fewer nanoparticles are formed before UV exposure cross-linking might be easier.

The high temperature heat treatment in the end of the process should also be investigated. For the conductive nanocomposite the exact time and temperature to achieve conductivity is unknown. It is also still a mystery why a direct placement on a hotplate set at 300°C did not result in a conductive nanocomposite.

10.2 Characterisation

As the final materials have not been obtained until very late in the project, some characterisations still need to be done. For all nanocomposite materials the actual amount of metal in the nanocomposite is unknown and should be investigated. No theoretical estimation can be made as it is unknown how much metal is lost during spinning.

Four point probe measurements on some of the nanocomposites also need to be done. These are especially important for conductive composites to find sheet and contact resistance, but also those materials which could be useful as super capacitors. These mea-

surements will also give information about how the current travels; surface currents or structural currents.

10.3 Applications

It was never accomplished to use the developed nanocomposites in any form of devices or applications. Some thoughts must however go into current and future possible applications for the material.

The characteristic plasmonic resonance for the nanoparticles is maintained within the composite. The material is therefore a great candidate to be used in different optical sensors. The exact application must, however, be chosen by experts within this field.

Another large field of applications are biological sensors. Silver nanoparticles are good for preventing bacterial growth while SU-8 has good biocompatibility. Before the material is used in biological applications is must however be investigated how well nanoparticles are encased in the polymer. Nanoparticles or metal ions could leak from the nanocomposite and this needs to be known to determine which kind of applications the nanocomposite can be used for. An interesting parameter to investigate would be whether nanoparticle or metal ion release could be controlled by adjusting a connected current.

The nanocomposite could also be interesting as a material for electrodes as composite electrodes in general have attracted a lot of attention during the last decade. Maybe the composite could be useful within electrochemistry, or as a material within a super capacitor.

If an acceptable conductive composite is achieved several applications also exists. An example could be easy readout SU-8 cantilevers where the impedance changes with vibration and attached particles. Easy depositioning and structured nanocomposites could also be preferred over the standard metal deposition used currently. If thin flexible conductors can be made this opens up an enormous window of opportunities to be explored.

There are also other projects at DTU Nanotech in which the conductive nanocomposite could be interesting. In one project gold electrodes are used for dielectrophoresis, but these are insufficient for the current needs.

So basically there is lot which can still be done, but the possibilities are equally large.

Bibliography

[1] Britannica Encyclopædia. composite, June 2014. URL http://www.britannica.com/EBchecked/topic/130093/composite-material. 3

[2] Anthony Kelly. Composite materials after seventy years. *Journal of Materials Science*, 41(3):905–912, February 2006. ISSN 0022-2461, 1573-4803. doi: 10.1007/s10853-006-6569-9. URL http://link.springer.com/article/10.1007/s10853-006-6569-9. 3

[3] Anna C. Balazs, Todd Emrick, and Thomas P. Russell. Nanoparticle Polymer Composites: Where Two Small Worlds Meet. *Science*, 314(5802):1107–1110, November 2006. ISSN 0036-8075, 1095-9203. doi: 10.1126/science.1130557. URL http://www.sciencemag.org/content/314/5802/1107. 3

[4] S R Bakshi, D Lahiri, and A Agarwal. Carbon nanotube reinforced metal matrix composites - a review. *International Materials Reviews*, 55(1):41–64, January 2010. ISSN 0950-6608. doi: 10.1179/095066009X12572530170543. URL http://www.maneyonline.com/doi/abs/10.1179/095066009X12572530170543. 3

[5] Hiroaki Miyagawa, Manjusri Misra, and Amar K. Mohanty. Mechanical properties of carbon nanotubes and their polymer nanocomposites. *Journal of Nanoscience and Nanotechnology*, 5(10):1593–1615, October 2005. ISSN 1533-4880. 3

[6] Aysha Chaudhary, Joseph O. Welch, and Richard B. Jackman. Electrical properties of monodispersed detonation nanodiamonds. *Applied Physics Letters*, 96(24):242903, 2010. ISSN 00036951. doi: 10.1063/1.3446966. URL http://link.aip.org/link/APPLAB/v96/i24/p242903/s1&Agg=doi. 3

[7] Michael Faraday. The Bakerian Lecture: Experimental Relations of Gold (and Other Metals) to Light. *Philosophical Transactions of the Royal Society of London*, 147:145–181, January 1857. ISSN 0261-0523,. doi: 10.1098/rstl.1857.0011. URL http://rstl.royalsocietypublishing.org/content/147/145. 3

[8] K. Lance Kelly, Eduardo Coronado, Lin Lin Zhao, and George C. Schatz. The Optical Properties of Metal Nanoparticles: The Influence of Size, Shape, and Dielectric Environment. *The Journal of Physical Chemistry B*, 107(3):668–677, January 2003. ISSN 1520-6106. doi: 10.1021/jp026731y. URL http://dx.doi.org/10.1021/jp026731y. 3

[9] Marie-Christine Daniel and Didier Astruc. Gold nanoparticles: assembly, supramolecular chemistry, quantum-size-related properties, and applications toward biology, catalysis, and nanotechnology. *Chemical Reviews*, 104(1):293–346, January 2004. ISSN 0009-2665. doi: 10.1021/cr030698+. 3

[10] Rainer H. Müller, Karsten Mäder, and Sven Gohla. Solid lipid nanoparticles (SLN) for controlled drug delivery – a review of the state of the art. *European Journal of Pharmaceutics and Biopharmaceutics*, 50(1):161–177, July 2000. ISSN 0939-6411. doi: 10.1016/S0939-6411(00)00087-4. URL http://www.sciencedirect.com/science/article/pii/S0939641100000874. 3

[11] Clarence Suh Yah, Geoffrey Simate Simate, and Sunny Esayegbemu Iyuke. Nanoparticles toxicity and their routes of exposures. *Pakistan Journal of Pharmaceutical Sciences*, 25(2):477–491, April 2012. ISSN 1011-601X. 3

[12] Gonçalo Doria, João Conde, Bruno Veigas, Leticia Giestas, Carina Almeida, Maria Assunção, João Rosa, and Pedro V. Baptista. Noble Metal Nanoparticles for Biosensing Applications. *Sensors*, 12(2):1657–1687, February 2012. doi: 10.3390/s120201657. URL http://www.mdpi.com/1424-8220/12/2/1657. 3

[13] V. V. Makarov, A. J. Love, O. V. Sinitsyna, S. S. Makarova, I. V. Yaminsky, M. E. Taliansky, and N. O. Kalinina. "Green" Nanotechnologies: Synthesis of Metal Nanoparticles Using Plants. *Acta Naturae*, 6(1):35–44, 2014. ISSN 2075-8251. URL http://www.ncbi.nlm.nih.gov/pmc/articles/PMC3999464/. 4

[14] Aiwei Tang, Shengchun Qu, Yanbing Hou, Feng Teng, Yongsheng Wang, and Zhanguo Wang. One-pot synthesis, optical property and self-assembly of monodisperse silver nanospheres. *Journal of Solid State Chemistry*, 184(8):1956–1962, August 2011. ISSN 0022-4596. doi: 10.1016/j.jssc.2011.05.041. URL http://www.sciencedirect.com/science/article/pii/S0022459611002908. 4

[15] Weipeng Lv, Yang Wang, Wenqian Feng, Junjie Qi, Guoliang Zhang, Fengbao Zhang, and Xiaobin Fan. Robust and smart gold nanoparticles: one-step synthesis, tunable optical property, and switchable catalytic activity. *Journal of Materials Chemistry*, 21(17):6173–6178, April 2011. ISSN 1364-5501. doi: 10.1039/C0JM04180G. URL http://pubs.rsc.org/en/content/articlelanding/2011/jm/c0jm04180g. 4

[16] Jun Natsuki and Takao Abe. Synthesis of pure colloidal silver nanoparticles with high electroconductivity for printed electronic circuits: The effect of amines on their

formation in aqueous media. *Journal of Colloid and Interface Science*, 359(1):19–23, July 2011. ISSN 0021-9797. doi: 10.1016/j.jcis.2011.03.079. URL http://www.sciencedirect.com/science/article/pii/S0021979711003778. 4

[17] Tao Zhao, Rong Sun, Shuhui Yu, Zhijun Zhang, Limin Zhou, Haitao Huang, and Ruxu Du. Size-controlled preparation of silver nanoparticles by a modified polyol method. *Colloids and Surfaces A: Physicochemical and Engineering Aspects*, 366(1–3):197–202, August 2010. ISSN 0927-7757. doi: 10.1016/j.colsurfa.2010.06.005. URL http://www.sciencedirect.com/science/article/pii/S0927775710003419. 4

[18] Paul Anastas and John Warner. *Green Chemistry: Theory and Practice*. OUP USA, March 2000. ISBN 978-0-19-850698-0. 4

[19] J. A. Linthorst. An overview: origins and development of green chemistry. *Foundations of Chemistry*, 12(1):55–68, April 2010. ISSN 1386-4238, 1572-8463. doi: 10.1007/s10698-009-9079-4. URL http://link.springer.com/article/10.1007/s10698-009-9079-4. 5

[20] Intel. ARK | Intel® Xeon® Processor E7-8850 v2 (24m Cache, 2.30 GHz). URL http://ark.intel.com/products/75253/Intel-Xeon-Processor-E7-8850-v2-24M-Cache-2_30-GHz. 5

[21] R. P. Clark, T. D. Preston, D. C. Gordon-Nesbitt, S. Malka, and L. Sinclair. The Size of Airborne Dust Particles Precipitating Bronchospasm in House Dust Sensitive Children. *The Journal of Hygiene*, 77(3):321–325, December 1976. ISSN 0022-1724. URL http://www.jstor.org.globalproxy.cvt.dk/stable/3861776. 5

[22] Robert William Cruden. Pollen grain size, stigma depth, and style length: the relationships revisited. *Plant Systematics and Evolution*, 278(3-4):223–238, April 2009. ISSN 0378-2697, 1615-6110. doi: 10.1007/s00606-008-0142-8. URL http://link.springer.com/article/10.1007/s00606-008-0142-8. 5

[23] J. Anthony Smith, Mira Josowicz, and Jiři? Janata. Polyaniline-Gold Nanocomposite System. *Journal of The Electrochemical Society*, 150(8):E384–E388, August 2003. ISSN 0013-4651, 1945-7111. doi: 10.1149/1.1589762. URL http://jes.ecsdl.org/content/150/8/E384. 6

[24] Min Hu, Jingyi Chen, Zhi-Yuan Li, Leslie Au, Gregory V. Hartland, Xingde Li, Manuel Marquez, and Younan Xia. Gold nanostructures: engineering their plasmonic properties for biomedical applications. *Chemical Society Reviews*, 35(11):1084–1094, October 2006. ISSN 1460-4744. doi: 10.1039/B517615H. URL http://pubs.rsc.org/en/content/articlelanding/2006/cs/b517615h. 6

[25] Munusamy Chamundeeswari, S. S. Liji Sobhana, Justin P. Jacob, M. Ganesh Kumar, M. Pandima Devi, Thotapalli P. Sastry, and Asit B. Mandal. Preparation, characterization and evaluation of a biopolymeric gold nanocomposite with antimicrobial activity. *Biotechnology and Applied Biochemistry*, 55(1):29–35, January 2010. ISSN 1470-8744. doi: 10.1042/BA20090198. URL http://onlinelibrary.wiley.com/doi/10.1042/BA20090198/abstract. 6

[26] Simona Badilescu Mohammed Alsawafta. Gold-Poly(methyl methacrylate) Nanocomposite Films for Plasmonic Biosensing Applications. *Polymers*, 3(4), 2011. ISSN 2073-4360. doi: 10.3390/polym3041833. 6

[27] J. Burunkova, I. Denisiuk, N. Vorzobova, L. Daroczi, Cs. Hegedus, S. Charnovych, and S. Kokenyesi. Fabrication and characterization of gold/acrylic polymer nanocomposites. *European Polymer Journal*, 49(10):3072–3077, October 2013. ISSN 0014-3057. doi: 10.1016/j.eurpolymj.2013.05.024. URL http://www.sciencedirect.com/science/article/pii/S0014305713002619. 6

[28] Shan-Hui Hsu, Cheng-Ming Tang, and Hsiang-Jung Tseng. Biocompatibility of poly(ether)urethane-gold nanocomposites. *Journal of Biomedical Materials Research. Part A*, 79(4):759–770, December 2006. ISSN 1549-3296. doi: 10.1002/jbm.a.30879. 6

[29] Dongxiang Li, Qiang He, and Junbai Li. Smart core/shell nanocomposites: Intelligent polymers modified gold nanoparticles. *Advances in Colloid and Interface Science*, 149(1–2):28–38, July 2009. ISSN 0001-8686. doi: 10.1016/j.cis.2008.12.007. URL http://www.sciencedirect.com/science/article/pii/S0001868609000025. 6

[30] Catalina Marambio-Jones and Eric M. V. Hoek. A review of the antibacterial effects of silver nanomaterials and potential implications for human health and the environment. *Journal of Nanoparticle Research*, 12(5):1531–1551, June 2010. ISSN 1388-0764, 1572-896X. doi: 10.1007/s11051-010-9900-y. URL http://link.springer.com/article/10.1007/s11051-010-9900-y. 7

[31] Christiane Beer, Rasmus Foldbjerg, Yuya Hayashi, Duncan S. Sutherland, and Herman Autrup. Toxicity of silver nanoparticles—Nanoparticle or silver ion? *Toxicology Letters*, 208(3):286–292, February 2012. ISSN 0378-4274. doi: 10.1016/j.toxlet.2011.11.002. URL http://www.sciencedirect.com/science/article/pii/S037842741101602X. 7, 8

[32] Yuan Gao and Robin Cranston. Recent Advances in Antimicrobial Treatments of Textiles. *Textile Research Journal*, 78(1):60–72, January 2008. ISSN 0040-5175, 1746-7748. doi: 10.1177/0040517507082332. URL http://trj.sagepub.com/content/78/1/60. 7

[33] Panagiotis Dallas, Virender K. Sharma, and Radek Zboril. Silver polymeric nanocomposites as advanced antimicrobial agents: Classification, synthetic paths, applications, and perspectives. *Advances in Colloid and Interface Science*, 166(1–2): 119–135, August 2011. ISSN 0001-8686. doi: 10.1016/j.cis.2011.05.008. URL http://www.sciencedirect.com/science/article/pii/S0001868611001175. 7

[34] Jaleh Mansouri, Simon Harrisson, and Vicki Chen. Strategies for controlling biofouling in membrane filtration systems: challenges and opportunities. *J. Mater. Chem.*, 20(22):4567–4586, April 2010. doi: 10.1039/B926440J. URL http://pubs.rsc.org/en/content/articlelanding/2010/jm/b926440j. 7

[35] Ammar T. Qureshi, W. Todd Monroe, Mandi J. Lopez, Marlene E. Janes, Vinod Dasa, Sunggook Park, Alborz Amirsadeghi, and Daniel J. Hayes. Biocompatible/bioabsorbable silver nanocomposite coatings. *Journal of Applied Polymer Science*, 120(5):3042–3053, June 2011. ISSN 00218995. doi: 10.1002/app.33481. URL http://www.readcube.com/articles/10.1002/app.33481? 7

[36] Stefanie Lischer, Enrico Körner, Dawn J. Balazs, Dakang Shen, Peter Wick, Kathrin Grieder, Dieter Haas, Manfred Heuberger, and Dirk Hegemann. Antibacterial burst-release from minimal Ag-containing plasma polymer coatings. *Journal of The Royal Society Interface*, 8(60):1019 –1030, July 2011. doi: 10.1098/rsif.2010.0596. URL http://rsif.royalsocietypublishing.org/content/8/60/1019.abstract. 7

[37] Rohan A Shirwaiker, Richard A Wysk, Subhashinie Kariyawasam, Hector Carrion, and Robert C Voigt. Micro-scale fabrication and characterization of a silver-polymer-based electrically activated antibacterial surface. *Biofabrication*, 3(1):015003, March 2011. ISSN 1758-5082, 1758-5090. doi: 10.1088/1758-5082/3/1/015003. URL http://iopscience.iop.org/1758-5082/3/1/015003. 7, 8

[38] P. Gonon and A. Boudefel. Electrical properties of epoxy/silver nanocomposites. *Journal of Applied Physics*, 99(2):024308, January 2006. ISSN 0021-8979, 1089-7550. doi: 10.1063/1.2163978. URL http://scitation.aip.org./content/aip/journal/jap/99/2/10.1063/1.2163978. 7

[39] Yang Rao and C.P. Wong. A novel ultra high dielectric constant epoxy silver composite for embedded capacitor application. In *2002 8th International Symposium on Advanced Packaging Materials, 2002. Proceedings*, pages 243–248, 2002. doi: 10.1109/ISAPM.2002.990394. 7

[40] L. Kabir and S.K. Mandal. Methanol sensing characteristics of conducting polypyrrole-silver nanocomposites. *The European Physical Journal Applied Physics*, 58(2):20402, May 2012. ISSN 1286-0042, 1286-0050. doi: 10.1051/epjap/2012110043. URL http://www.epjap.org/action/displayFulltext?type=1&fid=8598352&jid=JAP&volumeId=58&issueId=02&aid=8598350&bodyId=&membershipNumber=&societyETOCSession=. 7

[41] T. A. Kravchenko. Kinetics of oxygen reduction by nanocomposite silver-ion exchanger. *RUSSIAN JOURNAL OF PHYSICAL CHEMISTRY a*, 85(7):1196–1201, 2011. ISSN 1531863x. doi: 10.1134/S0036024411070181. 7

[42] Mariana Sendova. Plasmonic Coupling in Silver Nanocomposite Glasses. *JOURNAL OF PHYSICAL CHEMISTRY C*, 116(33):17764–17772, 2012. ISSN 19327455. doi: 10.1021/jp304778z. 7

[43] Hong-Ju Zhai. Catalytic properties of silica/silver nanocomposites. *JOURNAL OF NANOSCIENCE AND NANOTECHNOLOGY*, 6(7):1968–1972, 2006. ISSN 15334899. doi: 10.1166/jnn.2006.320. 7

[44] Özlem Kalaycı, Füsun Cömert, Baki Hazer, Turgay Atalay, Kevin Cavicchi, and Mukerrem Cakmak. Synthesis, characterization, and antibacterial activity of metal nanoparticles embedded into amphiphilic comb-type graft copolymers. *Polymer Bulletin*, 65(3):215–226, 2010. ISSN 0170-0839. doi: 10.1007/s00289-009-0196-y. URL http://www.springerlink.com./content/b84n434552r77867/abstract/. 8

[45] M. Rashidi Huyeh, M. Shirdel Havar, and B. Palpant. Thermo-optical properties of embedded silver nanoparticles. *Journal of Applied Physics*, 112 (10):103101, November 2012. ISSN 0021-8979, 1089-7550. doi: 10.1063/1.4766409. URL http://scitation.aip.org.globalproxy.cvt.dk/content/aip/journal/jap/112/10/10.1063/1.4766409. 8

[46] Wenjian Wu. Morphology controllable synthesis of silver nanoparticles: Optical properties study and SERS application. *JOURNAL OF ALLOYS AND COMPOUNDS*, 579:117–123, 2013. ISSN 18734669. doi: 10.1016/j.jallcom.2013.05.044. 8

[47] David J. Griffiths. *Introduction to Electrodynamics*. Addison Wesley, Upper Saddle River, N.J, 3rd edition edition, January 1999. ISBN 9780138053260. 8

[48] Nancy C. LaBianca and Jeffrey D. Gelorme. High-aspect-ratio resist for thick-film applications. volume 2438, pages 846–852, 1995. doi: 10.1117/12.210413. URL http://dx.doi.org/10.1117/12.210413. 8

[49] Y. Fang. Optical absorption of nanoscale colloidal silver: Aggregate band and adsorbate-silver surface band. *The Journal of Chemical Physics*, 108(10):4315–4318, March 1998. ISSN 0021-9606, 1089-7690. doi: 10.1063/1.475831. URL http://scitation.aip.org/content/aip/journal/jcp/108/10/10.1063/1.475831. 8, 23

[50] Krishnamurthy V. Nemani, Karen L. Moodie, Jeoffry B. Brennick, Alison Su, and Barjor Gimi. In vitro and in vivo evaluation of SU-8 biocompatibility. *Materials Science and Engineering: C*, 33(7):4453–4459, October 2013. ISSN 0928-4931. doi: 10.1016/j.msec.2013.07.001. URL http://www.sciencedirect.com/science/article/pii/S0928493113004049. 8

[51] Microchem. SU-8 2000 Permanent Epoxy Negative Photoresist Data sheet, 2014. URL http://www.microchem.com/pdf/SU-82000DataSheet2000_5thru2015Ver4.pdf. 9, 11, 77, 80, 81

[52] Microchem. SU-8 Series Resist Material Safety Data Sheet, April 2009. URL http://cnl.colorado.edu/cnl/images/MSDS/microchem%20su-8_resist.pdf. 11

[53] Microchem. Nano SU-8 Negative Tone Photoresist Formulations 2-25, 2015. URL https://www.microchem.com/pdf/SU8_2-25.pdf. 11

[54] Microchem. SU-8 2000 Series Resists Material Safety Data Sheet, April 2012. URL https://louisville.edu/micronano/files/documents/material-safety-data-sheets-msds/SU82000.pdf. 11

[55] Stephan Keller, Gabriela Blagoi, Michael Lillemose, Daniel Haefliger, and Anja Boisen. Processing of thin SU-8 films. *Journal of Micromechanics and Microengineering*, 18(12):125020, December 2008. ISSN 0960-1317. doi: 10.1088/0960-1317/18/12/125020. URL http://iopscience.iop.org/0960-1317/18/12/125020. 11

[56] Stephan Keller. *Fabrication of an autonomous surface stress sensor with the polymer SU-8*. PhD thesis, Technical University of Denmark, Department of Micro and Nanotechnology, April 2008. URL http://orbit.dtu.dk/fedora/objects/orbit:82544/datastreams/file_5007524/content. 11

[57] S. Jiguet, A. Bertsch, H. Hofmann, and P. Renaud. Conductive SU8-Silver Composite Photopolymer. *Micro Electro Mechanical Systems*, 2004. 11

[58] S. Jiguet, A. Bertsch, H. Hofmann, and P. Renaud. SU8-Silver Photosensitive Nanocomposite. *Advanced Engineering Materials*, 6(9):719–724, 2004. ISSN 1527-2648. doi: 10.1002/adem.200400068. URL http://onlinelibrary.wiley.com.globalproxy.cvt.dk/doi/10.1002/adem.200400068/abstract. 11, 81

[59] Ajit Khosla and B. L. Gray. Photopatternable Electrical Conductive Ag- SU-8 Nanocomposite for MEMS/MST. *ECS Transactions*, 33(8):313–318, October 2010. ISSN 1938-6737, 1938-5862. doi: 10.1149/1.3484135. URL http://ecst.ecsdl.org/content/33/8/313. 11, 93

[60] E. Tamjid and Bernd H. Guenther. Rheology and colloidal structure of silver nanoparticles dispersed in diethylene glycol. *Powder Technology*, 197(1–2):49–53, January 2010. ISSN 0032-5910. doi: 10.1016/j.powtec.2009.08.022. URL http://www.sciencedirect.com/science/article/pii/S0032591009004823. 11

[61] Ramanan Krishnamoorti and Tirtha Chatterjee. Rheology and Processing of Polymer Nanocomposites. In rianna Kontopoulou, editor, *Applied Polymer Rheology*, pages 153–177. John Wiley & Sons, Inc., 2011. ISBN 9781118140611. URL http://onlinelibrary.wiley.com/doi/10.1002/9781118140611.ch5/summary. 11

[62] S. Jiguet, A. Bertsch, H. Hofmann, and P. Renaud. Conductive SU8 Photoresist for Microfabrication. *Advanced Functional Materials*, 15(9):1511–1516, 2005. ISSN 1616-3028. doi: 10.1002/adfm.200400575. URL http://onlinelibrary.wiley.com.globalproxy.cvt.dk/doi/10.1002/adfm.200400575/abstract. 11, 95

[63] Jianwen Xu and C.P. Wong. Photodefinable High-k SU8 Nanocomposite for Embedded Capacitors. In *200611th International Symposium on Advanced Packaging Materials: Processes, Properties and Interface*, pages 133–138, 2006. doi: 10.1109/ISAPM.2006.1666022. 12

[64] Sébastien Jiguet, Arnaud Bertsch, Moshe Judelewicz, Heinrich Hofmann, and Philippe Renaud. SU-8 nanocomposite photoresist with low stress properties for microfabrication applications. *Microelectronic Engineering*, 83(10):1966–1970, October 2006. ISSN 0167-9317. doi: 10.1016/j.mee.2006.02.004. URL http://www.sciencedirect.com/science/article/pii/S0167931706002978. 12

[65] Shengxiang Wang, Pierre Campistron, Julien Carlier, Dorothée Callens-Debavelaere, Bertrand Nongaillard, Assane NDieguene, Georges Nassar, Caroline Soyer, and Xingzhong Zhao. SU-8-based nanocomposites for acoustical matching layer. *IEEE transactions on ultrasonics, ferroelectrics, and frequency control*, 56(7):1483–1489, July 2009. ISSN 1525-8955. doi: 10.1109/TUFFC.2009.1204. 12

[66] S. Jiguet, M. Judelewicz, S. Mischler, H. Hofmann, A. Bertsch, and P. Renaud. SU-8 nanocomposite coatings with improved tribological performance for MEMS. *Surface and Coatings Technology*, 201(6):2289–2295, December 2006. ISSN 02578972. doi: 10.1016/j.surfcoat.2006.03.041. URL http://infoscience.epfl.ch/record/99662. 12

[67] V Velmurugan and J. P. Raina. SU8 nanocomposite photoresist with enhanced thermal conductivity. *International Journal of ChemTech Research*, 6(4):2300–2305, August 2014. ISSN 0974-4290. 12

[68] John Turkevich, Peter Cooper Stevenson, and James Hillier. A study of the nucleation and growth processes in the synthesis of colloidal gold. *Discuss. Faraday Soc.*, 11:55–75, January 1951. doi: 10.1039/DF9511100055. URL http://pubs.rsc.org/en/content/articlelanding/1951/df/df9511100055. 19

[69] G. Frens. Controlled Nucleation for the Regulation of the Particle Size in Monodisperse Gold Suspensions. *Nature*, 241(105):20–22, January 1973. doi: 10.1038/10.1038/physci241020a0. URL http://www.nature.com/nature-physci/journal/v241/n105/abs/physci241020a0.html. 19

[70] Nikolai G. Khlebtsov, Vladimir A. Bogatyrev, Lev A. Dykman, and Andrei G. Melnikov. Spectral Extinction of Colloidal Gold and Its Biospecific Conjugates. *Journal of Colloid and Interface Science*, 180(2):436–445, June 1996. ISSN 0021-9797. doi:

10.1006/jcis.1996.0323. URL http://www.sciencedirect.com/science/article/pii/S0021979796903239. 20

[71] Lorraine Mulfinger, Sally D. Solomon, Mozghan Bahadory, Aravindan V. Jeyarajasingam, Susan A. Rutkowsky, and Charles Boritz. Synthesis and Study of Silver Nanoparticles. *J. Chem. Educ.*, 84(2):322, 2007. ISSN 0021-9584. doi: 10.1021/ed084p322. URL http://dx.doi.org/10.1021/ed084p322. 23, 24, 25

[72] J. Alan Creighton, Christopher G. Blatchford, and M. Grant Albrecht. Plasma resonance enhancement of Raman scattering by pyridine adsorbed on silver or gold sol particles of size comparable to the excitation wavelength. *Journal of the Chemical Society, Faraday Transactions 2: Molecular and Chemical Physics*, 75(0):790–798, January 1979. ISSN 0300-9238. doi: 10.1039/F29797500790. URL http://pubs.rsc.org/en/content/articlelanding/1979/f2/f29797500790. 23, 24

[73] P. C. Lee and D. Meisel. Adsorption and surface-enhanced Raman of dyes on silver and gold sols. *The Journal of Physical Chemistry*, 86(17):3391–3395, 1982. ISSN 0022-3654. doi: 10.1021/j100214a025. URL http://dx.doi.org/10.1021/j100214a025. 23, 24

[74] Prashant V. Kamat, Mark Flumiani, and Gregory V. Hartland. Picosecond Dynamics of Silver Nanoclusters. Photoejection of Electrons and Fragmentation. *The Journal of Physical Chemistry B*, 102(17):3123–3128, 1998. ISSN 1520-6106. doi: 10.1021/jp980009b. URL http://dx.doi.org/10.1021/jp980009b. 24, 26

[75] Salvatore Giuffrida, Giorgio Ventimiglia, and Salvatore Sortino. Straightforward green synthesis of "naked" aqueous silver nanoparticles. *Chem. Commun.*, (27): 4055–4057, May 2009. doi: 10.1039/B907075C. URL http://pubs.rsc.org/en/Content/ArticleLanding/2009/CC/b907075c. 25, 26

[76] Rachel K. O'Reilly, Craig J. Hawker, and Karen L. Wooley. Cross-linked block copolymer micelles: functional nanostructures of great potential and versatility. *Chemical Society Reviews*, 35(11):1068–1083, October 2006. ISSN 1460-4744. doi: 10.1039/B514858H. URL http://pubs.rsc.org/en/content/articlelanding/2006/cs/b514858h. 29

[77] Abraham Ulman. Formation and Structure of Self-Assembled Monolayers. *Chemical Reviews*, 96(4):1533–1554, January 1996. ISSN 0009-2665. doi: 10.1021/cr9502357. URL http://dx.doi.org/10.1021/cr9502357. 29

[78] Noriyuki Masuda. *New Nanoparticle Doped Polymer Materials for Micro- and Nanofabrication*. Master Thesis, Technical University of Denmark, 2010. 29, 35, 43

[79] Helmut Ritter. Functionalized polymers: synthesis and properties. *Beilstein Journal of Organic Chemistry*, 6, June 2010. ISSN 1860-5397. doi: 10.3762/bjoc.6.

55. URL http://www.beilstein-journals.org/bjoc/single/articleFullText.htm?vt=f&publicId=1860-5397-6-55&sn=9&tpn=0&bpn=singleSeries. 30

[80] Hyeon Suk Shin, Hyun Jung Yang, Seung Bin Kim, and Mu Sang Lee. Mechanism of growth of colloidal silver nanoparticles stabilized by polyvinyl pyrrolidone in γ-irradiated silver nitrate solution. *Journal of Colloid and Interface Science*, 274(1): 89–94, June 2004. ISSN 0021-9797. doi: 10.1016/j.jcis.2004.02.084. URL http://www.sciencedirect.com/science/article/pii/S0021979704002516. 31

[81] Cytodiagnostics. Gold Nanoparticle Handling and Storage, December 2014. URL http://www.cytodiagnostics.com/store/pc/Gold-Nanoparticle-Handling-and-Storage-d7.htm. 35

[82] Thermo Scientific. Convert between times gravity (x g) and centrifuge rotor speed (RPM), 2009. 35

[83] wiki. Phase diagram, December 2014. URL http://en.wikipedia.org/wiki/Phase_diagram. 37

[84] Wassim Abdelwahed, Ghania Degobert, Serge Stainmesse, and Hatem Fessi. Freeze-drying of nanoparticles: Formulation, process and storage considerations. *Advanced Drug Delivery Reviews*, 58(15):1688–1713, December 2006. ISSN 0169-409X. doi: 10.1016/j.addr.2006.09.017. URL http://www.sciencedirect.com/science/article/pii/S0169409X06001840. 39

[85] A. Toor, J.C. Cheng, and A.P. Pisano. Synthesis and characterization of gold nanoparticle/SU-8 polymer based nanocomposite. In *2014 9th IEEE International Conference on Nano/Micro Engineered and Molecular Systems (NEMS)*, pages 664–668, April 2014. doi: 10.1109/NEMS.2014.6908899. 47

[86] H. C. Chiamori, J. W. Brown, E. V. Adhiprakasha, E. T. Hantsoo, J. B. Straalsund, N. A. Melosh, and B. L. Pruitt. Suspension of nanoparticles in SU-8: Processing and characterization of nanocomposite polymers. *Microelectronics Journal*, 39(2): 228–236, February 2008. ISSN 0026-2692. doi: 10.1016/j.mejo.2007.05.012. URL http://www.sciencedirect.com/science/article/pii/S0026269207001188. 47, 56

[87] C. Jiang, L. Ouattara, C. Ingrosso, M. L. Curri, V. Krozer, A. Boisen, M. H. Jakobsen, and T. K. Johansen. Microwave absorption properties of gold nanoparticle doped polymers. *Solid-State Electronics*, 57(1):19–22, March 2011. ISSN 0038-1101. doi: 10.1016/j.sse.2010.10.021. URL http://www.sciencedirect.com/science/article/pii/S0038110110003801. 47

[88] Yue Chi, Liang Zhao, Qing Yuan, Xiao Yan, Yanjuan Li, Nan Li, and Xiaotian Li. In situ auto-reduction of silver nanoparticles in mesoporous carbon with multi-functionalized surfaces. *Journal of Materials Chemistry*, 22(27):13571–13577, June

2012. ISSN 1364-5501. doi: 10.1039/C2JM31854G. URL http://pubs.rsc.org/en/content/articlelanding/2012/jm/c2jm31854g. 55

[89] Da-Guang Yu, Wen-Ching Lin, Chien-Hong Lin, Li-Mei Chang, and Ming-Chien Yang. An in situ reduction method for preparing silver/poly(vinyl alcohol) nanocomposite as surface-enhanced Raman scattering (SERS)-active substrates. *Materials Chemistry and Physics*, 101(1):93–98, January 2007. ISSN 0254-0584. doi: 10.1016/j.matchemphys.2006.02.020. URL http://www.sciencedirect.com/science/article/pii/S0254058406000708. 55

[90] Biwen Yang, Zhiming Liu, Zhouyi Guo, Wen Zhang, Mingming Wan, Xiaochu Qin, and Huiqing Zhong. In situ green synthesis of silver–graphene oxide nanocomposites by using tryptophan as a reducing and stabilizing agent and their application in SERS. *Applied Surface Science*, 316:22–27, October 2014. ISSN 0169-4332. doi: 10.1016/j.apsusc.2014.07.084. URL http://www.sciencedirect.com/science/article/pii/S0169433214016122. 55

[91] Tatiana N. Smirnova, Lyudmila M. Kokhtych, Alexander S. Kutsenko, Oksana V. Sakhno, and Joachim Stumpe. The fabrication of periodic polymer/silver nanoparticle structures: in situ reduction of silver nanoparticles from precursor spatially distributed in polymer using holographic exposure. *Nanotechnology*, 20(40):405301, October 2009. ISSN 0957-4484. doi: 10.1088/0957-4484/20/40/405301. URL http://iopscience.iop.org/0957-4484/20/40/405301. 55

[92] P. K. Khanna, Narendra Singh, Shobhit Charan, and A. Kasi Viswanath. Synthesis of Ag/polyaniline nanocomposite via an in situ photo-redox mechanism. *Materials Chemistry and Physics*, 92(1):214–219, July 2005. ISSN 0254-0584. doi: 10.1016/j.matchemphys.2005.01.011. URL http://www.sciencedirect.com/science/article/pii/S0254058405000258. 55

[93] Zhongping Zhang, Lide Zhang, Shixing Wang, Wei Chen, and Yong Lei. A convenient route to polyacrylonitrile/silver nanoparticle composite by simultaneous polymerization–reduction approach. *Polymer*, 42(19):8315–8318, September 2001. ISSN 0032-3861. doi: 10.1016/S0032-3861(01)00285-3. URL http://www.sciencedirect.com/science/article/pii/S0032386101002853. 55

[94] W. Fritzsche, H. Porwol, A. Wiegand, S. Bornmann, and J. M. Köhler. In-situ formation of Ag-containing nanoparticles in thin polymer films. *Nanostructured Materials*, 10(1):89–97, January 1998. ISSN 0965-9773. doi: 10.1016/S0965-9773(98)00023-3. URL http://www.sciencedirect.com/science/article/pii/S0965977398000233. 55

[95] Shatabdi Porel, Shashi Singh, S. Sree Harsha, D. Narayana Rao, and T. P. Radhakrishnan. Nanoparticle-Embedded Polymer: In Situ Synthesis, Free-Standing Films with Highly Monodisperse Silver Nanoparticles and Optical Limiting. *Chemistry*

of Materials, 17(1):9–12, January 2005. ISSN 0897-4756. doi: 10.1021/cm0485963. URL http://dx.doi.org/10.1021/cm0485963. 55

[96] S. Porel, S. Singh, and T. P. Radhakrishnan. Polygonal gold nanoplates in a polymer matrix. *Chemical Communications*, (18):2387–2389, May 2005. ISSN 1364-548X. doi: 10.1039/B500536A. URL http://pubs.rsc.org/en/content/articlelanding/2005/cc/b500536a. 55

[97] *CRC Handbook of Chemistry and Physics, 95th Edition*. URL http://www.crcpress.com/product/isbn/9781482208672. 58, 94

[98] Salt Lake Metals. Solubility of Silver Nitrate, October 2014. URL http://www.saltlakemetals.com/Solubility_Of_Silver_Nitrate.htm. 58

[99] Kiper Anatolievich. Properties of substance: silver nitrate, October 2014. URL http://chemister.ru/Database/properties-en.php?dbid=1&id=862. 58

[100] Gaylord Chemicals. DMSO Solubility Data, October 2014. URL http://www.gaylordchemical.com/index.php?page=102b-dmso-solubility-data#102b-4. 58

[101] Christian Laurence and Jean-François Gal. Lewis Basicity and Affinity Measurement: Definitions and Context. In *Lewis Basicity and Affinity Scales*, pages 1–69. John Wiley & Sons, Ltd, 2009. ISBN 9780470681909. URL http://onlinelibrary.wiley.com/doi/10.1002/9780470681909.ch1/summary. 82

[102] F. Carmona. Conducting filled polymers. *Physica A: Statistical Mechanics and its Applications*, 157(1):461–469, May 1989. ISSN 0378-4371. doi: 10.1016/0378-4371(89)90344-0. URL http://www.sciencedirect.com/science/article/pii/0378437189903440. 93

[103] Dietrich Stauffer and Ammon Aharony. *Introduction To Percolation Theory*. CRC Press, July 1994. ISBN 9781420074796. 93

[104] J. Y. Li, L. Zhang, and Stephen Ducharme. Electric energy density of dielectric nanocomposites. *Applied Physics Letters*, 90(13):132901, March 2007. ISSN 0003-6951, 1077-3118. doi: 10.1063/1.2716847. URL http://scitation.aip.org/content/aip/journal/apl/90/13/10.1063/1.2716847. 93

[105] Sebastien Jiguet. GCM 3060 Datasheet, May 2005. 95

Appendix A

SU-8 2002 Certificate of Analysis

MICRO CHEM
90 Oak Street, PO Box 426 Newton, MA 02464-0002
TEL: (617) 965 - 5511 FAX: (617) 965 - 5818

SU-8 2002

NEGATIVE RADIATION SENSITIVE RESIST

29% in Cyclopentanone

Product No.	Y111029	Lot No.	14080525
Expiration	Sep-01-2015	Manufactured	Aug-01-2014

CERTIFICATE OF ANALYSIS

MicroChem Corp. has completed the analysis of the above lot of material with the results listed below.

	Specification	Result
Appearance Test Method: QA003	Clear, yellow	Clear, yellow
Solids Content, % Test Method: QA085	Calculated	29.7
Viscosity at 25° C, cst Test Method: QA004	7.50 +/-0.26	7.62
Filtration Level	0.2 μm	0.2 μm

MicroChem Corp. hereby certifies that the above material meets all specifications for this product and conforms to our Quality Assurance requirements.

Certified by:

Aug-05-2014

John D'Apollo
QA Technician

Appendix B

Materials and Methods

Throughout the thesis several processes for synthesis of nanoparticles and the like has been explained. In this appendix all have been collected and condensed for those who wish to do the experiments themselves.

B.1 Nanoparticles

The synthesis of nanoparticles involves in total five different methods divided in such a manner that there is two for gold and three for silver.

Both synthesis and coating is described in one step.

B.1.1 Gold

Gold(III) chloride hydrate ($HAuCl_4 \cdot 3H_2O$) $\geq$99.9 % and sodium citrate dihydrate ($Na_3C_6H_5O_7 \cdot 2H_2O$) $\geq$99 % was bought from Sigma Aldrich and Luviskol® VA 64, a Polyvinyl pyrrolidone co-vinyl acetate (PVP/VA) mixture was kindly gifted by BASF. Milli-Q water with a resistivity of 18.2 MΩ cm^{-1} was used for all solution.

Post Grafted Particles

45 ml of 0.2 % $HAuCl_4$ solution was diluted with 155 ml of Milli-Q water in a two necked 500 ml round bottomed flask equipped with a reflux condenser. The solution was heated to reflux with rapid magnetic stirring before 5 ml of 5 % of pre heated trisodium citrate was added through the second neck. The color changes from colorless through black to wine red. The solution is left to reflux with magnetic stirring for half an hour, before being cooled to room temperature.

40 ml of the particle solution was transferred to a 45 ml centrifuge tube before being coated with PVP/VA. 1.4 ml of 100 mg/ml PVP/VA was added to the centrifuge tube and the entire solution shaken over night.

Pre Grafted Particles

15 ml of 0.2 % $HAuCl_4$ solution was boiled with 15 ml of 10 mg/ml PVP/VA solution and 5 ml of Milli-Q water. While boiling, 5 ml of hot 3 % solution of trisodium citrate was added. Within a couple of minutes, wine red coloured PVP/VA coated gold nanoparticle suspension was obtained with a gold content of 15 mg and a gold to polymer ratio of 1:10.

B.1.2 Silver

Silver nitrate ($AgNO_3$) ≥99.0 %, silver acetylacetonate ($C_5H_7AgO_2$ 98 %) and sodium borohydride ($NaBH_4$ ≥98.0 %) was bought from Sigma Aldrich. Luviskol® VA 64, a Polyvinyl pyrrolidone co-vinyl acetate (PVP/VA) mixture was kindly gifted by BASF. Milli-Q water with a resistivity of 18.2 MΩ cm^{-1} was used for all solution. Argon ≥99.99 % was bought from AGA A/S.

Post Grafted Particles – Procedure 1

30 ml of 2.0 mM sodium borohydride in a 100 ml round bottomed flask was chilled in an ice bath. 10 ml of 1 mM silver nitrate was added at one drop pr. second under vigorously stirring. After complete addition the stirring is stopped.

40 ml of the particle solution was transferred to a 45 ml centrifuge tube before being coated with PVP/VA. 50 μl of 100 mg/ml PVP/VA was added to the centrifuge tube and the entire solution shaken over night.

Post Grafted Particles – Procedure 2

200 ml of water is saturated with argon in a gas washing bottle for 30 min. 10 mg of silver acetylacetonate is added to the water and dissolved using magnetic stirring. After complete dissolve the solution if left for several hours.

40 ml of the particle solution was transferred to a 45 ml centrifuge tube before being coated with PVP/VA. 40 μl of 100 mg/ml PVP/VA was added to the centrifuge tube and the entire solution shaken over night.

Pre Grafted Particles

1 g of PVP/VA and 0.1 g of silver nitrate is dissolved in 50 ml of absolute ethanol. 0.02 g of sodium borohydride and 0.2 g of PVP/VA dissolved in 10 ml of absolute ethanol is added to the solution at one drop pr. second under vigorously stirring. 30 s after complete addition the stirring is stopped.

B.2 Solvent Exchange

The solvent exchange is done using a rotary evaporator *Rotavapor® R-210* from *Buchi*. The procedure is can only be guaranteed to work for pre grafted particles.

Gold Nanoparticles

1. 10 ml of gold nanoparticle sol is attached to the rotary evaporator and 2 ml water evaporated.
2. 1 ml of cyclopentanone is added to the sol.
3. The process is repeated five times.

During evaporation two phases should be observable. After successful removal of the water only one phase should be observed.

Silver Nanoparticles

1. 10 ml of the nanoparticle sol is attached to the rotary evaporator and 1 ml of ethanol evaporated.
2. 1 ml of cyclopentanone is added to the sol.
3. 3 ml of ethanol is evaporated and 1 ml of cyclopentanone added.
4. The remaining 6 ml of ethanol is evaporated and 1 ml cyclopentanone added.

Appendix C

Cleanroom recipe

This process cook book contains a functional process flow for fabrication of an *in situ* silver nanocomposite. The process is optimised for the DTU Danchip cleanroom and the machines in there.

Equipment	Recipe/ Program	Time	Comments
100 mm double sided polished, 500 μm fused silica wafers or 100 mm double sided polished, 350 μm phosphor doped silicon wafers.			
1. Pretreatment			
250°C oven		4 hours	Preferably over night.
2. Precursor Preparation			
Fume hood			Prepare a precursor solution by weighing of a desired amount of $AgNO_3$ and dissolving it in acetonitrile.
3. Spinning			
Fume hood			0.5 ml of the precursor solution is mixed with 4 ml of SU-8 2002.
Manual spinner 1	1500 RPM	1 min	Add the freshly made nanocomposite mixture using a disposable transfer pipette.
4. Soft bake			

Continued on next page

Continued from previous page

Equipment	Recipe/ Program	Time	Comments
Hotplate	95°C	10 min	The hotplate is equipped with an extra aluminium plate for better homogeneity which lowers the temperature. The hotplate should be set at 105°C.
5. UV exposure			
EVG620 aligner	First print, constant time interval	7.5 min	The filter needs to be removed from the machine prior to exposure. The exposure should be done in 30 s intervals with 30 s wait in between. Use purge during exposure.
6. Post exposure bake			
Hotplate	95°C	10 min	The hotplate is equipped with an extra aluminium plate for better homogeneity which lowers the temperature. The hotplate should be set at 105°C.
7. Development			
PGMEA baths		2 min	Use dedicated beakers in the fumehood. Two baths, 2 min in each.
8. Hard bake			
Hotplate	150°C – 300°C	30 min	The cleanroom hotplates are normally confined to a maximum temperature of 220°C.

Appendix D

Conference Proceedings

Technical University of Denmark DTU

Joint author statement

If a thesis contains articles (i.e. published journal and conference articles, unpublished manuscripts, chapters etc.) made in collaboration with other researchers, a joint-author statement verifying the PhD student's contribution to each article should be made by all authors. However, if an article has more than three authors the statement may be signed by a representative sample, cf. article 12, section 4 and 5 of the Ministerial Order No. 1039 27 August 2013 about the PhD degree. We refer to the Vancouver protocol's definition of authorship.

A representative sample of authors is comprised of

- Corresponding author and/or principal/first author (defined by the PhD student), and if there are more authors:
- 1-2 authors (preferably international/non-supervisor authors)

Titel of the article	Gold Nanoparticle Doped Polymer Materials for Micro- and Nanofabrication
Author(s)	S. V. Fischer, N. Masuda, S. S. Keller, B. Uthuppu, M. H. Jakobsen
Journal/conference * if applicable	8th International Congress on Advanced Electromagnetic Materials in Microwaves and Optics – Metamaterials 2014
Name of PhD student	Søren Vang Fischer
Date of Birth	28/4-1986

Description of the PhD student's contribution to the abovementioned article

Main writer and confirmation of experiments

Signature of the PhD student S.V. Fischer Date 31/3 - 2015

Signatures of co-authors

As a co-author I state that the description given above to the best of my knowledge corresponds to the process and I have no further comments.

Date (DD/MM/YY)	Name	Signature
31 March 2015	BASIL UTHUPPU	
31/3 - 2015	MOGENS H. JAKOBSEN	Mogens Jakobsen

Joint author statements shall be delivered to the *PhD administration* along with the PhD thesis

Gold Nanoparticle Doped Polymer Materials for Micro- and Nanofabrication

S. V. Fischer[1], N. Masuda[1], S. S. Keller[1], B. Uthuppu[1], M. H. Jakobsen[1]

[1]Department of Nanotechnology, DTU, Kgs. Lyngby, Ørsteds plads, 2800, DK
Mogens.Jakobsen@nanotech.dtu.dk

New bottom-up approach to fabricate metal nanoparticle doped polymer photoresist (polymer nanocomposite) is presented. The nanocomposite holds a potential to fabricate hierarchically structured materials which have tailored functionalities spanning multiple length, scales and dimensions. Such materials will enable exiting new applications in micro- and nanotechnology1. However, simple mixture of nanoparticles with many polymers leads to non-uniform distribution, particle clustering or aggregation that impairs desired properties in the composite material[2].

Gold nanoparticle SU-8 composite was structured by UV photolithography and attained the lithographic resolution of 3.5 μm by soft contact (Figure 1). Point-wise light scattering was observed through dark field microscopy (Figure 2). Plasmonic extinction peaked at 550 nm and similar response was observed by brief Mie calculation at n=1.63, (Figure 3). Spherical gold nanoparticle possesses isotropic feature. However, the composite showed polarization dependency to incident light, indicating that the particles were self-organized chemically and/or physically during the fabrication. The material is speculated to be useful in various fields, such as biomedical optics and photonics. The technique may be a break-through for cost-effective and scalable development for plasmonic sensing devices for example, SPR spectroscopy/SERS substrate and ultra-thin photonic crystals which sometimes relay on time consuming top-down approach for the fabrication. Since SU-8, PVP/VA and gold nanoparticles have low biological toxicity there may be applications in life science and medicine with this technique[4, 5].

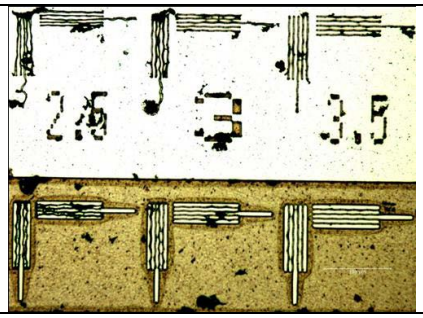

Figure 1: Bright field image from two SU-8 structures. Lithographic resolution, 3.5μm was achieved

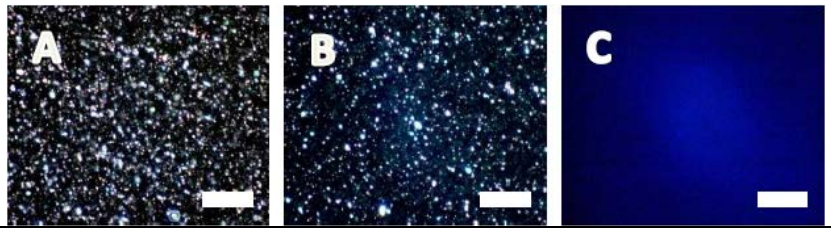

Figure 2: The image from dark field microscopy. From left to right, pictures were taken with (A) 1w/w% (8mg), (B) 0.25w/w (2mg) and (C) control respectively. The white bar is the scale bar (10μm).

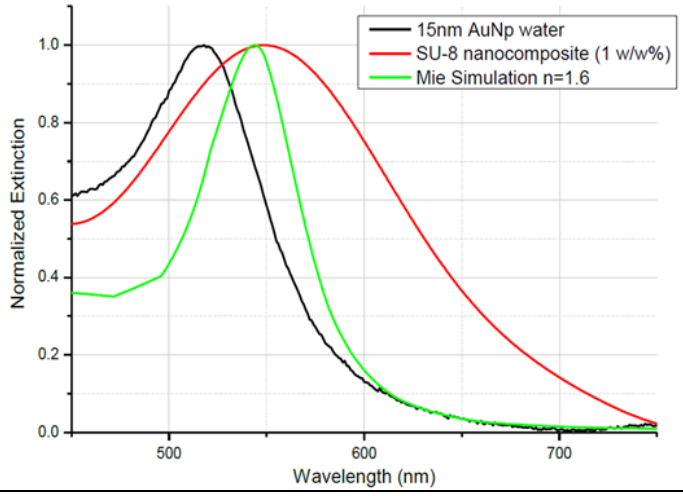

Figure 3: Normalized excitation spectra from 5um SU-8/15nm gold nanoparticle composite. From black, red to green spectra corresponds to phase in water, SU-8 nanocomposite (1 w/w %) and theoretical spectra from 15nm particle at n=1.6 respectively.

1. O.D. Velev & S. Gupta, *Adv. Mater.*, Vol.21, p.1897 (2009).
2. A.C. Balazs, T. Emrick & T.P. Russell, *Science*, Vol.314, p.1107 (2006).
3. B. Bilenberg, T. Nielsen, B. Clausen & A. Kristensen, *J. Micromech. Microeng.*, Vol.14, p.814 (2004).
4. C. Leuner, & J. Dressman, Eur. *J. Pharm. Biopharm.*, Vol.50, p.47 (2000).
5. G. Voskerician et al., *Biomaterials*, Vol.24, p.1959 (2003).

Technical University of Denmark DTU

Joint author statement

If a thesis contains articles (i.e. published journal and conference articles, unpublished manuscripts, chapters etc.) made in collaboration with other researchers, a joint-author statement verifying the PhD student's contribution to each article should be made by all authors. However, if an article has more than three authors the statement may be signed by a representative sample, cf. article 12, section 4 and 5 of the Ministerial Order No. 1039 27 August 2013 about the PhD degree. We refer to the Vancouver protocol's definition of authorship.

A representative sample of authors is comprised of

- Corresponding author and/or principal/first author (defined by the PhD student), and if there are more authors:
- 1-2 authors (preferably international/non-supervisor authors)

Titel of the article	Metal Nanocomposites
Author(s)	S. V. Fischer, B. Uthuppu, M. H. Jakobsen
Journal/conference * if applicable	8th International Congress on Advanced Electromagnetic Materials in Microwaves and Optics – Metamaterials 2014
Name of PhD student	Søren Vang Fischer
Date of Birth	28/4-1986

Description of the PhD student's contribution to the abovementioned article

Main writer and performer of experiments and charaterisation

Signature of the PhD student S.V. Fischer Date 31/3-2015

Signatures of co-authors

As a co-author I state that the description given above to the best of my knowledge corresponds to the process and I have no further comments.

Date (DD/MM/YY)	Name	Signature
31 March 2015	BASIL UTHUPPU	
31/3-2015	MOGENS H. JAKOBSEN	Mogens Jakobsen

Joint author statements shall be delivered to the *PhD administration* along with the PhD thesis

8th International Congress on Advanced Electromagnetic Materials in Microwaves and Optics - Metamaterials 2014
Copenhagen, Denmark, 25-30 August 2014

Metal Nanocomposites

S. V. Fischer[1], B. Uthuppu[1] and M. H. Jakobsen[1]

[1]Technical University of Denmark, DTU Nanotech, Ørsteds plads, 2800, Kgs. Lyngby, Denmark
Soren.Fischer@nanotech.dtu.dk

***Abstract* – We have made SU-8 gold nanoparticle composites in two ways, *ex situ* and *in situ*, and found that in both methods nanoparticles embedded in the polymer retained their plasmonic properties. The *in situ* method has also been used to fabricate a silver nanocomposite which is electrically conductive. The silver composite was structured using UV lithography, and initial results are very promising with regards to obtained resolution.**

I. INTRODUCTION

Metallic nanoparticle photoresist materials are of high interest for the microfabrication of new structures, to exploit the extraordinary optical properties of the metal nanoparticles. Photoresist materials in which the nanoparticles retain their localized surface plasmonic resonance will serve as a flexible template for next-generation optical and sensing applications. Furthermore, embedded metallic nanoparticles can improve the electrical conductivity of the materials allowing the construction of transparent flexible conducting optoelectronic devices.

In general two major approaches to fabricate nanoparticle photoresist materials exists: 1) synthesis and condition the nanoparticles and suspend them into the polymeric matrix followed by polymerization (*ex situ*) and 2) formation of the nanoparticles during crosslinking by adding the metal precursor into the polymeric matrix before polymerization (*in situ*). The *ex situ* method allows the synthesis of nanoparticles of controlled size, shape, and chemical composition [1], but also conditioning of these pre-formed particles is necessary to achieve uniform distribution in the photoresist. Conditioning of the pre-formed particles can be obtained by ligand exchange methods [2] to control the suspendability of the nanoparticles in relevant solvents.

SU-8 is a highly performing epoxy-based photoresist widely used for microfabrication of two or three dimensional components with high aspect ratios [3]. The excellent mechanical and optical properties of SU-8 makes it a highly suitable material for many micromechanical systems and optical components. Embedding metallic nanoparticles into SU-8 will further extend the possibility of using these materials to develop new photonic applications and optoelectronic devices.

II. MATERIALS

Gold(III) chloride hydrate ($HAuCl_4 \cdot 3H_2O$) 99.9+%, sodium citrate dihydrate $\geq$ 99%, $AgNO_3 \geq$ 99.0 %, DMSO $\geq$ 99.9 %, H_2SO_4 95.0-98.0 %, $H_2O_2 \geq$ 30 %, PGMEA 99 % and cyclopentanone $\geq$ 99,0% were purchased from Sigma Aldrich. SU-8 was bought from microchem, and Luviskol©VA 64, a Polyvinyl pyrrolidone-co-vinyl acetate (PVP-VA) mixture was kindly gifted by BASF.

All reagents were used without further purification.

III. METHODS

A. Ex situ Synthesis of Gold Nanoparticle SU-8 Composite

15 mL of 0.2 % $HAuCl_4$ solution was boiled with 15 mL of 10 mg/mL PVP-VA solution and 5 mL of milliQ Water. While boiling, 5 mL of hot 3 % solution of trisodium citrate was added. Within a couple of minutes, wine red coloured PVP-VA coated gold nanoparticle suspension was obtained with a gold content of 15 mg and a gold to polymer ratio of 1:10.

10 mL of this suspension was evaporated in a rotary evaporator under reduced pressure until the total volume became around 3 mL. Then 10 mL of cyclopentanone was added and the rotary evaporation process continued. This step was repeated until all water had evaporated and a stable suspension of PVP-VA coated Au nanoparticles in cyclopentanone was obtained.

1 mL of the above nanoparticle suspension was then mixed with 1 mL of SU-8 before being spun on a wafer and given a hard bake.

B. In situ Synthesis of Gold and Silver Nanoparticle SU-8 Composite

In situ generated gold and silver nanocomposites were spun on 2 inch wafers after a pre-treatment step consisting of a piranha clean (4:1 ratio of H_2SO_4 and H_2O_2) for 10 min, followed by a wash in milli-Q water for 10 min and then drying under nitrogen flow.

For the gold 1 g of $HAuCl_4 \cdot 3H_2O$ was dissolved in 2 mL of SU-8 and readily spun on the wafer before giving the wafer a hardbake on a hotplate.

For the silver 0.5 g of $AgNO_3$ were dissolved in 1 mL of DMSO and then mixed with 1 mL of SU-8. The solution was spun on the wafer and given a hardbake on a hotplate.

If the composite was to be structured, then it was given a softbake after spinning, followed by 30 s UV exposure using a dedicated mask. After UV the wafer was given another softbake and then developed in PGMEA for 2 min. After development the wafer was cleaned with propylene alcohol and water before being given a hardbake.

IV. Results

A. Gold Nanoparticle SU-8 Composite

Ex situ generated particles have successfully been transferred to cyclopentanone using PVP-VA as a stabiliser. The stable suspension in cyclopentanone has been used for mixing with SU-8 to make a nanocomposite, but the concentration of gold compared to polymer is low. High gold concentration in SU-8 has been achieved using *in situ* formation of nanoparticles within the SU-8. This process does however eliminate control of particle size and the possibility to functionalise the particles. Fig. 1 shows a SEM image of *in situ* synthesised gold SU-8 nanocomposite. The picture shows the presence of a large number of nanoparticles embedded in the polymer matrix. Fig. 2 shows preliminary results from fitted absorption spectra of gold SU-8 composites made by both the *in situ* and the *ex situ* method. It is evident that the embedded particles retain their plasmonic response in the

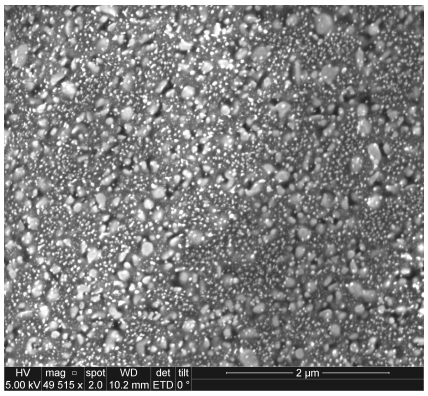

Fig. 1: SEM image of a gold nanocomposite, a large number of gold nanoparticles can be seen. The particles are divided into two groups, small particles of around 30 nm to 50 nm and large particles between 150 nm and 300 nm.

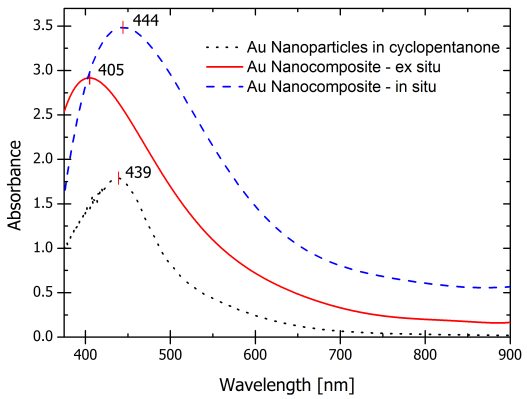

Fig. 2: Fitted Absorption spectra of *ex situ* generated gold nanocomposite (red solid line), and *in situ* generated gold nanocomposite (blue dashed line) and gold nanoparticles suspended in cyclopentanone (black dotted line). The lower wavelength for the absorption peak of the *ex situ* composite indicates smaller nanoparticles than in the *in situ* composite. The instrument went into saturation below 375 nm.

8th International Congress on Advanced Electromagnetic Materials in Microwaves and Optics - Metamaterials 2014
Copenhagen, Denmark, 25-30 August 2014

visible region. From the absorption peaks, it is also understood that the particles achieved by the *in situ* method are larger than with the *ex situ* synthesized particles. Why the bare particles in cyclopentanone show a peak at a significantly higher wavelength has not been investigated.

B. Silver Nanoparticle SU-8 Composite

Fig. 3 shows the SEM image of a silver nanocomposite obtained by an *in situ* synthesis. The silver nanocomposites are found to be electrically conductive. The electrical conductivity of the silver composite is evident from the better images of the silver composite as compared to the *in situ* gold composite shown in Fig. 1.

Comparing Fig. 1 with Fig. 3, large particles surrounded by smaller particles can be seen in case of the gold composite, while the silver composite shows a more homogeneous distribution of particle sizes. In both cases some larger agglomerates of small particles can be seen.

Fig. 4 shows the SEM image of silver SU-8 nanocomposite structured by UV lithography. The *in situ* formed silver nanoparticles are clearly visible and the straight line defined by the UV lithography indicates the possibility of patterning such materials for making devices. The large contamination in the across all areas is to be expected as the process has not been made in a sufficiently clean environment.

V. Conclusion

Gold nanoparticles are successfully embedded in two different ways *in situ* and *ex situ* into an epoxy photoresist material, SU-8, without losing their plasmonic response with visible light. The advantage of *in situ* generation of particles compared to *ex situ* synthesis is the possibility to achieve very high particle concentration, which has not otherwise been possible.

In situ formation of silver particles in the polymer matrix is also done to create a conductive nanocomposite which is subsequently structured using UV lithography, with promising results. We expect that this process will allow structuring with UV lithography at a resolution comparable to that of unmodified SU-8.

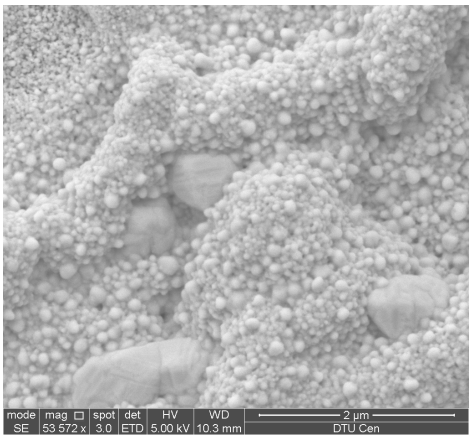

Fig. 3: SEM image of a silver nanocomposite, a complex structure of silver nanoparticles can be seen together with some significantly larger particles.

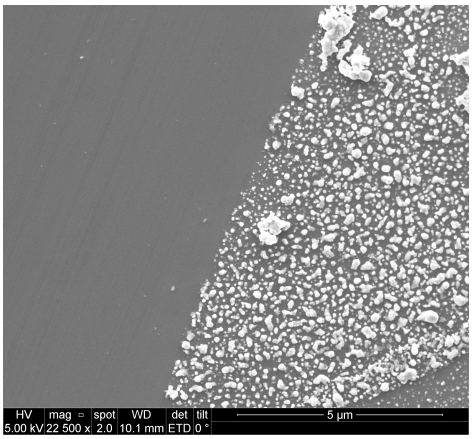

Fig. 4: SEM image of silver nanocomposite structured by UV lithography. A sharp edge defined by UV lithography can be seen between the composite and the substrate.

References

[1] D.V Talapin, J.S. Lee, M.V. Kovalenko, and E.V. Shevchenko, "Prospects of colloidal nanocrystals for electronic and optoelectronic applications," *Chem. Rev.,* vol. 110, pp. 389-458, 2010.
[2] R.A. Sperling and W.J. Parak, "Surface modification, functionalization and bioconjugation of colloidal inorganic nanoparticles," *Phil. Trans. R. Soc. A,* vol. 368 pp. 1333-1383, 2010.
[3] A del Campo and C.A. Geiner, "SU-8: a photoresist for high-aspect-ratio and 3D submicron lithography," *Micromech. Microeng.,* vol. 17 pp. R81-R95, 2007.

Technical University of Denmark

Joint author statement

If a thesis contains articles (i.e. published journal and conference articles, unpublished manuscripts, chapters etc.) made in collaboration with other researchers, a joint-author statement verifying the PhD student's contribution to each article should be made by all authors. However, if an article has more than three authors the statement may be signed by a representative sample, cf. article 12, section 4 and 5 of the Ministerial Order No. 1039 27 August 2013 about the PhD degree. We refer to the Vancouver protocol's definition of authorship.

A representative sample of authors is comprised of

- Corresponding author and/or principal/first author (defined by the PhD student), and if there are more authors:
- 1-2 authors (preferably international/non-supervisor authors)

Titel of the article	Polymer Coated Nanogold for Tracing Mobility of Engineered Nanoparticles in Subsurface Water
Author(s)	B. Uthuppu, A. S. Fjordbøge, S. V. Fischer, M. M. Broholm, M. H. Jakobsen
Journal/conference * if applicable	8th International Congress on Advanced Electromagnetic Materials in Microwaves and Optics – Metamaterials 2014
Name of PhD student	Søren Vang Fischer
Date of Birth	28/4-1986

Description of the PhD student's contribution to the abovementioned article

Correction of article and co-developer of nanoparticle synthesis and coating

Signature of the PhD student S.V. Fischer Date 9/4-2015

Signatures of co-authors

As a co-author I state that the description given above to the best of my knowledge corresponds to the process and I have no further comments.

Date (DD/MM/YY)	Name	Signature
31 March 2015	BASIL UTHUPPU	
07/04/15	Annika S. Fjordbøge	
07/04/15	Mette M. Broholm	

Joint author statements shall be delivered to the *PhD administration* along with the PhD thesis

8th International Congress on Advanced Electromagnetic Materials in Microwaves and Optics – Metamaterials 2014
Copenhagen, Denmark, 25-30 August 2014

Polymer Coated Nanogold for Tracing Mobility of Engineered Nanoparticles in Subsurface Water

B. Uthuppu [1], A. S. Fjordbøge [2], S. V. Fischer [1], M. M. Broholm [2], M. H. Jakobsen [1]

[1] Technical University of Denmark, Department of Micro- and Nanotechnology, Ørsteds Plads 345 B, 2800-Kongens Lyngby, Denmark
[2] Technical University of Denmark, Department of Environmental Engineering, Miljovej 113, 2800-Kongens Lyngby, Denmark
Basil.uthuppu@nanotech.dtu.dk

***Abstract* – Gold nanoparticles coated with amphiphilic block co-polymer PVP-VA are found to be extremely mobile in sand columns in laboratory based experiments. The ultra-stability obtained by such surface modification is also shown by diluting down to a concentration of 62.5 ppb in groundwater having other ions. Such a low level detection of particles is achieved by non-destructive simple UV-Vis spectroscopic technique equipped with liquid wave guide capillary cell (LWCC) units. These results propose the possibility of using surface engineered gold nanoparticles as model system for tracing the mobility of other engineered nanoparticles in the subsurface.**

I. INTRODUCTION

Nanoparticles (NPs) are manufactured for their specific properties providing possibilities for new and improved products and applications. The use of engineered nanoparticles (ENPs) has therefore brought significant innovation and advances to society, including benefits for human health and the environment. At the same time, little is known about the potential risk associated with the inevitable release of these new materials to the environment, and their new properties are poorly understood [1]. Recent advances in chemical synthesis resulted in increased colloidal stability of ENPs in high concentrations by coating with a large variety of natural and synthetic polymers [2]. This also resulted in their enhanced mobility in surface water and groundwater, which may lead to inadvertent impacts on aquatic ecosystems and human health. Hence, there is a need for tracing of ENP behaviour in the environment. Detection of ENPs in natural water systems, however, has proved very challenging [3]. In this paper, we report the possibility of using polymer stabilized gold nanoparticles for tracing the mobility of engineered nanoparticles (ENPs) in the subsurface. Colloidal gold has been of great interest for centuries due to its interaction with visible light to produce vibrant colors. In nanotechnology, the use of gold nanoparticles (AuNPs) as a model system for exploring various phenomena including self-assembly, biolabeling, catalysis, phase transfer, crystal growth and many more is evident from the number of articles found in the literature. The unusual optical-electronic properties, high chemical stability, relatively low toxicity and the rare possibility of natural occurrence in the subsurface have made AuNPs the model system of choice in this context. In this paper we show that otherwise immobile and unstable bare AuNPs achieve enhanced mobility in sand columns and extreme stability on dilution with groundwater containing various ions, when coated with an amphiphilic block co-polymer PVP-VA (polyvinyl pyrrolidone-co-vinyl acetate). It also addresses the possibility of detecting extremely stable colloidal gold in tracer amounts (at least 1000 fold lower than ENPs), to substantiate the use of such an expensive noble element for environmental monitoring.

II. SYNTHESIS OF GOLD NANOPARTICLES

Stable suspensions of AuNPs with high gold concentrations (0.5 mg mL^{-1}) and low size distribution were synthesized by the well-known citrate reduction method with slight modification as described in Li *et al* [4]. The surface modification of AuNPs is attained in two different ways. In a pre-grafting technique, the reduction of Au^{3+} ions by citrate is carried out in the presence of the polymer, PVP-VA (AuNP:PVP-VA_{Pre}) and in the post-grafting technique, AuNPs synthesized first and then the surfaces were modified by shaking with PVP-VA solution (AuNP:PVP-VA_{Post}).

978-1-4799-3452-2/14/$31.00 ©2014 IEEE

III. Mobility of PVP-VA coated gold nanoparticles

Mobility tests were conducted in three transparent PVC columns (30 cm long and 2.125 cm inner diameter) filled with tamped sand (DanSand 00) with a small grain size (0.32 mm-0.71 mm). The columns were feed by a bottom-up flow with a velocity of 1.0 mL/min. The feed solution (12 mL) was introduced to the column followed by tap water until the feed solution has passed through the column. Initially, the columns were fed by a non-reactive chloride tracer solution to determine the flow characteristics in the porous media as a base for comparison with the AuNP solutions. Secondly, three different AuNP solutions (0.3 mg/mL) were introduced to the columns: uncoated AuNPs, AuNP:PVP-VA$_{Pre}$ and AuNP:PVP-VA$_{Post}$. The column effluents were collected continuously (4 mL samples) and the concentrations were measured. The chloride concentration was measured by titration and the AuNP concentration was measured by spectroscopy (absorbance at 520 nm). The mobility of the different NPs was assessed based on breakthrough curves. The breakthrough of a non-reactive tracer occurs after a pore volume of one. Based on the breakthrough of the tracer, the pore volume of a sand filled column was 52.4 mL (equivalent to a porosity of 0.49). It was found that the surface modification with PVP-VA makes the AuNPs mobile in the porous media as shown in figure 1. The uncoated AuNPs have a very low mobility and never broke through the column; instead they were deposited at the column inlet resulting in clogging. However, both pre- and post-grafted AuNPs show no retardation compared to the water front (breakthrough around one pore volume similar to the tracer), while pre-grafted AuNPs show better performance in terms of recovery (larger area under the breakthrough curve). The recovery of pre-grafted AuNPs is 85% (tracer 87%), while only 66% of the post-grafted AuNPs are recovered in the effluent. The better recovery for AuNP:PVP-VA$_{Pre}$ is likely due to stronger ligand – metal particles interactions; the stronger the interaction the lesser the ligand lose during the transport in the porous media.

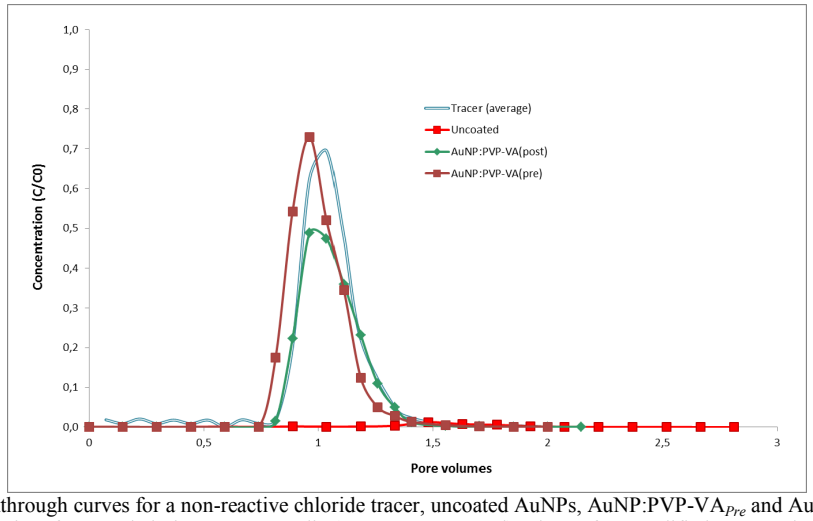

Fig. 1. Breakthrough curves for a non-reactive chloride tracer, uncoated AuNPs, AuNP:PVP-VA$_{Pre}$ and AuNP:PVP-VA$_{Post}$ with a flow velocity of 1.0 mL/min in a porous media (0.32-0.71 mm sand). The surface modified AuNPs show high mobility similar to the tracer (similar breakthrough curves), while unmodified AuNPs are immobile (no breakthrough).

IV. Detection of AuNPs at tracer level

PVP-VA coated AuNPs exhibit a strong plasmonic resonance in the visible spectrum allowing their detection by nondestructive optical methods at concentrations at least 1000 fold lower than most ENPs. Using a conventional UV-Vis spectrometer equipped with liquid waveguide capillary cell (LWCC), nanogold was detected at a very low concentration range (1 ppm – 62.5 ppb). In this technique, 1 m long capillary optical fiber is used instead of cuvettes to hold the sample, thus allowing very low detection limits using conventional UV-

8th International Congress on Advanced Electromagnetic Materials in Microwaves and Optics – Metamaterials 2014
Copenhagen, Denmark, 25-30 August 2014

Vis spectroscopy. Compared to uncoated particles, surface modified nanogold with polymers retains the plasmonic peaks at 528 nm when diluted with artificial ground water (Fig 2). The various ions (such as chloride, nitrate, sulphate etc.) present in the groundwater affect the zeta-potential of the bare nanoparticles and they tend to agglomerate whereas physically adsorbed polymer protects the nanoparticles from agglomeration even at high dilutions.

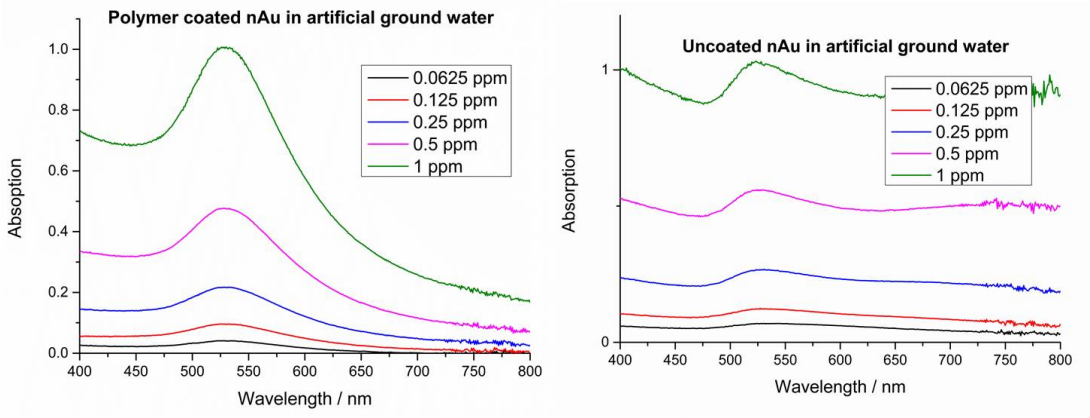

Fig. 2. Plasmonic peaks of gold nanoparticles at ~528 nm for 2-fold dilution series measured in liquid waveguide capillary cell (LWCC) connected with UV-Vis spectrometer. PVP-VA coated AuNPs shows higher stability in groundwater than bare AuNPs

V. CONCLUSION

Modifying surfaces of AuNPs with amphiphilic block co-polymers like PVP-VA make them extremely mobile in sand columns and highly stable even at very high dilutions with artificial groundwater containing other ions. Non-destructive UV-Vis spectroscopic methods equipped with fiber optic techniques (LWCC) allow detecting the gold nanoparticles at tracer concentrations. These findings can be instrumental to use them as model particles for tracing the behavior of other ENPs that are exposed to the subsurface environment for example zero-valent iron nanoparticles (nZVI) which are used for remediation.

ACKNOWLEDGEMENT

The low level detection of nanogold using LWCC was done at the department of nuclear and quantum engineering, KAIST (Korea Advance Institute of Science and Technology), 291 Daehak-ro, (373-1, Guseong-dong), Yuseong-gu, Daejeon 305-701, Republic of KOREA. We acknowledge Prof. Woojin Lee, Prof. Jong-Il Yun, Kim A Young and Tae Hyeong Kim for the same.

REFERENCES

[1] Joris T.K. Quik, Jan Arie Vonk, Steffen Foss Hansen, Anders Baun and Dik Van De Meent, “How to assess exposure of aquatic organisms to manufactured nanoparticles? ”, *Environment International*, vol. 37, pp. 1068-1077, 2011
[2] Wolfgang Schartl, ”Current directions in core-shell nanoparticles design”, *Nanoscale*, vol. 2, pp. 829–843, 2010
[3] Feng He, Dongye Zhao, Chris Paul, “Field assessment of carboxymethyl cellulose stabilized iron nanoparticles for in situ destruction of chlorinated solvents in source zone”, *WATER RESEARCH*, vol. 44, pp. 2360-2370, 2010
[4] Chunfang Li, Dongxiang Li, Ganggiang Wan, Jie Xu and Wanguo Hou, “Facile synthesis of concentrated gold nanoparticles with low size-distribution in water: temperature and pH control”, Nanoscale Research Letters, vol. 6, p. 440, 2011

Appendix E

Articles

PhD and Continuing Education
June 2014 | page 1/1

Technical University of Denmark

Joint author statement

If a thesis contains articles (i.e. published journal and conference articles, unpublished manuscripts, chapters etc.) made in collaboration with other researchers, a joint-author statement verifying the PhD student's contribution to each article should be made by all authors. However, if an article has more than three authors the statement may be signed by a representative sample. cf. article 12. section 4 and 5 of the Ministerial Order No. 1039 27 August 2013 about the PhD degree. We refer to the Vancouver protocol's definition of authorship.

A representative sample of authors is comprised of

- Corresponding author and/or principal/first author (defined by the PhD student)
- 1-2 authors (preferably international/non-supervisor authors)

Titel of the article	Blueshift of the surface plasmon resonance in silver nanoparticles studied with EELS
Author(s)	S. Raza, N. Stenger, S. Kadkhodazadeh, S. V. Fischer, N. Kostesha, A.-P. Jauho, A. Burrows, M. Wubs, and N. A. Mortensen
Journal/conference * if applicable	Nanophotonics 2, 131 (2013)
Name of PhD student	Søren Vang Fischer
Date of Birth	28-04-1986

Description of the PhD student's contribution to the abovementioned article

Synthesised the used nanoparticles and corrected the paper.

Signature of the PhD student S.V. Fischer Date 4/2-15

Signatures of co-authors

As a co-author I state that the description given above to the best of my knowledge corresponds to the process and I have no further comments.

Date (DD/MM/YY)	Name	Signature
30/01/2015	N. A. MORTENSEN	
30/01/2015	Nicolas Stenger	
04/02/2015	Shima Kadkhodazadeh	

Joint author statements shall be delivered to the *PhD administration* along with the PhD thesis

© 2013 Science Wise Publishing & DE GRUYTER DOI 10.1515/nanoph-2012-0032 — Nanophotonics 2013; 2(2): 131–138

Søren Raza[a], Nicolas Stenger[a], Shima Kadkhodazadeh, Søren V. Fischer, Natalie Kostesha, Antti-Pekka Jauho, Andrew Burrows, Martijn Wubs and N. Asger Mortensen*

Blueshift of the surface plasmon resonance in silver nanoparticles studied with EELS

Abstract: We study the surface plasmon (SP) resonance energy of isolated spherical Ag nanoparticles dispersed on a silicon nitride substrate in the diameter range 3.5–26 nm with monochromated electron energy-loss spectroscopy. A significant blueshift of the SP resonance energy of 0.5 eV is measured when the particle size decreases from 26 down to 3.5 nm. We interpret the observed blueshift using three models for a metallic sphere embedded in homogeneous background material: a classical Drude model with a homogeneous electron density profile in the metal, a semiclassical model corrected for an inhomogeneous electron density associated with quantum confinement, and a semiclassical nonlocal hydrodynamic description of the electron density. We find that the latter two models provide a qualitative explanation for the observed blueshift, but the theoretical predictions show smaller blueshifts than observed experimentally.

Keywords: Electron energy loss spectroscopy; nonlocal response; plasmonics.

[a]Both authors contributed equally.
***Corresponding author: N. Asger Mortensen,** Department of Photonics Engineering, Technical University of Denmark, DK-2800 Kgs. Lyngby, Denmark; and Center for Nanostructured Graphene (CNG), Technical University of Denmark, DK-2800 Kgs. Lyngby, Denmark, e-mail: asger@mailaps.org
Søren Raza, Nicolas Stenger and Martijn Wubs: Department of Photonics Engineering, Technical University of Denmark, DK-2800 Kgs. Lyngby, Denmark
Søren Raza, Shima Kadkhodazadeh and Andrew Burrows: Center for Electron Nanoscopy, Technical University of Denmark, DK-2800 Kgs. Lyngby, Denmark
Nicolas Stenger and Antti-Pekka Jauho: Center for Nanostructured Graphene (CNG), Technical University of Denmark, DK-2800 Kgs. Lyngby, Denmark
Søren V. Fischer, Natalie Kostesha and Antti-Pekka Jauho: Department of Micro and Nanotechnology, Technical University of Denmark, DK-2800 Kgs. Lyngby, Denmark

Edited by Javier Garcia de Abajo

1 Introduction

Surface plasmons are collective excitations of the electron gas in metallic structures at the metal/dielectric interface [1]. The ability to concentrate light with SPs [2] and to enhance light-matter interaction on a subwavelength scale enables few and even single-molecule spectroscopy when the size of the metallic structures is decreased to a few nanometers [3]. These collective excitations are usually well-described by the classical Drude model for nanoparticles with dimensions of tens of nanometer and larger [1]. In the quasistatic limit, i.e., when the wavelength of the exciting electromagnetic wave considerably exceeds the dimensions of the structure, the local-response Drude theory predicts that the resonance energy of localized SPs is independent of the size of the nanostructure [4], and that the field enhancement created in the gap between two metallic nanostructures diverges for vanishing gap size [5]. These predictions are however in conflict both with earlier [6–9] and with more recent experimental results, which have shown a size dependency of the localized SP resonance in noble metal nanoparticles in the size range of 1–10 nm [10] and pronounced deviations for dimer geometries [11, 12].

This dependence of the SP resonance on the size of noble metal nanostructures is believed to be a signature of quantum properties of the free-electron gas. With decreasing sizes of the nanoparticles, the quantum wave nature of the electrons is theoretically expected to manifest itself in the optical response due to the effects of quantum confinement [13–17], quantum tunneling [17–20], as well as nonlocal response [21–27]. Nonlocal effects are a direct consequence of the inhomogeneity of the electron gas, which arises due to the quantum wave nature and the many-body properties of the electron gas.

The recent developments in analytical scanning transmission electron microscopes (STEM) equipped with a monochromator and electron energy-loss spectroscopy (EELS) [28] give the possibility of accessing the near-field energy distribution of the plasmon resonance of individual nanoparticles on a subnanometer scale with an energy resolution better than 0.2 eV. This method has

been used for the imaging of surface plasmons in many different metallic nanostructures [10, 29–32]. With STEM EELS it is possible to correlate the structural and chemical information on the nanometer scale, such as the shape and the presence of organic ligands, with the spectral information of the SP resonance of single isolated nanoparticles. STEM EELS is thus perfectly suited to probe and access plasmonic nanostructures and SP resonances at length scales where quantum mechanics is anticipated to become important.

In this paper we report the experimental study of the SP resonance of chemically grown single Ag nanoparticles dispersed on 10 nm thick Si_3N_4 membranes with STEM EELS. Our measurements present a significant blueshift of the SP resonance energy from 3.2 to 3.7 eV for particle diameters ranging from 26 down to 3.5 nm. Our results also confirm very recent experiments made with Ag nanoparticles on different substrates using different STEM operating conditions [10], thereby strengthening the interpretation that the blueshift is predominantly associated with the tight confinement of the plasma and the intrinsic quantum properties of the electron gas itself rather than having an extrinsic cause.

We compare our experimental data to three different models: a purely classical local-response Drude model which assumes a constant electron density profile in the metal nanoparticle, a semiclassical local-response Drude model where the electron density is determined from the quantum mechanical problem of electrons moving in an infinite spherical potential well [16], and finally, a semiclassical model based on the hydrodynamic description of the motion of the electron gas which takes into account nonlocal response through the internal quantum kinetics of the electron gas in the Thomas-Fermi (TF) approximation [33, 34]. We find good qualitative agreement between our experimental data and the two semiclassical models, thus supporting the anticipated nonlocal nature of SPs of Ag nanoparticles in the 1–10 nm size regime. The experimentally observed blueshift is however significantly larger than the predictions by the two semiclassical models.

2 Materials and methods

The nanoparticles are grown chemically following the method described in Ref. [35] and subsequently stabilized in an aqueous solution with borohydride ions. The mean size of the nanoparticles is 12 nm with a very broad size distribution ranging from 3 to 30 nm. The nanoparticle solution is dispersed on a 10 nm thick commercially available Si_3N_4 membrane (TEMwindows.com), which has a refractive index of approximately $n \approx 2.1$ [36]. To characterize our nanoparticles we have used an aberration-corrected STEM FEI Titan (www.FEI.com) operated at 120 kV with a probe diameter of approximately 0.5 nm, and convergence and collection angles of 15 mrads and 17 mrads, respectively. The Titan is equipped with a monochromator allowing us to perform EELS with an energy resolution of 0.15±0.05 eV. We systematically performed EELS measurements at the surface and in the middle of each nanoparticle. The EELS spectra were taken with an exposure time of 90 ms to avoid beam damage as much as possible. To improve the signal-to-noise ratio we accumulated 10–15 spectra for each measurement point. We observed no evidence of damage after each measurement.

The experimental data were analyzed with the aid of commercially available software (Digital Micrograph) and three different methods were used to reconstruct and remove the zero-loss peak (ZLP): the first method is the reflected tail (RT) method, where the negative-energy half part of the ZLP is reflected about the zero-energy axis to approximate the ZLP at positive energies, while the second method is based on fitting the ZLP to the sum of a Gaussian and a Lorentzian functions. The third method is to prerecord the ZLP prior to each set of EELS measurements. All three methods yielded consistent results.

The energies of the SP resonance peaks were determined by using a nonlinear least-squares fit of our data to Gaussian functions. The error in the resonance energy is given by the 95 % confidence interval for the estimate of the position of the center of the Gaussian peak. Nanoparticle diameters were determined by calculating the area of the imaged particle and assigning to the area an effective diameter by assuming a perfect circular shape. The error bars in the size therefore correspond to the deviation from the assumption of a circular shape, which is estimated as the difference between the largest and smallest diameter of the particle.

3 Theory

In the following theoretical analysis our hypothesis is that the blueshift of the SP resonance energy is related to the properties of the electron density profile in the metal nanoparticle. Therefore, we use three different approaches to model the electron density of the Ag nanoparticle. In all three approaches, we calculate the optical response and thereby also the resonance energies of the nanoparticle through the quasistatic polarizability α of a sphere embedded in a homogeneous background dielectric with

permittivity ε_B. With this approach, we make two implicit assumptions: the first is that we can neglect retardation effects and the second is that we can neglect the symmetry-breaking effect of the substrate. We have validated the quasistatic approach by comparing to fully retarded calculations [37], which shows excellent agreement in the particle size range we consider. The effect of the substrate will be taken into account indirectly by determining an effective homogeneous background permittivity ε_B using the average resonance frequency of the largest particles ($2R$>20 nm) as the classical limit.

The first, and simplest, approach is to assume a constant free-electron density n_0 in the metal particle, which drops abruptly to zero outside the particle. This assumption is the starting point of the classical local-response Drude model for the response of the Ag nanoparticle, where the polarizability is given by the Clausius-Mossotti relation, which is well-known to be size independent for subwavelength particles. The classical local-response polarizability α_L is [1]

$$\alpha_L(\omega)=4\pi R^3\frac{\varepsilon_D(\omega)-\varepsilon_B}{\varepsilon_D(\omega)+2\varepsilon_B}, \tag{1}$$

where R is the radius of the particle and $\varepsilon_D(\omega)=\varepsilon_\infty(\omega)-\omega_p^2/(\omega^2+i\gamma\omega)$ is the classical Drude permittivity taking additional frequency-dependent polarization effects such as interband transitions into account through $\varepsilon_\infty(\omega)$, not included in the plasma response of the free-electron gas itself.

The second approach is to correct the standard approximation in local-response theory of a homogeneous electron density profile by using insight from the quantum wave nature of electrons to model the electron density profile and take into account the quantum confinement of the electrons. For nanometer-sized spheres, the classical polarizability given by the Clausius-Mossotti relation must be altered to take into account an inhomogeneous electron density. In Ref. [16], it is shown that in general the local-response polarizability for a sphere embedded in a homogeneous material is given as

$$\alpha_{LQC}(\omega)=12\pi\int_0^R r^2 dr\frac{\varepsilon(r,\omega)-\varepsilon_B}{\varepsilon(r,\omega)+2\varepsilon_B}, \tag{2}$$

now with a spatially varying Drude permittivity [16, 17]

$$\varepsilon(r,\omega)=\varepsilon_\infty(\omega)-\frac{\omega_p^2}{\omega(\omega+i\gamma)}\frac{n(r)}{n_0}. \tag{3}$$

Here, $n(r)$ is the electron density in the metal nanoparticle. Clearly, if $n(r)=n_0$ we arrive at the classical Clausius-Mossotti relation Eq. (1) as expected. To determine the density profile in this local-response model, we follow the approach of Ref. [16] and assume that the free electrons move in an infinite spherical potential well. The approach just outlined of a local-response theory with an inhomogeneous electron density is very similar to the theoretical model used in Ref. [10] for explaining their experimental results. It should be noted that any effects due to electron spill-out and quantum tunneling are neglected in all of the approaches that we consider.

The third and final approach is to compare our experimental data with a linearized nonlocal hydrodynamic model in which the electron density is allowed to deviate slightly from the constant electron density used in classical local-response theories [22, 38–40]. The dynamics of the electron gas is governed by the semiclassical hydrodynamic equation of motion [25, 26, 34], which results in an inhomogeneous electron density profile. The nonlocal hydrodynamic polarizability $\alpha_{NL}(\omega)$ is exactly given as

$$\alpha_{NL}(\omega)=4\pi R^3\frac{\varepsilon_D(\omega)-\varepsilon_B(1+\delta_{NL})}{\varepsilon_D(\omega)+2\varepsilon_B(1+\delta_{NL})}, \tag{4}$$

$$\delta_{NL}=\frac{\varepsilon_D(\omega)-\varepsilon_\infty(\omega)}{\varepsilon_\infty(\omega)}\frac{j_1(k_LR)}{k_LRj_1'(k_LR)}, \tag{5}$$

and these results constitute our nonlocal-response generalization of the Clausius-Mossotti relation of classical optics. Here, $k_L=\sqrt{\omega^2+i\omega\gamma-\omega_p^2/\varepsilon_\infty}/\beta$ is the wave vector of the additional longitudinal wave allowed to be excited in the hydrodynamic nonlocal theory [25, 34], and j_1 is the spherical Bessel function of first order. Finally, within TF theory $\beta^2=3/5v_F^2$, where v_F is the Fermi velocity [34]. We emphasize that for $\beta\to0$, the local-response Drude result is retrieved, since $\delta_{NL}\to0$ and Eq. (4) simplifies to the classical Clausius-Mossotti relation Eq. (1).

The SP resonance energy follows theoretically from the Fröhlich condition, i.e., we must consider the poles of Eq. (4). For sufficiently small blueshifts and neglecting damping, the resonance frequency can be approximated by

$$\omega=\frac{\omega_P}{\sqrt{\mathrm{Re}[\varepsilon_\infty(\omega)]+2\varepsilon_B}}+\sqrt{\frac{2\varepsilon_B}{\mathrm{Re}[\varepsilon_\infty(\omega)]}}\frac{\beta}{2R}+O\left(\frac{1}{R^2}\right), \tag{6}$$

where the first term is the common size-independent local-response Drude result for the SP resonance that also follows from Eq. (1), and the second term gives the size-dependent blueshift due to nonlocal corrections. At this stage, we note that a $1/(2R)$ dependence was experimentally observed in Refs. [6, 7] using optical spectroscopy. However, Eq. (6) reveals, besides a $1/(2R)$ dependence, that there is a delicate interplay in the blueshift between the material parameters of the metal, through $\varepsilon_\infty(\omega)$ and

β, and the background medium ε_B. Furthermore, Eq. (6) shows that the blueshift can be enhanced with a large-permittivity background medium.

4 Results

Figures 1(A–C) display STEM images of Ag nanoparticles with diameters of 15.5, 10.0, and 5.5 nm, respectively. The images show that no chemical residue is left from the synthesis and that the particles are faceted. We find that approximately 70% of the studied nanoparticles have a relative size error (i.e., the ratio of the size error bar to the particle diameter) below 20% (determined from the 2D STEM images), verifying that the shape of the nanoparticles is to a first approximation overall spherical (see Supplementary Figure 1). On a subset of the particles, thickness measurements using image recordings at different tilt angles were performed, revealing information about the shape of the nanoparticle in the third dimension. Such 3D investigations confirmed that the shape is overall spherical, but however could not be completed for all particles due to stability issues: the positions of tiny nanoparticles fluctuate under too long exposure of the electron beam, thus preventing accurate determination of the shape of the nanoparticle in the third dimension perpendicular to the substrate.

Figures 1(D–F) display raw normalized EELS data, acquired on Ag nanoparticles with diameters 14.1, 9.8, and 6.6 nm, respectively. The peaks correspond to the excitation of the SP. When the diameter of the nanoparticle decreases, the SP resonance clearly shifts progressively to higher energies. Figures 1(D–F) also display that the amplitude and linewidth of the SP resonances can vary from particle to particle (with the same size) and at times show narrowing instead of the expected broadening of the resonance for decreasing nanoparticle sizes [6, 13, 14]. This is for example seen in the linewidths in Figures 1(D–F) which seem to decrease with size. However, as will be explained in more detail in the next paragraph, we did not find a systematic trend of the linewidths in our EELS measurements probably due to the shape variations in our ensemble of nanoparticles.

Figure 2 displays the resonance energy of the SP as a function of the diameter of the nanoparticles. A significant blueshift of the SP resonance of 0.5 eV is observed when

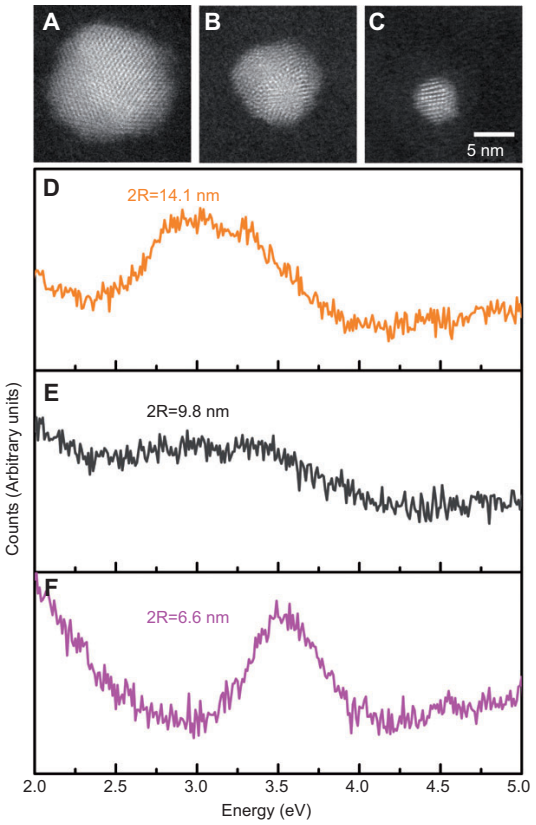

Figure 1 Aberration-corrected STEM images of Ag nanoparticles with diameters (A) 15.5 nm, (B) 10 nm, and (C) 5.5 nm, and normalized raw EELS spectra of similar-sized Ag nanoparticles (D-F). The EELS measurements are acquired by directing the electron beam to the surface of the particle.

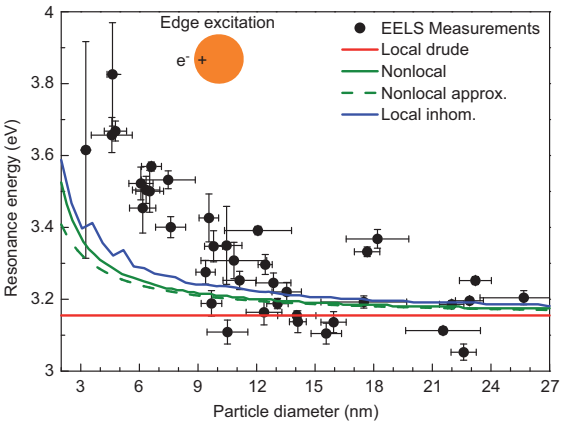

Figure 2 Nanoparticle SP resonance energy as a function of the particle diameter. The dots are EELS measurements taken at the surface of the particle and analyzed using the RT method, and the lines are theoretical predictions. We use parameters from Ref. [41]: $\hbar\omega_p$=8.282 eV, $\hbar\gamma$=0.048 eV, n_0=5.9×10^{28} m^{-3} and v_F=1.39×10^6 m/s. From the average large-particle ($2R$>20 nm) resonances we determine ε_B=1.53.

the nanoparticle diameter decreases from 26 to 3.5 nm. This trend is in good agreement with the results shown in Ref. [10], despite the difference in the substrate and the STEM operating conditions, a strong indication that the blueshift of Ag nanoparticles is robust to extrinsic variations. Another prominent feature in Figure 2 is the scatter of resonance energies at a fixed particle diameter. We mainly attribute the spread in resonance energies at a given particle size to shape variations in our ensemble of nanoparticles (see Supplementary Material). Slight deviations from perfect circular shape in the STEM images will result in a delicate dependency on the location of the electron probe and give rise to splitting of SP resonance energies due to degeneracy lifting. In this regard, we also note that even a perfectly circular particle on a 2D STEM image may still possess some weak prolate or oblate deformation in the third dimension, resulting in a departure from spherical shape. Calculations using the local response model show that a 20% deformation of a sphere into an oblate or prolate spheroid results in a 0.4 eV spread in resonance energy (see Supplementary Figure 2), which is approximately the spread in resonance energy we observe for particles larger than 10 nm. Furthermore, shape deviations may also impact the linewidth of the SP resonance, since the electron probe can excite the closely-spaced non-degenerate resonance energies simultaneously, which may appear as a single broadened peak. This broadening mechanism could explain the apparent linewidth narrowing for decreasing particle size seen in Figures 1(D–F). However, we cannot rule out that other effects beyond shape deviations contribute to the spread of resonance energies and impact the SP resonance linewidth. These could for example be the facets or the particle-to-substrate interface [42].

Along with the EELS measurements in Figure 2, we show Eq. (1) for the local-response Drude model (red line) and the semiclassical local-response model Eq. (3) (blue line). Furthermore, the nonlocal relation of Eq. (3) (green solid line) and the approximate nonlocal relation of Eq. (6) (green dashed line) are also depicted, and we see that Eq. (6) is accurate for particle sizes $2R \gtrsim 10$ nm.

Due to the narrow energy range in consideration (~3.0–3.9 eV), we approximate $\varepsilon_\infty(\omega)$ as a second-order Taylor polynomial based on the frequency-dependent values given for Ag in Ref. [41]. We find $\varepsilon_\infty(\omega)=(59.8+i55.1)(\omega/\omega_p)^2-(40.3+i42.4)(\omega/\omega_p)+(10.5+i8.6)$. Since the refractive index of the Si_3N_4 substrate varies hardly ($n\approx2.1$) in the narrow energy range we consider [36], we assume that the background permittivity ε_B is constant and determine it by approximating the average resonance energy of the largest particles ($2R>20$ nm) as the classical limit, i.e., the first term of Eq. (6).

It is known that local Drude theory produces size-independent resonance frequencies of subwavelength particles, but this theory is clearly inadequate to describe the measurements of Figure 2. The nonlocal quasistatic hydrodynamic model predicts a blueshift in agreement with the experimental EELS measurements. Interestingly, the measured blueshift is even larger than predicted. We also see that the local-response model with an inhomogeneous electron density profile shows a similar trend as the nonlocal hydrodynamic model, indicating that these two different models describe very similar physical effects. The oscillations in the resonance energy in the inhomogeneous local-response model seen for small particle diameter are due to small variations in the density profile with decreasing size (i.e., discrete changes in the number of electrons), as also stated in Ref. [10].

The inhomogeneous local-response model and the nonlocal hydrodynamic model, when applied to a sphere in a homogeneous background medium, agree qualitatively with the EELS measurements. However, they do not provide the full picture. One of the probable issues arising is that the substrate is taken into account indirectly through a homogeneous background medium, a state-of-the-art procedure [10] which however may not be adequate to describe the effects of the presence of a dielectric substrate. It has been shown that the dielectric substrate modifies the absorption spectrum of an isolated sphere [43] and also the waveguiding properties of nanowires [31, 44, 45]. In an attempt to include the symmetry breaking effect of the substrate in our theoretical analysis, we apply a simple image charge model. The main effect of the substrate in this picture stems from the interaction of the dipole mode of the nanoparticle with the induced dipole mode in the substrate [46–48]. However, we find that such a dipole-dipole model for the substrate is inadequate to describe the large blueshift observed experimentally (see Supplementary Material). Indeed, it has been shown that the induced image charges in the substrate can make the contributions of higher order multipoles in the nanoparticle important [49], and it has also been observed theoretically that higher order multipoles produce larger blueshifts in the nonlocal hydrodynamic model (Figure 2 in Ref. [50]). The impact of the substrate on the electron density inhomogeneity and thereby the SP resonance energy depends on the thickness and refractive index of the substrate, which may explain the quantitative agreement between theory and experiment reported in Ref. [10], since thinner substrates with smaller refractive indexes were used in their experiments. In order to completely address this issue, one would need to go beyond the dipole-dipole model for the substrate, thus future 3D EELS simulations taking nonlocal effects

and/or inhomogeneous electron densities into account would be needed.

Another complementary explanation in the context of the inhomogeneity of the free-electron density could be the combined contribution of both the inhomogeneous static equilibrium electron density and nonlocality. It is well-known that the static equilibrium electron density is inhomogeneous, even in a semi-infinite metal [51], due to Friedel oscillations and the electron spill-out effect at the metal surface. The Friedel oscillations are modeled in the local quantum-confined model given by Eq. (3) while nonlocality is neglected, and *vice versa* in the nonlocal hydrodynamic model given by Eq. (3). As seen in Figure 2, the two effects separately give rise to similar-sized blueshifts, suggesting that the contribution of both effects simultaneously could add up to the significantly larger experimentally observed blueshift. Simply put, an extension of the nonlocal hydrodynamic model to include an inhomogeneous equilibrium free-electron density could produce a larger blueshift, which may be in accordance with the experimental observations. Furthermore, such a model could also take into account the electron spill-out effect, which in free-electron models has been argued to produce a redshift of the SP resonance [21, 50, 52–54], describing adequately simple metals. In contrast, it has also been shown that the spill-out effect in combination with the screening from the *d* electrons gives rise to the blueshift seen in Ag nanoparticles [55].

Additional size effects such as changes of the electronic band structure of the smallest nanoparticles, which are considerably more difficult to take into account, also impact the shift in SP resonance energy [6].

5 Conclusion

We have investigated the surface plasmon resonance of spherical silver nanoparticles ranging from 26 down to 3.5 nm in size with STEM EELS and observed a significant blueshift of 0.5 eV of the resonance energy. We have compared our experimental data with three different models based on the quasistatic optical polarizability of a sphere embedded in a homogeneous material. Two of the models, a nonlocal hydrodynamic model and a generalized local model, incorporate an inhomogeneity of the electron density induced by the quantum wave nature of the electrons. These two different models produce similar results in the SP resonance energy and describe qualitatively the blueshift observed in our measurements. Although our exact hydrodynamic generalization of the Clausius-Mossotti relation predicts a nonlocal blueshift that grows fast [as $1/(2R)$] when decreasing the diameter and increases even faster for the smallest particles ($2R$<10 nm), the observed blueshifts are nevertheless larger than predicted.

The quantitative agreement between the two different theoretical models and the discrepancy with the larger observed blueshift suggest that a more detailed theoretical description of the system is needed to fully understand the influence of the substrate and the effect of the confinement of free electrons on the SP resonance shift in silver nanoparticles. On the experimental side, further EELS studies of other metallic materials and on different substrates could unveil the mechanism behind the size dependency of the SP resonance of nanometer scale particles.

Acknowledgments: We thank S. I. Bozhevolnyi for directing our attention to the theoretical model in Ref. [16] and G. Toscano for fruitful discussions. The Center for Nanostructured Graphene is sponsored by the Danish National Research Foundation, Project DNRF58. The A. P. Møller and Chastine Mc-Kinney Møller Foundation is gratefully acknowledged for the contribution toward the establishment of the Center for Electron Nanoscopy. N. Stenger acknowledges financial support by a Lundbeck Foundation Grant Nbr. R95-A10663.

Received October 9, 2012; accepted February 19, 2013; previously published online March 23, 2013

References

[1] Maier SA. Plasmonics: fundamentals and applications. New York: Springer; 2007.
[2] Schuller JA, Barnard ES, Cai W, Jun YC, White JS, Brongersma ML. Plasmonics for extreme light concentration and manipulation. Nat Mater 2010;9:193–204.
[3] Kneipp K. Surface-enhanced Raman scattering. Phys Today 2007;60:40–6.
[4] Wang F, Shen YR. General properties of local plasmons in metal nanostructures. Phys Rev Lett 2006;97:206806.
[5] Romero I, Aizpurua J, Bryant GW, García de Abajo FJ. Plasmons in nearly touching metallic nanoparticles: singular response in the limit of touching dimers. Opt Express 2006;14:9988–99.
[6] Kreibig U, Genzel L. Optical absorption of small metallic particles. Surf Sci 1985;156:678–700.

[7] Charlé K-P, Schulze W, Winter B. The size dependent shift of the surface-plasmon absorption-band of small spherical metal particles. Z Phys D 1989;12:471–5.
[8] Ouyang F, Batson P, Isaacson M. Quantum size effects in the surface-plasmon excitation of small metallic particles by electron-energy-loss spectroscopy. Phys Rev B 1992;46:15421–5.
[9] Berciaud S, Cognet L, Tamarat P, Lounis B. Observation of intrinsic size effects in the optical response of individual gold nanoparticles. Nano Lett 2005;5:515–8.
[10] Scholl JA, Koh AL, Dionne JA. Quantum plasmon resonances of individual metallic nanoparticles. Nature 2012;483:421–7.
[11] Ciracì C, Hill RT, Mock JJ, Urzhumov Y, Fernández-Domínguez AI, Maier SA, Pendry JB, Chilkoti A, Smith DR. Probing the ultimate limits of plasmonic enhancement. Science 2012;337:1072–4.
[12] Kern J, Grossmann S, Tarakina NV, Häckel T, Emmerling M, Kamp M, Huang J-S, Biagioni P, Prangsma J, Hecht B. Atomic-scale confinement of resonant optical fields. Nano Lett 2012;12:5504–9.
[13] Genzel L, Martin TP, Kreibig U, Dielectric function and plasma resonance of small metal particles. Z Phys B 1975;21:339–46.
[14] Kraus WA, Schatz GC. Plasmon resonance broadening in small metal particles. J Chem Phys 1983;79:6130.
[15] Halperin WP, Quantum size effects in metal particles. Rev Mod Phys 1986;58:533–606.
[16] Keller O, Xiao M, Bozhevolnyi S. Optical diamagnetic polarizability of a mesoscopic metallic sphere: transverse self-field approach. Opt Comm 1993;102:238–44.
[17] Öztürk ZF, Xiao S, Yan M, Wubs M, Jauho A-P, Mortensen NA. Field enhancement at metallic interfaces due to quantum confinement. J Nanophot 2011;5:051602.
[18] Zuloaga J, Prodan E, Nordlander P. Quantum description of the plasmon resonances of a nanoparticle dimer. Nano Lett 2009;9:887–91.
[19] Mao L, Li Z, Wu B, Xu H. Effects of quantum tunneling in metal nanogap on surface-enhanced Raman scattering. Appl Phys Lett 2009;94:243102.
[20] Esteban R, Borisov AG, Nordlander P, Aizpurua J. Bridging quantum and classical plasmonics with a quantum-corrected model. Nat Commun 2012;3:825.
[21] Ljungbert A, Lundqvist S. Non-local effects in the optical absorption of small metallic particles. Phys Rev Lett 1985;156:839–44.
[22] García de Abajo FJ. Nonlocal effects in the plasmons of strongly interacting nanoparticles, dimers, and waveguides. J Phys Chem C 2008;112:17983–7.
[23] David C, García de Abajo FJ. Spatial nonlocality in the optical response of metal nanoparticles. J Phys Chem C 2012;115:19470–5.
[24] Aizpurua J, Rivacoba A. Nonlocal effects in the plasmons of nanowires and nanocavities excited by fast electron beams. Phys Rev B 2008;78:035404.
[25] Raza S, Toscano G, Jauho A-P, Wubs M, Mortensen NA. Unusual resonances in nanoplasmonic structures due to nonlocal response. Phys Rev B 2011;84:121412(R).
[26] Toscano G, Raza S, Jauho A-P, Mortensen NA, Wubs M. Modified field enhancement and extinction in plasmonic nanowire dimers due to nonlocal response. Opt Express 2012;20:4176.
[27] Fernández-Domínguez AI, Wiener A, García-Vidal FJ, Maier SA, Pendry JB. Transformation-optics description of nonlocal effects in plasmonic nanostructures. Phys Rev Lett 2012;108:106802.
[28] García de Abajo FJ. Optical excitations in electron microscopy. Rev Mod Phys 2010;82:209–75.
[29] Nelayah J, Kociak M, Stephan O, García de Abajo FJ, Tence M, Henrard L, Taverna D, Pastoriza-Santos I, Liz-Marzan LM, Colliex C. Mapping surface plasmons on a single metallic nanoparticle. Nat Phys 2007;3:348–53.
[30] Koh AL, Bao K, Khan I, Smith WE, Kothleitner G, Nordlander P, Maier SA, McComb DW. Electron energy-loss spectroscopy (EELS) of surface plasmons in single silver nanoparticles and dimers: influence of beam damage and mapping of dark modes. ACS Nano 2009;3:3015–22.
[31] Nicoletti O, Wubs M, Mortensen NA, Sigle W, van Aken PA, Midgley PA. Surface plasmon modes of a single silver nanorod: an electron energy loss study. Opt Express 2011;19:15371.
[32] Koh AL, Fernández-Domínguez AI, McComb DW, Maier SA, Yang JKW. High-resolution mapping of electron-beam-excited plasmon modes in lithographically defined gold nanostructures. Nano Lett 2011;11:1323–30.
[33] Bloch F. Bremsvermögen von Atomen mit mehreren Elektronen. Z Phys A 1933;81:363–76.
[34] Boardman A. Electromagnetic surface modes. Hydrodynamic theory of plasmon-polaritons on plane surfaces. Chichester: John Wiley and Sons; 1982.
[35] Mulfinger L, Solomon SD, Bahadory M, Jeyarajasingam A, Rutkowsky SA, Boritz C. Synthesis and study of silver nanoparticles. J Chem Educ 2007;84:322–5.
[36] Bååk T. Silicon oxynitride; a material for GRIN optics. Appl Opt 1982;21:1069–72.
[37] Ruppin R. Optical properties of a plasma sphere. Phys Rev Lett 1973;31:1434–7.
[38] Pendry JB, Aubry A, Smith DR, Maier SA. Transformation optics and subwavelength control of light. Science 2012;337:549–52.
[39] Dasgupta BB, Fuchs R. Polarizability of a small sphere including nonlocal effects, Phys Rev B 1981;24:554–61.
[40] Fuchs R, Claro F. Multipolar response of small metallic spheres: nonlocal theory. Phys Rev B 1987;35:3722–7.
[41] Rakić AD, Djurišić AB, Elazar JM, Majewski ML. Optical properties of metallic films for vertical-cavity optoelectronic devices. Appl Opt 1998;37:5271–83.
[42] Noguez C. Surface plasmons on metal nanoparticles: the influence of shape and physical environment. J Phys Chem C 2007;111:3806–19.
[43] Ruppin R. Optical absorption by a small sphere above a substrate with inclusion of nonlocal effects. Phys Rev B 1992;45:11209–15.
[44] Li Z, Bao K, Fang Y, Guan Z, Halas NJ, Nordlander P, Xu H. Effect of a proximal substrate on plasmon propagation in silver nanowires. Phys Rev B 2010;82:1.
[45] Zhang S, Xu H. Optimizing substrate-mediated plasmon coupling toward high-performance plasmonic nanowire waveguides. ACS Nano 2012;6:8128–35.
[46] Yamaguchi T, Yoshida S, Kinbara A. Optical effect of the substrate on the anomalous absorption of aggregated silver films. Thin Solid Films 1974;21:173–87.
[47] Jain PK, Huang W, El-Sayed MA. On the universal scaling behavior of the distance decay of plasmon coupling in metal

nanoparticle pairs: a plasmon ruler equation. Nano Lett 2007;7:2080–8.
[48] Novotny L, Hecht B. Principles of nano-optics. New York: Cambridge; 2006.
[49] Ruppin R. Surface modes and optical absorption of a small sphere above a substrate. Surf Sci 1983;127:108–18.
[50] Boardman AD, Paranjape BV. The optical surface modes of metal spheres. J Phys F Met Phys 1977;7:1935.
[51] Lang ND, Kohn W. Theory of metal surfaces: charge density and surface energy. Phys Rev B 1970;1:4555–68.
[52] Ascarelli P, Cini M. "Red shift" of the surface plasmon resonance absorption by fine metal particles. Solid State Commun 1976;18:385–8.
[53] Ruppin R. Plasmon frequencies of small metal spheres. J Phys Chem Solids 1978;39:233–7.
[54] Apell P, Ljungbert Å. Red shift of surface plasmons in small metal particles. Solid State Commun 1982;44:1367–9.
[55] Liebsch A. Surface-plasmon dispersion and size dependence of Mie resonance: silver versus simple metals. Phys Rev B 1993;48:11317–28.

Technical University of Denmark

Joint author statement

If a thesis contains articles (i.e. published journal and conference articles, unpublished manuscripts, chapters etc.) made in collaboration with other researchers, a joint-author statement verifying the PhD student's contribution to each article should be made by all authors. However, if an article has more than three authors the statement may be signed by a representative sample, cf. article 12, section 4 and 5 of the Ministerial Order No. 1039 27 August 2013 about the PhD degree. We refer to the Vancouver protocol's definition of authorship.

A representative sample of authors is comprised of

- Corresponding author and/or principal/first author (defined by the PhD student), and if there are more authors:
- 1-2 authors (preferably international/non-supervisor authors)

Titel of the article	In Situ SU-8 Silver Nanocomposites
Author(s)	S. V. Fischer, B. Uthuppu, M. H. Jakobsen
Journal/conference * if applicable	Beilstein Journal of Nanotechnology
Name of PhD student	Søren Vang Fischer
Date of Birth	28/4-1986

Description of the PhD student's contribution to the abovementioned article

Main writer and performer of experiments and characterisation

Signature of the PhD student S. V. Fischer Date 31/3 - 2015

Signatures of co-authors

As a co-author I state that the description given above to the best of my knowledge corresponds to the process and I have no further comments.

Date (DD/MM/YY)	Name	Signature
31 March 2015	BASIL UTHUPPU	
31/3-2015	MOGENS H. JAKOBSEN	Mogens Jakobsen

Joint author statements shall be delivered to the *PhD administration* along with the PhD thesis

In Situ SU-8 Silver Nanocomposites

Søren V. Fischer*[1], Basil Uthuppu[1] and Mogens H. Jakobsen[1]

Address: [1]DTU Nanotech, Technical University of Denmark, Anker Engelundsvej 1, 2800 Kgs. Lyngby, Denmark

Email: Søren V. Fischer – soren.fischer@nanotech.dtu.dk

* Corresponding author

Abstract

Nanocomposite materials containing metal nanoparticles are of considerable interest in photonics and optoelectronics applications. However, device fabrication of such materials always encounters the challenge of incorporation of pre-formed nanoparticles into photoresist materials. As a solution to this problem, an easy new method of fabricating silver nanocomposites by an in situ reduction of precursors within the epoxy-based photoresist SU-8 has been developed. AgNO3 dissolved in acetonitrile and mixed with the epoxy-based photoresist SU-8 forms silver nanoparticles primarily during the pre- and post-exposure soft bake steps at 95ºC. A further high temperature treatment at 300ºC resulted in formation of densely homogeneously distributed silver nanoparticles in the photoresist matrix. No particle growth or agglomeration of nanoparticles is observed at this point. The reported new in situ Silver Nanocomposite materials can be spin coated as homogeneous thin films and structured using UV lithography. A resolution of 5 µm is achieved in the lithographic process. The UV exposure time is found to be independent of nanoparticle concentration. The fabricated silver nanocomposites exhibit high

plasmonic responses suitable for development of new optoelectronic and optical sensing devices.

Keywords

Functional photoresist; *in situ* synthesis; metal nanoparticles; micro and nanofabrication; nanocomposite

Introduction

Introduction text

Noble metal nanoparticles (NPs) have been of high interest for many years as their unique properties make them useable in a large variety of applications [1]. The application of these NPs ranges from optical imaging, optoelectronics and electrochemistry to catalysts [2].

However, it is difficult to use such NPs in conjunction with standard top down micro- and nanofabrication processes as the positioning and control of the nanoparticles are impossible to maintain. Homogeneous polymeric thin film metal nanocomposites are therefore of great interest within micro- and nanofabrication. The nanoparticles encased in a polymeric matrix should maintain their physical properties, while the nanocomposite can be structured using standard fabrication methods allowing development of new optoelectronic and sensing devices.

A good candidate for a polymeric matrix is the epoxy-based photoresist SU-8 which is widely used for making high aspect ratio structures [3]. SU-8 is good for optical sensors being highly transparent in the visible region [4] and also useful in biological sensing applications being quite biocompatible [5].

SU-8 thin films are deposited on wafers using standard spin coating techniques [6]. However, high loadings of pre-formed NPs in the polymer change the rheological behaviour and might hinder the ability to use spin-coating for thin film

nanocomposites [7, 8]. Furthermore, it is difficult to obtain a stable suspensions of pre-formed NPs in SU-8 without aggregation and phase separation.

In situ synthesis methods where the particles are formed directly within the polymeric matrix from a precursor can circumvent this problem.

Here we report a fast and simple method for fabricating homogeneous SU-8 based metal nanocomposite thin films with in situ generated silver nanoparticles. These composite materials can be deposited on wafers using standard spin coating techniques and subsequently structured with UV lithography.

The nanocomposite is prepared by dissolving a $AgNO_3$ precursor in acetonitrile in a two-fold dilution series: 500 mg mL^{-1}, 250 mg mL^{-1}, 125 mg mL^{-1}, 62.5 mg mL^{-1}, 31.3 mg mL^{-1}, and 15.6 mg mL^{-1}. 0.5 mL of the freshly prepared precursor solutions or 0.5 mL acetonitrile as reference is added to 4 mL of SU-8 2002, which is a formulation of SU-8 with cyclopentanone as the main solvent. As $AgNO_3$ is not soluble in cyclopentanone, acetonitrile is chosen as a co-solvent. $AgNO_3$ precursor solutions with a concentration above 500 mg mL^{-1} are immiscible with SU-8 using the described protocol.

The SU-8 mixture is then spun on a 100 mm fused silica or silicon wafer, at 1500 RPM for 1 min followed by heating at 95°C on a hotplate for 10 min. After heating, a UV of 5 min is performed to cross-link the polymer followed by a post exposure bake at 95°C on a hotplate for 10 min. In case of structuring, a mask is used during the exposure and the wafer is then developed for 2 min in propylene glycol monomethyl ether acetate (PGMEA) followed by rinsing with 2-propanol (IPA). After development or post exposure bake some of the wafers are further heated to 300°C for 30 min on a hotplate. The UV exposure is done without any filters in the aligner.

Acetonitrile, the chosen co-solvent for the precursor $AgNO_3$, is a mild reducing agent. This precursor solution must therefore be prepared fresh, and added to the SU-8 just before spin coating, to minimise unwanted nanoparticle formation.

Mostly, AgNPs are formed during the heat treatments before and after UV exposure. The exact process is not known as acetonitrile and the many constituents of SU-8 play a role in the NP formation. The AgNPs formed in the SU-8 polymer matrix shows strong plasmonic absorption in the visible region as seen in Fig. 1.

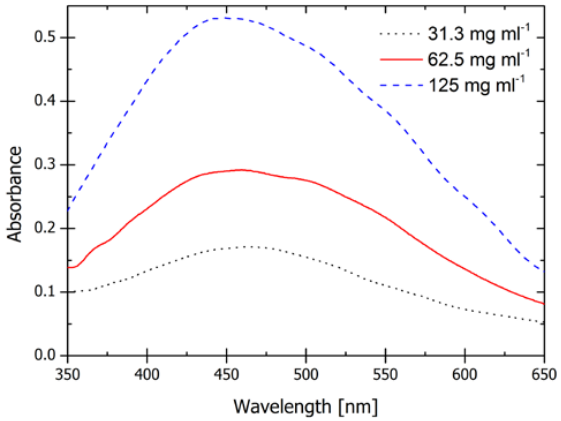

Figure 1: UV-Vis absorption spectra of silver nanocomposites at silica wafers after post-exposure bake at 95°C with varying $AgNO_3$ precursor concentrations. The absorption increases with increasing amounts of $AgNO_3$ precursor added.

The high temperature post-exposure bake at 300°C resulted in the formation of densely populated silver nanoparticles in the polymer matrix. They appeared to be single nanoparticles entities, smaller than the clusters that formed during the baking steps at 95ºC. This is evident from the UV-Vis absorption spectra shown in Fig. 2 and the SEM images shown in Fig. 3. The plasmonic peak of a nanocomposite baked at 95ºC is broad; indicating particles or agglomerates of many sizes, whereas the peak corresponding to the composite material treated at 300ºC is sharper, enhanced and more defined with a λ_{max} of 434 nm. The peak position at 434 nm is a typical value for the absorption band of AgNPs [9]. Also; this peak resembles the plasmonic peak

obtained for AgNPs in water. The shoulders appearing at higher wavelengths indicate the retention of AgNP clusters, formed during the lower temperature treatments, in the polymer matrix. These results are visually reinforced in the SEM images shown in Fig. 3.

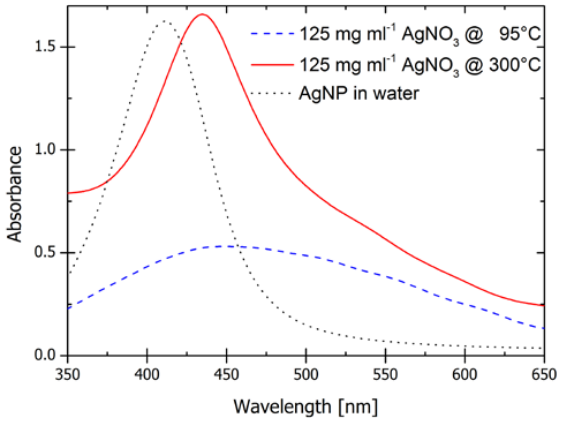

Figure 2: UV-Vis absorption spectra of a nanocomposite on a silica wafer containing 0.5 mL of 125 mg mL^{-1} $AgNO_3$ precursor solution after two different post-exposure heat treatments. Blue dashed curve – after 95°C for 10 min, red solid curve – after an additional 300°C for 30 min and black dotted curve – 15 nm sized AgNPs in water for comparison.

The formation of AgNPs is also confirmed with SEM by looking at the cross sectional area of a fabricated nanocomposite wafer as shown in Fig. 3. The images confirm that individual NPs of 25 nm in diameter are formed, although the randomly distributed NP clusters of roughly 80-100 nm are easy to spot when looking at the composite treated at 95°C. The SEM image further confirms that the additional heat treatment of 300°C results in the generation of more 25 nm sized nanoparticles. It is important to note that further growth of already formed agglomerated NPs does not happen during this last heat treatment.

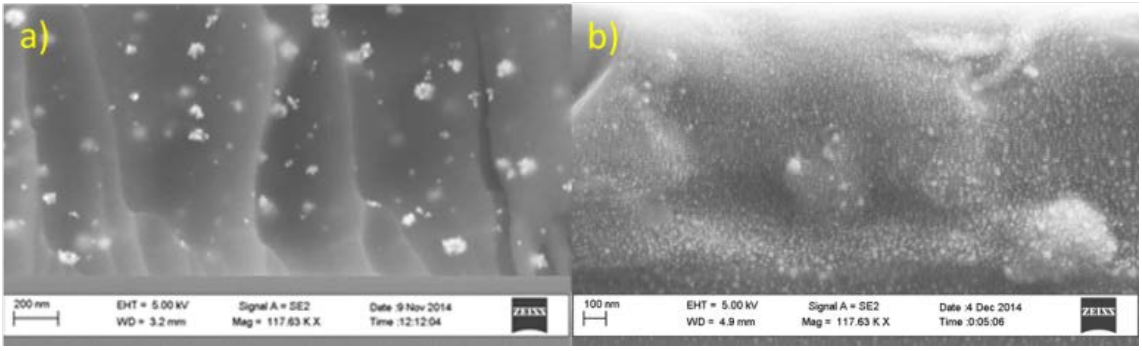

Figure 3: SEM images of a cross section of a nanocomposite on a silicon wafer containing 0.5 mL of 125 mg mL^{-1} $AgNO_3$ precursor solution. a) after a post bake at 95°C for 10 min and b) after an additional bake at 300°C for 30 min.

Structuring of the nanocomposite is important if to be used in micro- and nanofabrication. Although not fully optimized a resolution of 5 µm is obtained using UV-lithography as shown in Fig. 4.

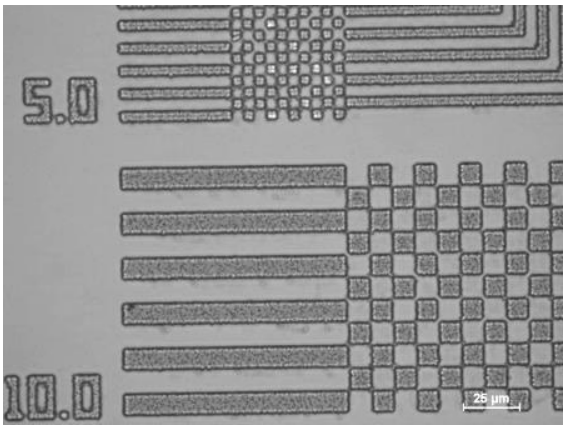

Figure 4: Microscope image at 20 times magnification of a nanocomposite containing 0.5 mL of 125 mg mL^{-1} $AgNO_3$ precursor solution after structuring using UV lithography.

The UV exposure results in the formation of a Lewis acid which cross-links the resist in the exposed areas.

The prolonged exposure of 5 min compared to a standard exposure time of 10 s is required because of the absorption and shadowing effects of the formed AgNPs. Further optimisation of the exposure time needs to be done for improving the currently obtained resolution of 5 µm. However, preliminary experiments show that the exposure time is independent of the added precursor solution for the structured nanocomposites with concentrations up to 125 mg mL^{-1} $AgNO_3$.

With a concentration of 250 mg mL^{-1} precursor solution added to the SU-8, larger amounts of homogeneously distributed micron sized AgNP agglomerates are formed after the post-exposure bake at 95°C. This is easily seen in the microscope image (Fig 5a). With a concentration of 500 mg mL^{-1} precursor solution large, more than 100 µm, randomly distributed phase separated islands of Ag is formed as well (Fig 5b). Heating to 300°C in both cases increases the amount of AgNPs in the nanocomposite but with large inhomogeneity across the wafer.

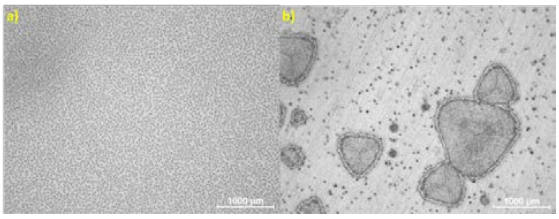

Figure 5: Microscope images at 2.5 times magnification of SU-8 nanocomposites after post-exposure bake at 95°C; a) with 250 mg mL^{-1} of $AgNO_3$ precursor solution added and, b) 500 mg mL^{-1} of $AgNO_3$ precursor solution added.

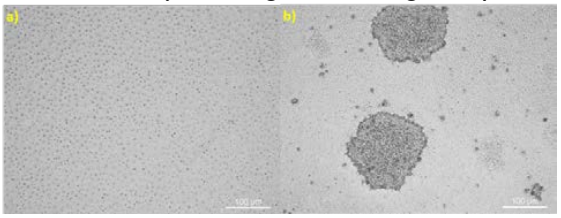

Figure 6: Microscope images at 5 times magnification of SU-8 nanocomposites after bake at 300°C; a) with 250 mg mL^{-1} of $AgNO_3$ precursor solution added and, b) 500 mg mL^{-1} of $AgNO_3$ precursor solution added.

In conclusion, we have developed a method for making in situ SU-8 silver nanocomposites with use of the precursor $AgNO_3$ dissolved in the SU-8 compatible solvent acetonitrile. The nanocomposite can easily be deposited and structured using standard micro- and nanofabrication processes such as spin coating and UV lithography. High resolution of 5 µm has been achieved with UV lithography. The UV exposure time is found to be independent of $AgNO_3$ precursor concentration. We have shown that a bake at 300°C results in further AgNP formation in the composite and not particle growth or agglomeration. The plasmonic absorption maximum is close to 434 nm and is independent of the $AgNO_3$ precursor concentration up to 125 mg mL^{-1}. The AgNPs formed in the SU-8 matrix is approximately 25 nm and distributed evenly in the composite matrix. At higher precursor concentrations, larger agglomerated NPs are dominant and large islands of phase separated Ag are formed in the composite.

1. Daniel, M.-C.; Astruc, D.; *Chem. Rev.,* **2004,** *104,* 293–346.

2. Fedlheim, D. L.; Foss, C. A.; Overview. In *Metal Nanoparticles: Synthesis, Characterization, and Applications,* Marcel Dekker, Inc.: New York, **2002;** pp 1–15.

3. LaBianca, N. C., Gelorme, J. D.; High-aspect-ratio resist for thick-film applications. In *Proceedings of SPIE*: *Advances in Resist Technology and Processing XII,* Santa Clara, CA, February 19, 1995; Allen, R. D., Ed.; 1995; pp 846-852.

4. Serbin, J.; Ovsianikov, A.; Chichkov, B.; *Opt. Express,* **2004,** *12,* 5221-5228.

5. Nemani, K. V.; Moodie, K. L.; Brennick, J. B.; Su, A.; Gimi, B.; *Mat. Sci. Eng. C,* **2013,** 33, 4453-4459.

6. Flack, W.; Soong, D.; Bell, A.; Hess, D.; *Appl. Phys.,* **1984,** 56, 1199-1206.

7. Jiguet, S.; Bertsch, A.; Hofmann, H.; Renaud, P.; *Adv. Eng. Mater.,* **2004,** 6, 719-724.

8. Jiguet, S.; Bertsch, A.; Hofmann, H.; Renaud, P.; *Adv. Funct. Mater.,* **2005,** 15, 1511-1516.

9. Fang, Y.; *J. Chem. Phys.,* **1998,** 108, 4315-4318.

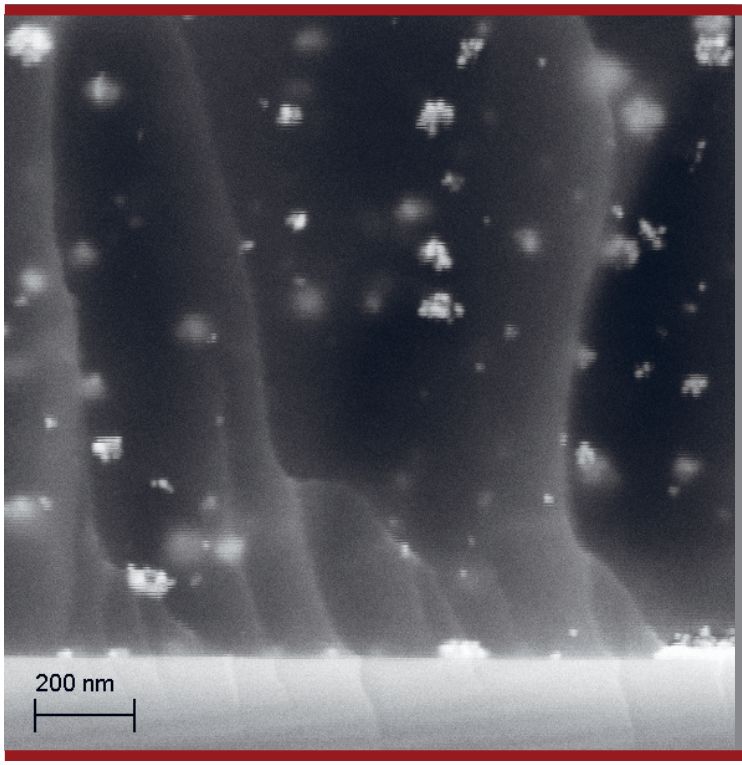

Published by:
DTU Nanotech
Department of Micro- and Nanotechnology
Technical University of Denmark
Ørsteds Plads, building 345B
DK-2800 Kgs. Lyngby